Development of Polylactide-based Reduction-responsive Degradable Nanomaterials for Multifunctional Biomedical Applications

Na Re Ko

A Thesis

In the Department

of

Chemistry and Biochemistry

Presented in Partial Fulfillment of the Requirements

For the Degree of

Doctor of Philosophy in Chemistry at

Concordia University

Montréal, Quebec, Canada

July 2015

CONCORDIA UNIVERSITY

SCHOOL OF GRADUATE STUDIES

This is to certify that the thesis prepared

By: <u>Na Re Ko</u>

Entitled: **Development of polylactide-based reduction-responsive degradable nanomaterials for multifunctional biomedical applications**

and submitted in partial fulfillment of the requirements for the degree of

Doctor of Philosophy in Chemistry

complies with the regulations of the University and meets the accepted standards with respect to originality and quality.

Signed by the final examining committee:

_____ Chair

_____ External Examiner
                    Dr. Ashok Kakkar

_____ External to Program
                    Dr. Christopher Brett

_____ Examiner
                    Dr. Christopher J. Wilds

_____ Examiner
                    Dr. Pat Forgione

_____ Thesis Supervisor
                    Dr. John Oh

Approved by

_____
Chair of Department or Graduate Program Director

_____ 2015   _____
                                        Dean of Faculty

Abstract

Development of Polylactide-based Reduction-responsive Degradable Nanomaterials for Multifunctional Biomedical Applications

Na Re Ko, Ph. D.

Concordia University, 2015

Polylactide (PLA)-based nanomaterials have been extensively explored in biomedical applications due to their biocompatibility and biodegradability. However, PLA has two main limitations: hydrophobicity and slow degradation rate. My Ph.D. research focuses on the exploration of potential approaches to circumvent these challenges by synthesis of PLA-based amphiphilic block copolymers (ABPs) with stimuli-responsive degradation (SRD) and these ABPs are used to fabricate novel PLA-based nanomaterials.

SRD is highly desirable in the design of multi-functional polymer-based drug delivery systems. SRD involves the incorporation of dynamic covalent bonds into nanomaterials that can be cleaved in response to external stimuli such as light, ultrasound, low pH, and enzymes. This process leads to chemical or physical changes of nanomaterials to enhance the release of therapeutics or tune the morphologies. Reduction-responsive degradation uses disulfide-thiol chemistry. Disulfide linkages are cleaved either in response to a reductive environment or a disulfide-thiol exchange reaction in the presence of thiols. Using this unique system, PLA-based nanomaterials with disulfide linkages can be developed for tumor-targeting drug delivery.

Amphiphilic micellar aggregates have attracted much interest as a promising candidate for effective polymeric drug delivery. Micelles are formed through aqueous self-assembly of ABPs consisting of both hydrophilic and hydrophobic blocks. Hydrophobic cores encapsulate hydrophobic therapeutics and the surrounding hydrophilic coronas enhance colloidal stability. Adjusting this unique structure of ABP is a promising strategy for circumventing the hydrophobicity of PLA. Uniformed micelles in the nanoscale size range can prolong the blood

residence and minimize side effects, and possess multiple cargos into a single vehicle, allowing multi-functional drug delivery.

In this thesis, several reduction-responsive degradable PLA-based ABPs have been reported. They were further used to fabricate various nanomaterials including micellar drug carriers; polyplexes; and nanofibers. These ABPs were synthesized by a combination method of ring opening polymerization and atom transfer radical polymerization. Due to their amphiphilic nature, ABPs can be self-assembled to form the micellar platforms possessing hydrophobic therapeutics in the core, which is surrounded with hydrophilic coronas. ABPs with positively charged hydrophilic blocks enable the formation of cationic micellar aggregates. These cationic micelles have subsequently been used as dual delivery carriers of drugs and genes. Furthermore, incorporating dual-located disulfide linkages at both the hydrophobic PLA core and the interface leads to a synergistically enhanced release of encapsulated drugs in cellular environments. Moreover, PLA nanofibers were fabricated via air-spinning technique of high-molecular weight PLAs. Their hydrophobic surface was modified with hydrophilic polymers via facile surface-initiated ATRP. The resulting surface-modified PLA fibers exhibit enhanced hydrophilicity and thermal stability, as well as tunable surface properties upon the cleavage of disulfide linkages. Under a reductive environment, these novel PLA-based nanomaterials are rapidly degraded upon the cleavage of disulfides, leading to controlled release of drugs and genes, as well as change of surface properties. These results suggest the disulfide-labeled PLA-based nanomaterials offer great potential and versatility in biomedical applications.

Acknowledgements

First, I would like to express my appreciation to my graduate adviser Dr. John Oh for his support and advice in conducting this scientific research, publishing the manuscripts, and writing this thesis throughout all four years. I also would like to thank my dissertation committee members: Dr. Christopher J. Wilds, Dr. Pat Forgione, Dr. Ashok Kakkar, and Dr. Christopher Brett for their helpful comments and suggestions that have been great value for this research and thesis. Additionally, I am grateful to all faculty members in chemistry department including Dr. Heidi Muchall and my proposal committee members: Dr. Yves Gélinas and Dr. Guillaume Lamoureux, for their encouragement and helpful advices during my Ph.D. program.

I would like to specially thank all my collaborators, Dr. Anne Noronha and Jack Cheong in the Dr. Wilds group and Dr. Gaétan Laroche and Gad Sabbatier at Université Laval, for all their support and achievements in the successful completion of my research. I would like to acknowledge all the members of the Dr. Oh's group that I had the pleasure to work with, particularly; Andrew, Behnoush, Sam, Qian, Alex, Nick, Mathias, Soyoung, Yasaman, Natalie, Yifen, Puzhen, Kaiwan, Dipa, Seonghwa, Tongbing, and Arun. I also must thank my great friends Hayline and Natalie, for their love and encouragement. I consider myself fortunate to have been able to make amazing memories with you.

A great deal of thanks is owed to all my family and friends in Korea. Thank you for all your great support. I am also thankful to Sergei, Dr. Cho, and SH. You were the key of my Ph.D. program over the past four years.

Finally and most importantly, this work is dedicated in loving memory to Anna and Dalsong.

List of Publications

(Equal contribution is denoted with *.)

1. Nicky Chan, <u>Na Re Ko</u>, So Young An, Jung Kwon Oh, *Controlled Radical Polymerization: Materials, Vol. 1188*, American Chemical Society, **2015**, pp. 273-291.

2. <u>Na Re Ko,</u> Jack Cheong, Anne Noronha, Christopher J. Wilds, Jung Kwon Oh. Reductively-sheddable cationic nanocarriers for dual chemotherapy and gene therapy with enhanced release. *Colloids and Surfaces B: Biointerfaces* **2015**, *126*, 178-187.

3. <u>Na Re Ko,</u> Jung Kwon Oh. Glutathione-triggered disassembly of dual disulfide located degradable nanocarriers of polylactide-based block copolymers for rapid drug release. *Biomacromolecules* **2014**, *15(8)*, 3180-3189.

4. Alexander Cunningham, <u>Na Re Ko</u>, Jung Kwon Oh. Synthesis and reduction-responsive disassembly of PLA-based mono-cleavable micelles. *Colloids and Surfaces B: Biointerfaces* **2014,** *122*, 693–700.

5. <u>Na Re Ko,</u> Gad Sabbatier*, Alexander Cunningham, Gaétan Laroche, Jung Kwon Oh. **(2014)**. Air-Spun PLA Nanofibers Modified with Reductively Sheddable Hydrophilic Surfaces for Vascular Tissue Engineering: Synthesis and Surface Modification. *Macromolecular Rapid Communications* **2014**, *35(4)*, 447-453.

6. <u>Na Re Ko,</u> Kejian Yao, Chuanbing Tang, Jung Kwon Oh. Synthesis and thiol-responsive degradation of polylactide-based block copolymers having disulfide junctions using ATRP and ROP. *Journal of Polymer Science Part A: Polymer Chemistry*, **2013**, *51(14)*, 3071-3080.

7. Qian Zhang, <u>Na Re Ko</u>, Jung Kwon Oh. Modulated morphologies and tunable thiol-responsive shedding of aqueous block copolymer aggregates. *RSC Advances*, **2012**, *2(21)*, 8079-8086.

8. Qian Zhang, <u>Na Re Ko</u>, Jung Kwon Oh. Recent advances in stimuli-responsive degradable block copolymer micelles: synthesis and controlled drug delivery applications. *Chemical Communications,* **2012**, *48(61)*, 7542-7552.

Contribution of Authors

The majority of the research presented in this thesis was conducted by the author of this thesis. Here are the specific contributions of collaborators.

In Chapter 3, dehydroabietic ethyl methacrylate (DAEMA) monomer was synthesized and offered by Dr. Kejian Yao in the Dr. Chuanbing Tang's group at the University of South Carolina.

In Chapter 4, the ssDNA synthesis and gel electrophoresis were conducted by Dr. Anne Noronha and Jack Cheong in the Dr. Christopher J. Wilds's group at Concordia University.

In Chapter 6, fabrication of nanofibers of high molecular weight PLAs was conducted by Gad Sabbatier in the Dr. Gaétan Laroche's group at Université Laval. Most high molecular weight PLAs were synthesized by myself and Alexander Cunningham also contributed to the synthesis of several PLAs described in Table 6.1.

Table of Contents

List of Figures

List of Schemes

List of Tables

List of Abbreviations

ABP	Amphiphilic block copolymer
ATRP	Atom transfer radical polymerization
BCA assay	Bicinchoninic acid assay
BCP	Block copolymer
Br-iBuBr	α-Bromoisobutyryl bromide
CLSM	Confocal laser scanning microscopy
CMC	Critical micellar concentration
cPDMA	Cationic poly(N,N-dimethylaminoethyl methacrylate)
C-ssABP	Polylactide-ss-cationic poly(N,N-dimethylaminoethyl methacrylate)
CuBr	Copper(I) bromide
D,L-LA	D,L-Lactide
DAEMA	Dehydroabietic ethyl methacrylate
DAPI	2-(4-Amidinophenyl)-1H-indole-6-carboxamidine
DCC	*N,N'*-Dicyclohexyl carbodiimide
DLS	Dynamic light scattering
DL-ssABP	POEOMA-ss-(PLA-ss-PLA)-ss-POEOMA triblock copolymer
DMA	N,N-Dimethylaminoethyl methacrylate
DMAP	4-(Dimethylamino)pyridine
DMEM	Dulbecco's modified Eagle's medium
DNA	Deoxyribonucleic acid
DOX	Doxorubicin
DP	Degree of polymerization
DSC	Differential scanning calorimetry

DTT	DL-Dithiothreitol
FBS	Fetal bovine serum
FC	Flow cytometry
FDA	Food and Drug Administration
FRP	Free radical polymerization
GC	Gas chromatography
GPC	Gel permeation chromatography
GSH	Glutathione
HMS	High molecular weight shoulder
HMssEt	Pendant disulfide-labeled methacrylate monomer
HO-ss-iBuBr	2-Hydroxyethyl-2-(bromoisobutyryl)ethyl disulfide
LA	3,6-Dimethyl-1,4-dioxane-2,5-dione (lactide)
LiBr	Lithium bromide
Me$_6$TREN	Tris[2-(dimethylamino)ethyl]amine
MeI	Iodomethane
MMA	Methyl methacrylate
M$_n$	Number-average molecular weight
MTT	3-(4,5-dimethylthiazol-2-yl)-2,5-diphenyltetrazolium bromide
M$_w$	Weight-average molecular weight
MWCO	Molecular weight cut-off
NMR	Nuclear magnetic resonance
NR	Nile Red
OEOMA	Oligo(ethylene glycol) monomer
PBS	Phosphate buffered saline
PCL	Polycaprolactone

PDDS	Polymeric drug delivery systems
PDI	Polydispersity index
PDLA	Poly(D-lactide)
PDLLA	Poly(D,L-lactide)
PDMA	Poly(*N,N*-dimethylaminoethyl methacrylate)
PDS	Pyridyl disulfide
PEG	Polyethylene glycol
PEO	Polyethylene oxide
PEOH	poly(ethylene oxide monomethyl ether
PET	Poly(ethylene terephthalate)
PLA	Polylactide
PLLA	Poly(L-lactide)
PMDETA	*N,N,N',N'',N''*-pentamethyldiethylenetriamine
PMMA	Poly(methyl methacrylate)
POEOMA	Poly oligo(ethylene glycol) monomethyl ether methacrylate
PSt	Polystyrene
PTFE	Polytetrafluoroethylene
RAFT	Reversible addition-fragmentation chain transfer polymerization
RI	Refractive index
ROP	Ring opening polymerization
SA	Succinic anhydride
SEM	Scanning electron microscopy
SI-ATRP	Surface-initiated atom transfer radical polymerization
Sn(Oct)$_2$	Tin(II) 2-ethylhexanoate
SRD	Stimuli-responsive degradation

ssDNA	Single-stranded DNA
ss-DOH	2-Hydroxyethyl disulfide
St	Styrene
tBA	*tert*-Butyl acrylate
TEM	Transmission electron microscopy
T_g	Glass transition temperatures
TGA	Thermal gravimetric analysis
TPMA	Tris(2-pyridylmethyl)amine
UV/Vis	Ultraviolet-visible Spectroscopy

Chapter 1 Introduction

1.1 Brief overview of the research

My Ph.D. research is aimed at exploring stimuli-responsive degradation (SRD), particularly reduction-responsive degradation, to develop a variety of novel disulfide-labeled polylactide (PLA)-based amphiphilic block copolymers (ABPs) and their nanomaterials, including self-assembled micelles, polyplexes, and nanofibers for biomedical applications. Ring opening polymerization (ROP) and atom transfer radical polymerization (ATRP) have been mainly used to synthesize well-defined PLA-based ABPs. They have subsequently been used as building blocks for fabricating micellar aggregates through aqueous self-assembly and nanofibers via the air-spinning method. Under a reductive environment, PLA-based nanomaterials degraded upon the cleavage of disulfide linkages, exhibiting the rapid release of anticancer drugs and genes, as well as tuning the surface properties. Furthermore, the proposed PLA-based micellar aggregates were evaluated for their prospective intracellular drug delivery applications through *in vitro* cell experiments.

1.2 Polylactide (PLA) as a promising material

Polylactide (PLA), polycaprolactone (PCL), and polyglycolide (PGA) are a class of hydroxyalkanoic acid-based aliphatic polyesters. In particular, PLA and its copolymers are commonly used in biomedical applications due to their great biocompatibility.[1] PLA is biodegraded *in vivo* by a simple hydrolysis of the ester linkage to the corresponding water-soluble oligomers and lactic acid monomers.[2] In mammalian physiology, lactic acid is naturally produced as a by-product of anaerobic respiration (a form of respiration using electron acceptors other than oxygen). It is then metabolized into carbon dioxide and water.[3] In addition, PLA is renewable and FDA-approved for clinical uses.[4] These unique properties make PLA-based materials useful for extensive applications in biomedical fields, including sutures, bone fixation implants, drug delivery carriers, and stents.[5]

The main application of PLA and its copolymer is in a drug delivery system. Due to the good biocompatibility and biodegradability of PLAs, many studies have made progress in the development of PLA-based drug delivery carriers. Such polymeric drug delivery systems

(PDDS) are ideal candidates for the transportation of therapeutics to target sites, which helps improve therapeutic efficacy by minimizing undesired side effects that commonly occur with small drugs.[6] During blood circulation, small therapeutics with a molecular weight less than 45 kDa (or diameter <5nm) are rapidly cleared through renal clearance (kidney filtration).[7] Small drugs can also be accumulated in normal tissues, causing harmful side effects.[8] In addition, most hydrophobic drugs are easily recognized by specific proteins (called opsonins) and cleared by the mononuclear phagocytic system (MPS), known as the reticuloendothelial system (RES).[9] For these reasons, high doses or frequent administrations of small therapeutics are required to achieve the desired therapeutic efficacy. PDDS have been extensively explored in the field of pharmaceutical science and nanotechnology.[10] To achieve targeted therapeutic potential and minimize side-effects common to small drugs, polymeric drug carriers must be designed considering several important properties:[11] I) appropriate particle size (50 - 150 nm) with uniform size distribution to minimize undesired clearance by kidney, liver, and spleen;[12] II) biocompatibility for prolonged blood circulation;[13] III) controlled rapid drug release at the target site;[14] and IV) biodegradability to avoid polymeric residue remaining after drug release.[15] Considering the versatile advantages of PDDS, the development of PLA-based drug carriers has been extensively explored in the form of pellets, microcapsules, and nanoparticles.[16] PLA-based nanoparticles are increasingly the subject of investigation for effective delivery with sustained release of therapeutics,[17] peptides or proteins,[18] and nucleic acids (RNA or DNA).[19]

1.3 Challenges of PLA applications in the use of biomedical fields

For successful biomedical applications, PLA has two obvious drawbacks to be addressed: hydrophobicity and slow degradation (Table 1.1).[20] PLA is hydrophobic due to the presence of methyl groups on the backbone. Hydrophobic PLA can produce inflammation through immune system recognition of host tissue.[21] In addition, PLA-based drug carriers can induce delayed diffusion of therapeutics due to the hydrophobic interaction between PLA and therapeutics, leading to a low drug efficacy.[22] One of the most promising strategies for overcoming the hydrophobicity of PLA is an introduction of hydrophilic polymers including poly(meth)acrylates, polypeptides, and polysaccharides.[23] This strategy can facilitate the development of PLA-based ABPs and their self-assembled micellar aggregates consisting of hydrophobic PLA cores

2

surrounded with hydrophilic coronas. These micellar platforms have been mainly used as effective drug carriers and they will be reviewed in section 1.6.[24]

Table 1.1. Advantages and disadvantages of PLA for biomedical applications.
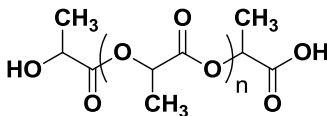
	Advantages	Applications
PLA	Biocompatibility	Sutures
	Biodegradability	Bone fixation implants
	Renewable source	Drug delivery carriers
	FDA-approval	Tissue engineering
	Disadvantages	**Solutions**
	Hydrophobicity	Amphiphilic block copolymer
	Slow degradation rate	Stimuli-responsive degradation

Another critical challenge associated with the successful application of PLA is its slow degradation rate. PLA can be naturally degraded via hydrolysis under acidic conditions or enzymatic reactions with lipase PL[25] or *proteinase K*.[26] However, this process sometimes takes a few years for PLA to be completely resorbed *in vivo*[27] and such a slow degradation impedes the use of PLA alone in biomedical applications.[28] One of the promising approaches for circumventing the slow degradation of PLA involves the introduction of SRD in the design of PLA-based nanomaterials. SRD uses the dynamic covalent bonds that can be cleaved in response to external stimuli such as light, ultrasound, and enzyme, as well as low pH and reduction reactions. Using the unique disulfide-thiol chemistry as an initial thought, the OH research group at Concordia University has extensively explored the synthesis of reduction-responsive PLA-based block copolymers (BCPs) and their nanostructured materials.[29] Based on these demonstrated experiments, my Ph.D. research has focused on the development of novel disulfide-labeled PLA-based nanomaterials.

1.4 Stimuli-Responsive Degradation (SRD)

SRD is a promising strategy that involves the introduction of dynamic covalent bonds into the design of nanomaterials.[30] In response to external stimuli, the covalent bonds are cleaved, causing destabilization or morphological change of nanomaterials,[31] thus leading to controlled release of therapeutics to desired sites.[32] As illustrated in Figure 1.1, the SRD can be classified into three categories: physical stimuli, including light and ultrasound; chemical stimuli, including pH and reductive reaction; and biological stimuli, such as enzymes.[33]
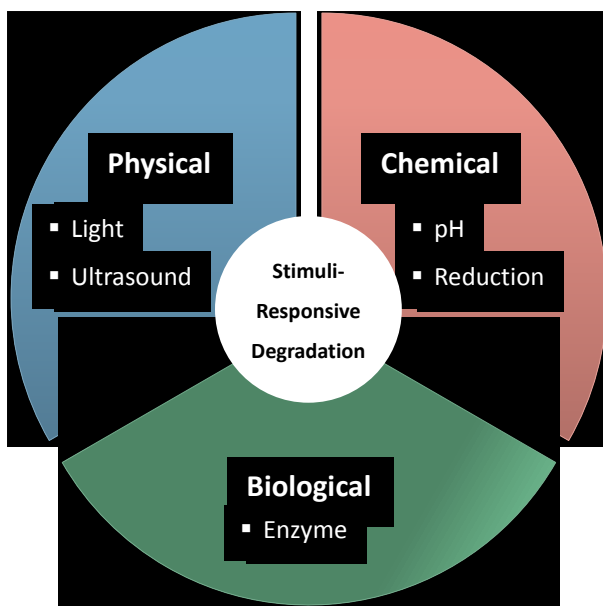
Figure 1.1. Three categories of stimuli-responsive degradation system.

Light-responsive degradation uses the incorporation of photo-sensitive linkages, such as 2-diazo-1,2-napthoquinone (coumarin dimers) and o-nitrobenzyl derivatives.[34] The cleavage of pendant photo-sensitive linkages changes the hydrophobic-hydrophilic balance of the copolymers, which causes the destabilization of drug carriers (Figure 1.2).[35]
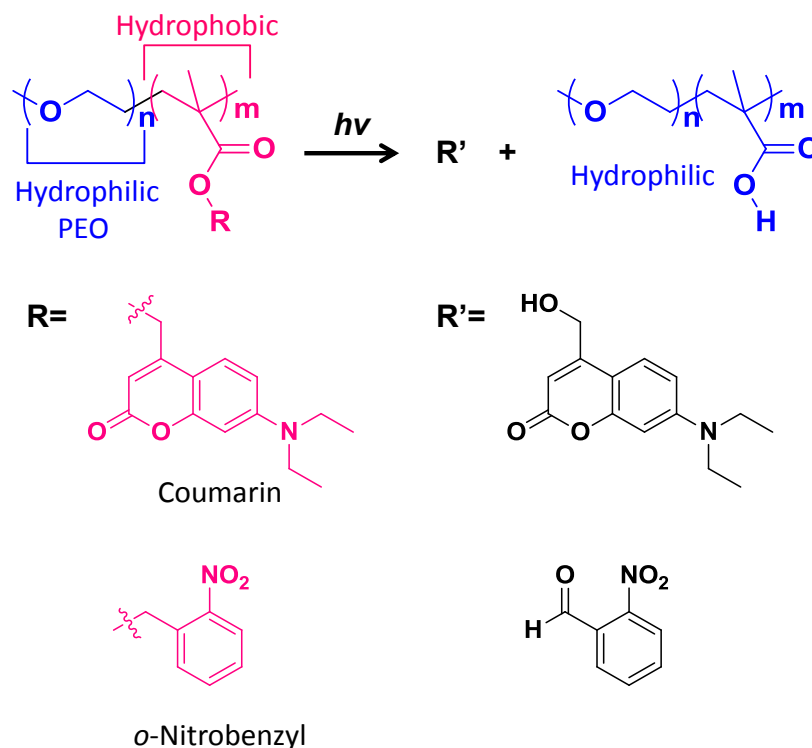
Figure 1.2. Illustration of light- responsive degradable coumarin and o-nitrobenzyl moieties.

An ultrasound-responsive degradation system uses an ultrasound contrast agent (called microbubble) which is filled with heavy gases like sulphur hexafluoride, perfluoropropane, perfluorohexane, and nitrogen.[36] The core of the microbubble is designed to strongly reflect ultrasound and temperature, and the shell is typically composed of either a lipid or protein linked with drugs.[37] The ultrasound wave is not much absorbed by water or tissue, and its tissue penetration depth can be easily controlled by tuning wave frequency and exposure time.[38] When the microbubbles are exposed to high frequency ultrasound, they are destroyed and release therapeutics by cavitation, when the gas inside the microbubble core becomes highly compressed,[39] or hyperthermia, when the temperature of the target site increases.[40]

Biologically-responsive degradation uses specific enzymes, such as proteases, phospholipases, or glycosidases, which are only found in tumor tissues or inflammation tissues.[41] The enzymatic activity associated with particular tissues increases the concentration of the enzyme and numerous diseases can be detected by enzyme dysregulation, which involves

poor modulation of enzyme.[42] These features can promote the use of enzymes as effective biological triggers with high selectivity in the development of tumor-targeting drug delivery nanocarriers.[43]

A pH-responsive degradation system uses acid-labile linkages like acetal, orthoester, imine, hydrazone, and oxime.[13, 44] Compared to a physiological condition (pH = 7.2–7.4), most tumor tissues are slightly acidic, including pH = 6.5–7.2 in extracellular fluids, pH = 5–6.5 in endosomes, and pH = 4.5–5 in lysosomes.[45] When these nanomaterials are exposed to an acidic environment, the acid-labile linkages are cleaved, and pH-responsive nanocarriers are rapidly degraded, leading to enhanced release of encapsulated therapeutics.[46]

1.4.1 Reduction-responsive degradation system

A typical reduction-responsive degradation system uses unique disulfide-thiol chemistry. Disulfide linkages are cleaved either in response to a reductive environment or a disulfide-thiol exchange reaction in the presence of thiols. Glutathione (GSH) is a naturally occurring isotripeptide, consisting of glycine, glutamic acid, and cysteine. GSH is also highly sensitive for cell functionality and viability.[47] It is found at higher level concentrations in intracellular environments (2-10 mM) than in extracellular environments (<20 μM).[48] Further, GSH is 7-10 times more common in cancer cells than in normal cells.[49] This significant variation in GSH levels has promoted the development of GSH-triggered tumor-targeting drug delivery systems.[50] Upon the cleavage of disulfides in response to GSH, reduction-responsive drug carriers are rapidly destabilized and release anti-cancer therapeutics.[51]

1.5 Various reduction-responsive drug delivery platforms

A variety of polymeric drug delivery carriers exhibiting reduction-responsive degradation and drug release have been explored. Typical examples include polymer-drug conjugates, dendrimers, crosslinked nanogels, and amphiphilic micelles (Figure 1.3).[52]

6
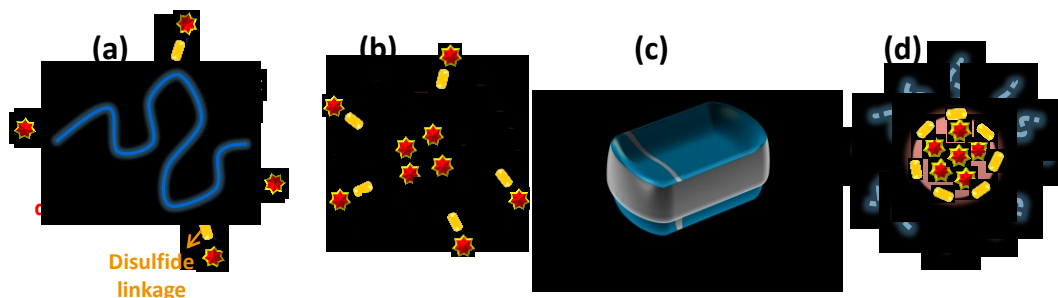
Figure 1.3. Different types of reduction-responsive drug carriers; (a) polymer-drug conjugates, (b) dendrimers, (c) nanogels, and (d) micelles.

A polymer-drug conjugate (also called as polymeric prodrug) is a nanosized hybrid drug carrier that consists of therapeutics covalently bound to a polymer chain (Figure 1.3a).[11] Generally, biodegradable and biocompatible water-soluble polymers are used as building blocks of polymer-drug conjugates.[53] Disulfide linkages are located between drugs and the polymer backbone, so the linked drugs can be released upon the cleavage of disulfides. Su et al. reported the synthesis and release kinetic of doxorubicin (DOX) anticancer drug conjugated chitosan oligosaccharide copolymer via disulfide linkage.[54] *In vitro* cell experiments showed a time-dependent release of DOX from the conjugates in response to the reducing agent, DL-dithiothreitol (DTT). After internalization into human breast cancer cells, DOX was rapidly released upon the cleavage of the disulfide bonds mediated by an abundance of GSH.

A dendrimer is a three-dimensional spherical symmetric macromolecule that contains a central core and hyperbranched polymeric chains, displaying a dense shell structure (Figure 1.3b). [55] It has terminal functional groups and interior void spaces, and therefore allows not only covalent bond with drugs but the physical entrapment of therapeutics through non-covalent interactions.[56] Lim et al. synthesized disulfide labeled poly(monochlorotriazine) dendrimer conjugated with the anti-cancer drug, paclitaxel.[57] The conjugates were further modified with polyethylene glycol (PEG) to enhance the hydrophilic properties of the conjugates. *In vivo* cytotoxicity studies showed enhanced toxicity of PC-3 cells (human prostate cancer cells) in the presence of the DTT reducing agent.

A nanogel is a cross-linked network of polymer chains confined in nanometer-size,[58] and therapeutics can be encapsulated inside these nanogel networks (Figure 1.3c).[59] Under a

reductive environment, the entrapped therapeutics can be rapidly released from nanogels through diffusion,[60] swelling,[61] or degradation processes.[62] The synthesis of reduction-responsive DOX-loaded PEG nanogels via crosslinking of disulfide-labeled PEG polymers was reported.[63] In the presence of 5 mM GSH, these nanogels were rapidly dissociated upon the cleavage of disulfides, exhibiting enhanced release of entrapped DOX over time.

1.6 Amphiphilic micellar drug carriers

Amphiphilic micelles can be prepared through self-assembly of ABPs in aqueous solution. ABPs consist of both hydrophilic and hydrophobic blocks, which are covalently attached. They possess important properties for effective drug delivery approaches.[64] First, amphiphilic micelles consist of a hydrophobic core, enabling the encapsulation of hydrophobic therapeutics, surrounded with hydrophilic coronas, enhancing colloidal stability (Figure 1.3d).[65] Second, they are designed with the size ranging of 50 - 150 nm in diameter with uniform size distribution, minimizing side effects common to small drugs.[7a, 66] Third, they can encapsulate multiple cargos such as diagnosis and imaging agents or other therapeutics together with drugs into a single vehicle.[67] Finally, they can be bioconjugated with specific proteins to promote active targeting, capable of enhancing selective delivery of the drug to target tissues by receptor-mediated endocytosis.[68]

1.6.1 Various approaches in the design of reduction-responsive degradable micelles

Numerous strategies to synthesize novel reduction-responsive ABPs and their nanometerials have been reported for tumor-targeting drug delivery. These degradable ABPs can be characterized with different numbers and locations of disulfide cleavable linkages (Figure 1.4).[30b] Depending on the location of disulfide linkages, micelles can have cleavable linkages either in their micellar cores (Figure 1.4a-c) or at interfaces between micelle cores and coronas (Figure 1.4d). Recently, multi-cleavable reduction-responsive micelles with disulfides at both the core and the interfaces have been reported (Figure 1.4e).[29d, 69]
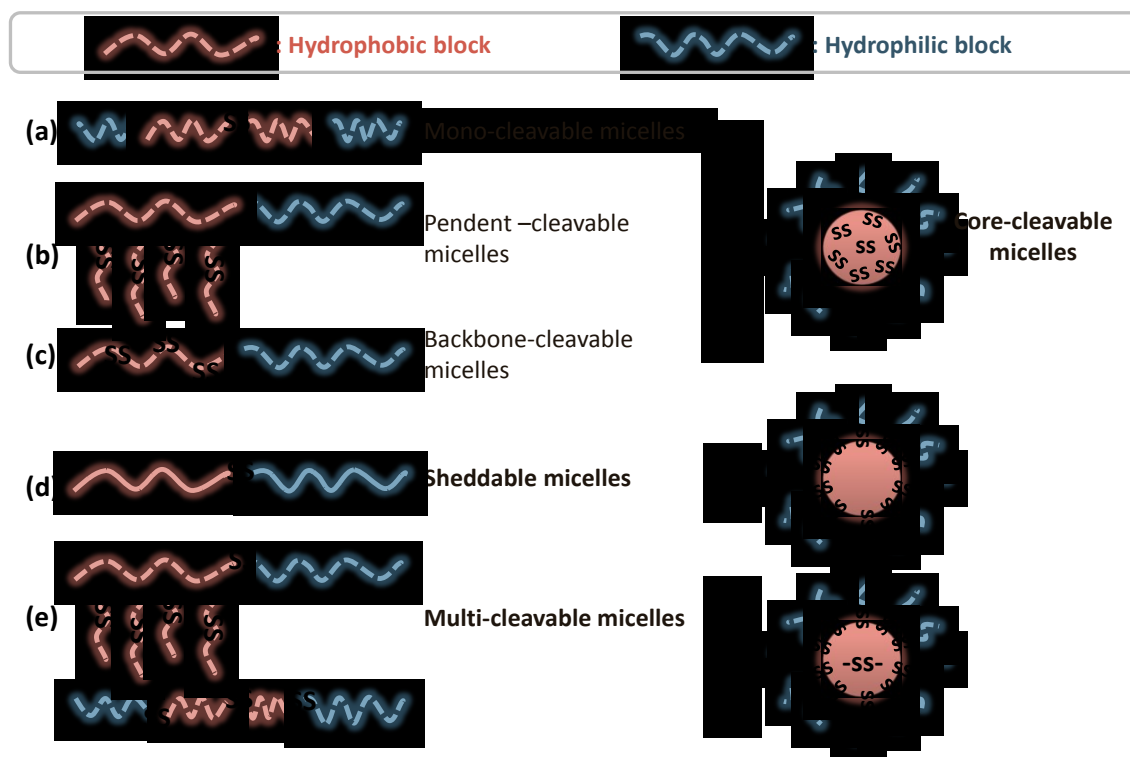
Figure 1.4. Schematic illustration of various strategies to synthesize reduction-responsive degradable amphiphilic micelles.

Mono-cleavable micelles (Figure 1.4a) consist of amphiphilic triblock copolymers with a single disulfide linkage in the middle of the triblock copolymer (hydrophilic-hydrophobic-ss-hydrophobic-hydrophilic blocks). Upon the cleavage of the disulfide bond under a reductive environment, their molecular weight can be halved from the original triblock copolymers, leading to a change in micellar morphologies and sizes in aqueous solution. However, degraded polymers still retain their amphiphilic nature (hydrophobic-hydrophilic-SH) and thus form smaller-sized micelles. Since these small micelles can re-encapsulate therapeutics, mono-cleavable micelles exhibit a slow release of drugs and low drug efficacy. Several mono-cleavable micellar drug carriers with disulfides in the cores were reported, including poly(oligo(propylene oxide) monononylphenyl ether acrylate)-poly(oligo(ethylene oxide) monomethyl ether methacrylate) amphiphilic micelles,[70] hydrophobic PLA-based ABP micelles consisting of hydrophilic POEOMA[71] or PEG blocks.[29c]

Pendent-cleavable micelles (Figure 1.4b) involve the synthesis and aqueous self-assembly of degradable ABPs with disulfide cleavable linkages positioned in the side chain of hydrophobic blocks. Upon the cleavage of pendant disulfide linkages in the hydrophobic cores, micelles change their polarity from hydrophobic to hydrophilic, leading to the destabilization of micelles.[72] Various pendent-cleavable ABPs have been designed based on disulfide-labeled hydrophobic monomers such as pendant disulfide-labeled methacrylate monomer (HMssEt),[73] 2-((2-hydroxyethyl)disulfanyl)ethyl methacrylate monomer,[74] pyridyl disulfide-based methacrylate monomer (2-pyridyldisulfide ethylmethacrylate),[75] and pyridyl disulfide-functionalized cyclic carbonate monomer.[76]

Backbone-cleavable micelles (Figure 1.4c) can be formed by self-assembly of ABPs with disulfide linkages regularly located on hydrophobic backbones. The cleavage of disulfide linkages in the micellar cores causes disintegration of the micelles due to the loss of colloidal stability in aqueous solution. Several ABPs consisting of a disulfide-labeled polyester backbone synthesized by polycondensation of 3,3′-dithiodipropionic acid and various diols with or without disulfide have been reported.[64, 77]

1.6.2 Sheddable micellar drug carriers

Unlike other core-cleavable micelles described above (mono-, pendant-, and backbone-cleavable micelles) that have disulfide bonds located in the micellar cores, sheddable type micelles have disulfides at interfaces between the hydrophobic core and hydrophilic coronas (Figure 1.4d). These micelles consist of ABPs with disulfides at the junction of hydrophobic and hydrophilic blocks.[78] The location of disulfides positioned at interfaces of sheddable micelles offers facile access of hydrophilic GSH.[29b, 79] Sun et al. reported disulfide-linked sheddable PEG-PCL micelles, encapsulating DOX as a model anticancer drug.[80] Compared with the reduction-insensitive control (PEG-b-PCL micelles with no disulfides), reduction-responsive PEG-ss-PCL micelles showed higher anticancer efficacy. Similarly, Wang et al. introduced disulfide-bridged PCL-poly(ethyl ethylene phosphate) (PEEP) micelles.[81] Compared with reduction-irresponsive micelles (PCL-b-PEEP with no disulfides), these sheddable PCL-ss-PEEP micelles exhibited rapid intracellular release and enhanced accumulation of drugs in cancer cells under a reductive environment. These experiments clearly indicate the great potential of reduction-responsive sheddable micelles as tumor-targeting drug carriers, and numerous papers

have demonstrated various applications for thiol-responsive sheddable micelles. Wen et al. reported a new sheddable micelle composed of a PEG shell and a poly(ε-benzyloxycarbonyl-L-lysine) core.[82] Upon exposure to GSH reducing agent, reductive cleavage of the disulfides initiates micellar rearrangement associated with the rapid release of the encapsulated DOX. Li et al. designed reduction-responsive hyaluronic acid-deoxycholic acid amphiphilic micelles as anti-cancer drug carriers.[83] They exhibit excellent GSH-sensitive drug-releasing capacities for paclitaxel, a model hydrophobic anticancer drug. Sun et al. fabricated reduction-degradable sheddable micelles based on polyamide amine-PEG ABPs with disulfides.[84] Through aqueous self-assembly, these ABPs form the sheddable micelles, bearing disulfides at micellar interfaces. These micelles exhibit colloidal stability in a physiological condition and quickly disassemble under a reductive environment due to the cleavage of the disulfide linkages, releasing the encapsulated DOX.

1.6.3 Multi-cleavable micelles

Recently, multiple stimuli-responsive degradable nanomaterials with more than two stimuli-responsive cleavable linkages have been developed.[85] Compared with conventional single stimulus-responsive degradable micelles, these novel systems exhibited dual- or triple-responses for release of drugs. However, the cleavage linkages are located at only one position (either the core or the interface) in the micellar drug carriers. To achieve more efficient therapeutic efficacy, the OH research group at Concordia University has explored a new dual-location of single stimulus strategy to develop multi-cleavable micelles with disulfide linkages at dual locations (Figure 1.4e). Upon the cleavage of dual-located disulfides in response to a GSH trigger, this new system accelerates the destabilization of nanocarriers, thus synergistically enhancing the release of therapeutics. As a proof-of-concept, a novel design of micellar nanocarriers with disulfide linkages at both the hydrophobic core and the interface has been developed (Figure 1.5).[69a] These micelles are formed from multi-cleavable ABPs consisting of a hydrophobic PHMssEt block and a hydrophilic polyethylene oxide (PEO) block. Disulfide linkages are located at the block junction and side chains of hydrophobic blocks, thus forming PEO-ss-PHMssEt ABPs. Under a reductive environment, disulfides present at the interface and hydrophobic core are rapidly cleaved and generate a water-soluble PEO segment (PEO-SH) and short hydrophobic chains (PHM-SH and HS-Et), leading to destabilization of the micelle. *In*

vitro cellular experiments exhibit accelerated release of encapsulated DOX upon cell internalization in response to a high concentration of intracellular GSH in HeLa cancer cells.
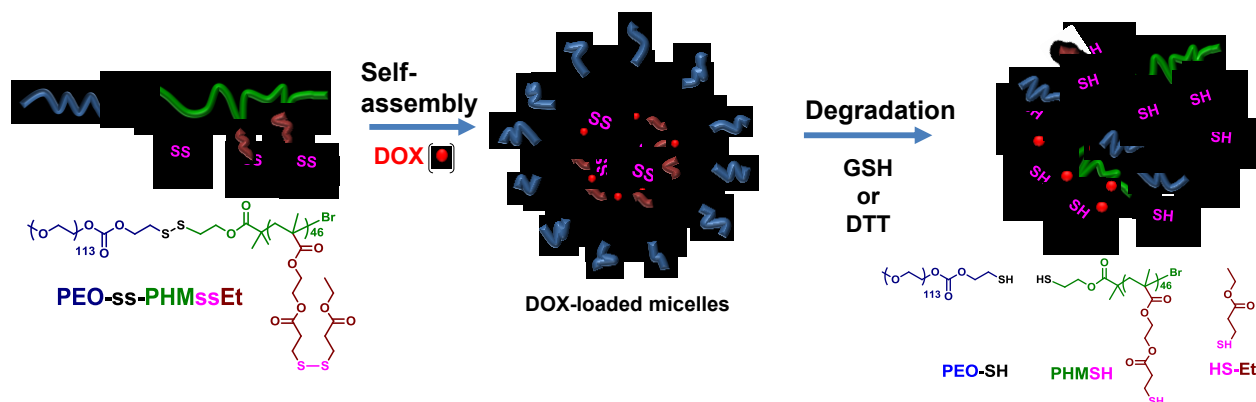
Figure 1.5. Design, aqueous micellization, and degradation of PEO-ss-PHMssEt ABPs having disulfide linkages located in both hydrophobic core and interface between core/corona.[69a]

1.7 Thesis organization

This thesis consists of seven chapters, namely the general introduction, principles of synthesis and characterization, four research projects, and the conclusion. Figure 1.6 illustrates a summary of overall approaches in my Ph.D. research.
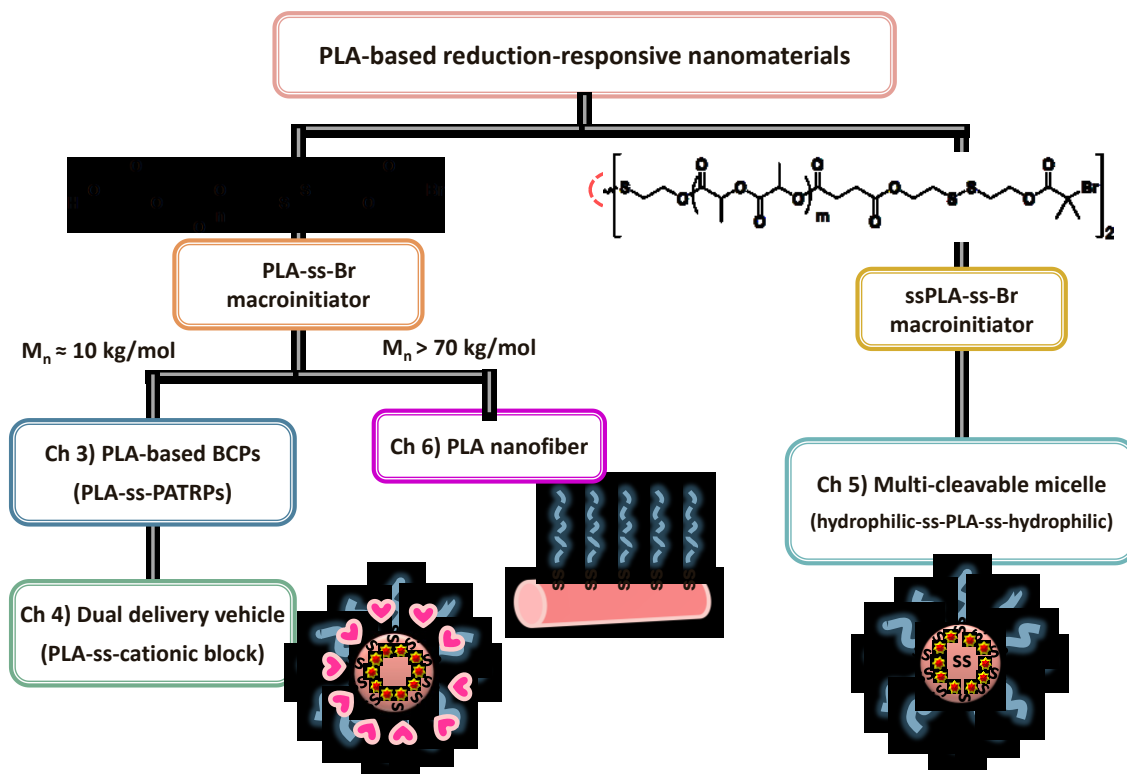
Figure 1.6. A summary of overall projects of reduction-responsive PLA-based nanomaterials in my Ph.D. research.

Chapter 2 describes the principles of synthesis and characterization of PLA-based ABPs and their nanomaterials.

Chapter 3 describes the development of various PLA-based BCPs with disulfide linkages at block junctions (PLA-ss-PATRPs). The ROP of D,L-lactide (D,L-LA) for the synthesis of novel disulfide-labeled PLAs was established in the presence of a newly synthesized double-headed initiator. The effects of the amount of tin catalyst and polymerization time were investigated on the control of ROP. Using these well-defined PLAs as a macroinitiator, a series of ATRP with various monomers, including methacrylates, acrylates, and aromatic monomers, were synthesized. These well-controlled PLA-ss-PATRPs were further characterized for the thermal properties and thiol-responsive degradation upon the cleavage of their disulfide linkages.

Chapter 4 describes the novel PLA-based polyplexes for dual delivery of drugs and genes. As a part of further works from Chapter 3, the hydrophilic block of PLA-based ABPs was

replaced with a positively charged hydrophilic polymer, resulting in cationic ABPs with a disulfide linkage at the block junctions. By aqueous self-assembly, hydrophobic cores encapsulate therapeutics, and cationic coronas interact with negatively-charged oligonucleotides through electrostatic interactions. In a reductive environment, the cleavage of disulfides at micellar interfaces enabled the enhanced release of both encapsulated drugs and oligonucleotides. In collaboration with Dr. Wilds' group at Concordia University, this project offers effective nanocarriers for dual chemotherapy and gene therapy.

Chapter 5 describes reduction-responsive multi-cleavable PLA-based micellar drug carriers. PLA-based triblock copolymers with a single disulfide in the middle of hydrophobic PLA and two disulfides at block junctions form the self-assembled micelles with disulfides positioned in both the core and the interface. The dual-located disulfide linkages were cleaved in response to GSH, resulting in a synergistically enhanced release of encapsulated anticancer drugs.

Chapter 6 describes the surface-modified PLA-nanofibers for tissue engineering applications. In collaboration with Dr. Laroche's group at Université Laval, high molecular weight PLAs with disulfide linkages and bromine functional groups can be used for the fabrication of nanofibers via air-spinning method. The hydrophobic surface of PLA-nanofibers was modified via surface-initiated ATRP with hydrophilic polymers, and the resulting surface-modified PLA fibers exhibit enhanced hydrophilicity and thermal stability. In response to a reductive environment, disulfide linkages on the surface of PLA fibers were cleaved, thus tuning the surface properties.

Finally, Chapter 7 summarizes the principal observations and conclusions with future perspectives that can be further explored.

Chapter 2

Principles of experimental methods and techniques

2.1 Polymer synthesis

2.1.1 Ring opening polymerization (ROP)

Polylactide (PLA) can be synthesized by two techniques: polycondensation of lactic acid and ROP of lactide (LA).[86] Polycondensation of lactic acid produces water as a by-product during polymerization (Scheme 2.1). Since a trace amount of water causes depolymerization of PLA via hydrolysis, the polymerization requires the removal of water by using organic solvent under extreme conditions (high temperature >180 °C, low pressure <5 mmHg).[87] Although polymerization can be accelerated by the addition of acidic catalysts such as boric or sulfuric acid, side reactions including hydrolysis can also occur due to the presence of catalysts at temperatures above 120 °C.[88]
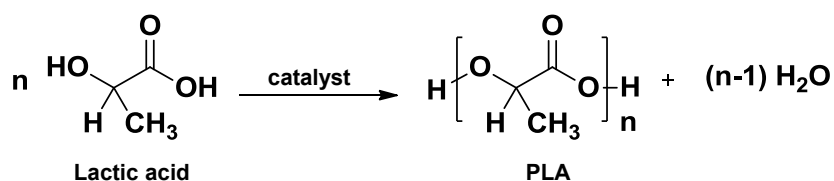
Scheme 2.1. Direct polycondensation of lactic acid.

ROP is the most common polymerization method to synthesize linear polymer chains from cyclic ester monomers such as lactones, anhydrides, and carbonates.[89] PLA with narrow molecular weight distribution is generally synthesized by ROP of LA initiated by hydroxyl- or amine-containing initiators. Scheme 2.2 shows the coordination-insertion mechanism of ROP in the presence of hydroxyl-functionalized initiator.[90] The hydroxyl initiator first forms the complex with a metal catalyst and this initiator/catalyst complex is coordinated with LA monomer, leading to the insertion of LA into the metal-oxygen bond by a rearrangement of

electrons.[86] Tin(II) 2-ethylhexanoate (Sn(Oct)$_2$) is the commonly used catalyst in the PLA synthesis due to its low toxicity, good solubility, high catalytic activity, and FDA approval as a food additive.[91] For biomedical uses, however, the residue of tin must be removed as it becomes toxic Sn(IV) by oxidation. Note that the permitted level of tin for commercial uses is 20 – 50 ppm.[92] In this thesis, Sn(Oct)$_2$ was used to synthesize well-controlled PLAs. They were then further used as macroinitiators for the synthesis of various PLA-based (amphiphilic) block copolymers and used as effective building blocks for fabrication of various nanomaterials.
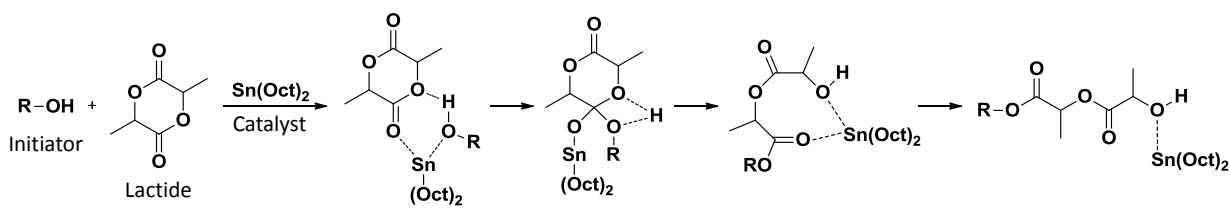
Scheme 2.2. Coordination-insertion mechanism for PLA chain growth.

Scheme 2.3 shows three stereoisomeric forms of LA monomers: D-LA, L-LA, and D,L-LA. ROP of these isomers yields three different PLAs, which exhibit different physical, thermal, and mechanical properties, as well as degradation kinetics.[93] Isotatic poly(D-LA) (PDLA) and poly(L-LA) (PLLA) synthesized from D-LA and L-LA are semi-crystalline, exhibiting high melting point (~180 °C) and glass transition temperature (55-80 °C), as well as increased mechanical strength.[94] Despite their excellent physical-mechanical properties, such semi-crystalline polymers are not suitable for biomedical applications due to high crystallinity and relatively longer degradation time.[95] On the other hand, poly(D,L-LA) (PDLLA) synthesized from D,L-LA is atactic and amorphous; thus they have relatively lower mechanical strength and shorter degradation kinetics, compared with PDLA and PLLA.[96]
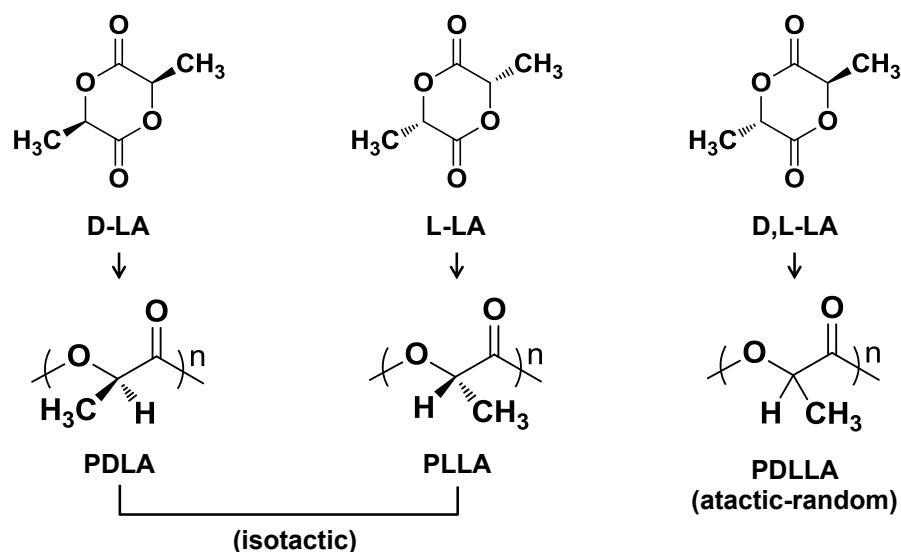
Scheme 2.3. Three different stereoisomers of LA and their corresponding PLAs.

2.1.2 Atom transfer radical polymerization (ATRP) for block copolymer synthesis

Free radical polymerization (FRP) is a conventional chain-growth polymerization that utilize reactive radical species.[97] The mechanism of FRP consists of initiation, propagation, and termination (Figure 2.1). The common radical initiators including azo and peroxide compounds are decomposed by several mechanisms to generate radicals called primary radicals.[98] These species are reactive to break carbon-carbon double bonds of monomers, allowing for the growth of polymeric chains through propagation. Because of high flux of radicals during FRP, the chains are subjected to irreversible termination or chain transfer, resulting in the formation of dead polymers with broad molecular weight distribution.[99]
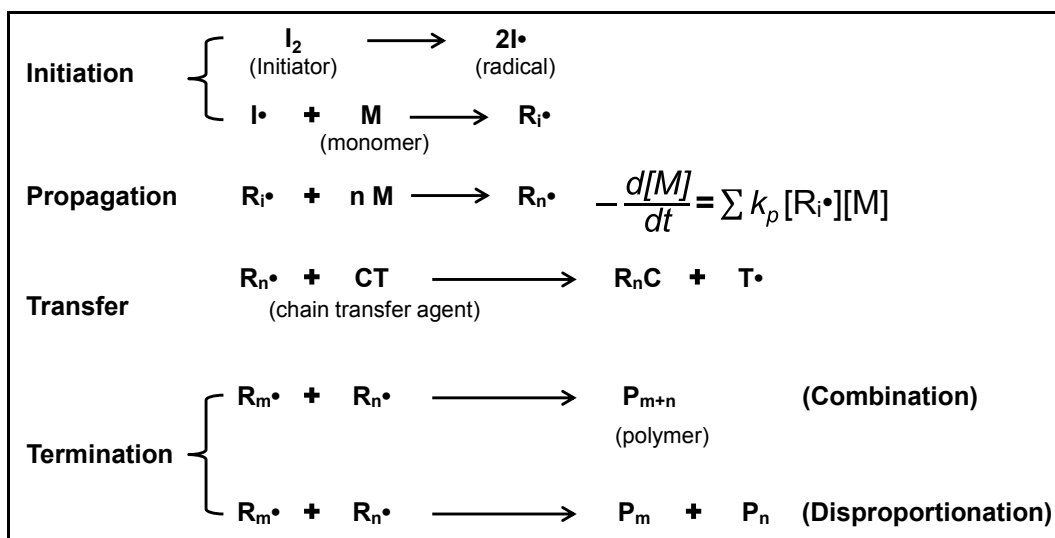
Figure 2.1. General mechanism of FRP.[100]

ATRP is one of the most successful controlled radical polymerization (CRP) techniques,[101] along with reversible addition-fragmentation chain transfer polymerization (RAFT)[102] and nitroxide-mediated polymerizations (NMP).[103] The ATRP allows the synthesis of well-controlled (co)polymers with predetermined molecular weight and narrow molecular weight distribution. This technique also allows for the synthesis of well-defined block copolymers with various architectures, such as linear, hyper branched, star, graft, and brushes.

In the mechanism as illustrated in Figure 2.2, ATRP utilizes equilibrium between dormant species and active species. The dormant species (R-X) react with a transition metal complex in a lower oxidation state (Mt^n/L) with the rate constant of activation (k_{act}). This activation process generates polymer radicals (R•) and transition metal complexes in the higher oxidation state ($X-Mt^{n+1}/L$) as deactivators. The formed radicals are involved in the propagation with the rate constant of propagation (k_p). Alternatively, they react with deactivators ($X-Mt^{n+1}/L$) to regenerate the dorman species and the activators. This deactivation process characterized with the rate constant of deactivation (k_{deact}). The equilibrium between activation and deactivation is preferred to dormant species ($k_{deact} \gg k_{act}$). In this way, the concentration of radicals can be minimized and thus the probability toward irreversible termination expressed with the rate constant of termination (k_t) can be suppressed. Consequently, such reversible deactivation allows the control of polymerization, yielding well-defined polymers with low polydispersity.[101]

Irreversible termination (k_t)

R-X + M_t^n/L $\xrightleftharpoons[k_{deact}]{k_{act}}$ R• + X-M_t^{n+1}/L

(Dormant) (Activator) (Deactivator)

+M

Propagation (k_p)

- R-X: Alkyl halide initiator
- M_t^n/L: Metal/Ligand complex
- M: monomer
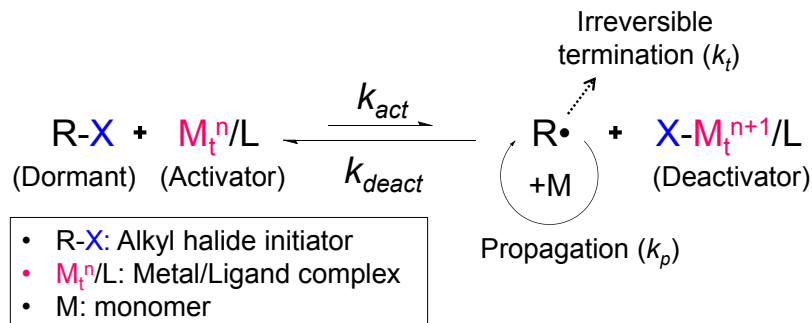
Figure 2.2. ATRP mechanism.[104]

2.2 Polymer characterization

2.2.1 Gel Permeation Chromatography (GPC)

Determination of molecular weight and molecular weight distribution of polymers is important to characterize the features of polymers, which significantly affect their properties such as viscosity, mechanical strength, and toughness.[105] Molecular weight is defined as weight-average molecular weight (M_w) and the number-average molecular weight (M_n). M_w is determined by the weight fraction of polymer samples. As seen in Figure 2.3a, the mass of the polymer is the probability factor in the calculation so that M_w is correlated to polymer properties that depends on polymer chain length such as melting viscosity.[106] M_n is determined by the number fraction of polymer chains. As shown in Figure 2.3b, M_n is calculated by dividing the total polymer weight by the total number of polymer molecules. Molecular weight distribution (known as the polydispersity index, PDI) is determined by the ratio of M_w to M_n (M_w/M_n) (Figure 2.3c). The M_w/M_n is close to 1.0 for monodispersed polymers, while it becomes larger as the polymer distribution broadens.

(a)

$$M_w = \frac{\sum N_i M_i^2}{\sum N_i M_i}$$

(b)

$$M_n = \frac{\sum N_i M_i}{\sum N_i}$$

(c)

$$PDI = \frac{M_w}{M_n}$$

- N_i: the number of polymers
- M_i: the molecular weight of each polymer

Figure 2.3. Formula of M_w (a), M_n (b), and PDI (c).

GPC, a type of size exclusion chromatography (SEC), is a commonly-used separation technique that allows the determination of relative molecular weight and molecular weight distribution of polymer samples by differences in effective molecular size in solution.[107] A polymer sample dissolved in an organic solvent is injected into a solvent stream which then flows through separation columns. By entropic effect, most polymer chains are folded to form random coils in the solution called hydrodynamic volumes, which are correlated with their chain lengths. In general, shorter chain polymer has smaller hydrodynamic volume and longer chain polymer has larger hydrodynamic volume and this relationship is used as a basis of sample separation in GPC. GPC columns are packed with highly cross-linked polymeric beads with various sizes of pores. For example, cross-linked poly(styrene-co-divinyl benzene) beads have pore sizes ranging between 5-10^5 nm. As illustrated in Figure 2.4, small molecular weight polymers pass through most of the pores in the beads and have relatively longer flow-path through column, thus they elute later. In contrast, larger molecular weight polymers are excluded from all the bead pores and have shorter flow-path, thus they elute earlier. The retention time of each polymer sample is analyzed using a calibration curve of typical calibration standards having pre-determined molecular weight such as poly(methyl methacrylate) (PMMA) and polystyrene (PSt).
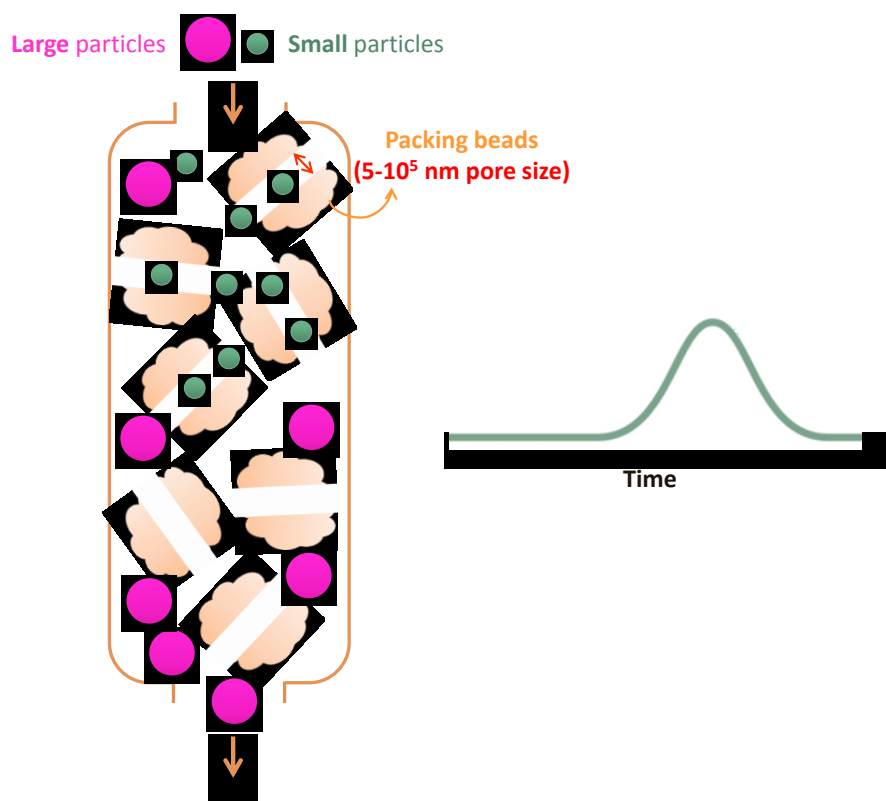
Figure 2.4. Illustration of principles of size exclusion chromatography for the separation of polymers through the GPC column.

2.2.2 Differential scanning calorimetry (DSC)

DSC is one of the techniques used to measure thermal transitions of polymers, such as heats of fusion, melting points, glass transitions, and specific heat capacities.[108] When polymer samples are heated or cooled under a given constant pressure, the heat flow (the flow of energy into or out of the sample) occurs. Typically, the dried sample is hermetically sealed into a small aluminum pan and loaded at the top of the temperature sensor of DSC with a reference (an empty aluminum pan). As the temperature of both pans is increased, the energy absorbed or released by the sample is recorded and compared with the signal from the corresponding reference. When the sample reaches to a phase transition point as temperature increases, the additional energy from the heater is delivered to the temperature sensor beneath the sample pan. When the transition is completed, the sample absorbs the additional heat again so that no energy is supplied to the sensor. On the other hand, the reference is empty so the recorded temperature keeps increasing

constantly as the heat is supplied. Based on this mechanism, the thermal behavior of the sample is monitored by comparing these two signals. The integral under this signal gives the total enthalpy change (ΔH) and the calculation   n of sample heat capacity is shown in Figure 2.5.[109] The unit of the heat flow is mW = mJ/s, which means the flow of energy in unit time.[110]

$$\Delta H = \int \left(\frac{dH}{dT} \right)$$

$$\Delta C_p = \Delta \left(\frac{dH}{dT} \right) = \Delta \frac{dH}{dt} \frac{dt}{dT}$$

$$\Delta C_p = C_p \text{ (sample)} - C_p \text{(reference)}$$

- ΔH : total enthalpy change
- ΔC_p : heat capacity change

Figure 2.5. Calculation of the heat flow over time of DSC.[110]

2.2.3 Thermal Gravimetric Analysis (TGA)

TGA scans the mass change (gain or loss) of a sample as a function of temperature or as time in the isothermal condition. When high temperature is applied, polymers become softer and melt which they are then degraded in three ways: side-group elimination, random chain scission, or depolymerisation. The side-group elimination takes place in two steps. First, the side groups attached to a polymer backbone are eliminated to produce an unstable polyene. Due to its weaker bond, the side groups are then removed from the main chain under high temperature before the backbone is broken into smaller pieces. For example, HCl can be eliminated from the polyvinyl chloride (PVC) under 100 °C. Random scission produces radicals, which attack polymer chains randomly to break down to smaller species than monomers. Such reactive species also can attack other polymer chains leading to cross-linked polymers or termination. Depolymerisation is a free radical mechanism that the end of polymer chain initiates and the polymer loses monomer units one by one. Typically, this mechanism is common for polymethacrylate and polystyrene. TGA is generally used to determine the thermal/oxidative stabilities, decomposition kinetics, and estimation of life times of polymer samples.[111] TGA also enables the characterization of the compositional analysis of multi-component polymer blends.[112] When TGA heats the sample and then holds it under isothermal conditions, the instrument detects a significant weight loss. If the sample polymer contains different segments having specific thermal stabilities, it is available to

22

quantitatively analyze the certain copolymers. Indeed, thermogravimetric curves are varied depending on monomer compositions of copolymers. In this thesis, TGA was used to identify polymer components using such unique decomposition patterns of monomers.

2.3 Characterization of amphiphilic micelles

2.3.1 Critical micellar concentration (CMC)

CMC is the concentration of polymers when micelles start to form. In general, the aqueous micellization of small surfactant molecules and well-defined ABPs obeys the closed association model for micellization.[113] The close association model is based on a dynamic equilibrium between the monomers and the molecules associated in an aggregate. Below CMC, polymers exists as single chains in aqueous solution, while at the CMC, physical properties of solution such as solubilisation, turbidity, surface tension, and electrical conductivity significantly changes.[114] CMC can be determined by fluorescence spectroscopy using Nile Red (NR) fluorescence dye. NR is highly fluorescent in hydrophobic environments (such as organic solvents and micellar cores) and nonfluorescent in aqueous solution.[115] NR generally absorbs(excites) at 485 nm and emits at 525 nm; however, its fluorescence can vary depending on the solvent used.[116] Due to high sensitivity, NR undergoes a large solvatochromic shift (change color of a chemical substance by a change of solvent polarity) in the fluorescence spectra, and therefore it can be used as a polarity probe for the CMC determination of PLA-ABPs. NR is entrapped in the hydrophobic PLA core via self-assembly and upon the cleavage of disulfides in the micelles, NR are released from the micelles, leading to the quenching of fluorescence.[117] Thus, NR serves as an excellent fluorescent hydrophobic probe.

2.3.2 Dynamic light scattering (DLS)

The size of self-assembled micellar aggregates can be determined by DLS. In aqueous solution, the micelles undergo Brownian motion, the random motion of particles driven by collision with water molecules. Through the Brownian motion, the translational diffusion coefficient (D) is proportional to the particle size, solution viscosity, and temperature. When the laser is applied on the micelles, light is scattered from the particle and DLS measures the light intensity fluctuations. Under the same condition of temperature and viscosity, the small particle

moves faster than the large particles, resulting in rapid fluctuation. The hydrodynamic diameter (*d(H)*) of the particles is calculated from the translational diffusion coefficient by using the Stokes-Einstein equation;

$$d(H) = \frac{kT}{3\pi\eta D}$$

- *d(H)* : hydrodynamic diameter
- *D*: translational diffusion coefficient
- *k*: Boltzmann's constant
- *T*: absolute temperature
- *η*: viscosity

2.3.3 Transmission electron microscopy (TEM)

TEM is a common technique capable of imaging dried particle morphology at a high resolution. When electrons are emitted by a source with high energy levels and focused on a specimen, they can interact with the specimen as it passes through.[118] Since a TEM image is obtained from the electrons that have transmitted the specimen, a thin specimen is required (the thickness of sample <100nm).[119] In this thesis, carbon-coated copper grids having 400 mesh were used as TEM substrates. For sample preparation, micellar dispersions were dropped onto the grids and air-dried at room temperature. Due to the hydrophobic surface of the copper grids, hydrophilic coronas of micelles may shrink upon drying on the grids,[120] and therefore, the average diameter of hydrophobic micellar cores can be analyzed.

2.3.4 *In vitro* cell toxicity using MTT assay

MTT (3-(4,5-dimethythiazol-2-yl)-2,5-diphenyl tetrazolium bromide) assay is commonly used to determine cytotoxicity of polymeric nanomaterials due to its simple process, safety, and high reproducibility. Yellow MTT is reduced to a purple formazan by mitochondrial succinate dehydrogenase in the living cells (Figure 2.6). Consequently, the cell viability can be determined by quantification of formazan in the cells. Formazan is insoluble in water and forms purple solution in an organic solvent (eg. dimethyl sulfoxide). The number of living cells can be directly

quantified by measuring intensity of this colored formazan solution at a certain wavelength (usually between 500 and 600 nm).[121]
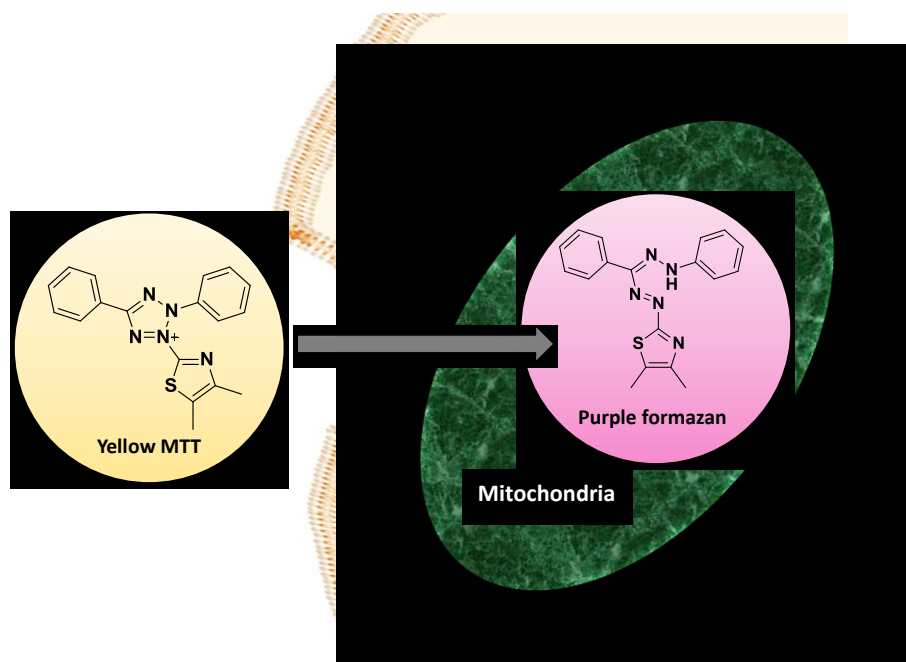
Figure 2.6. MTT mechanism by mitochondrial reduction.

Chapter 3

Synthesis and thiol-responsive degradation of polylactide-based block copolymers having disulfide junctions using ATRP and ROP
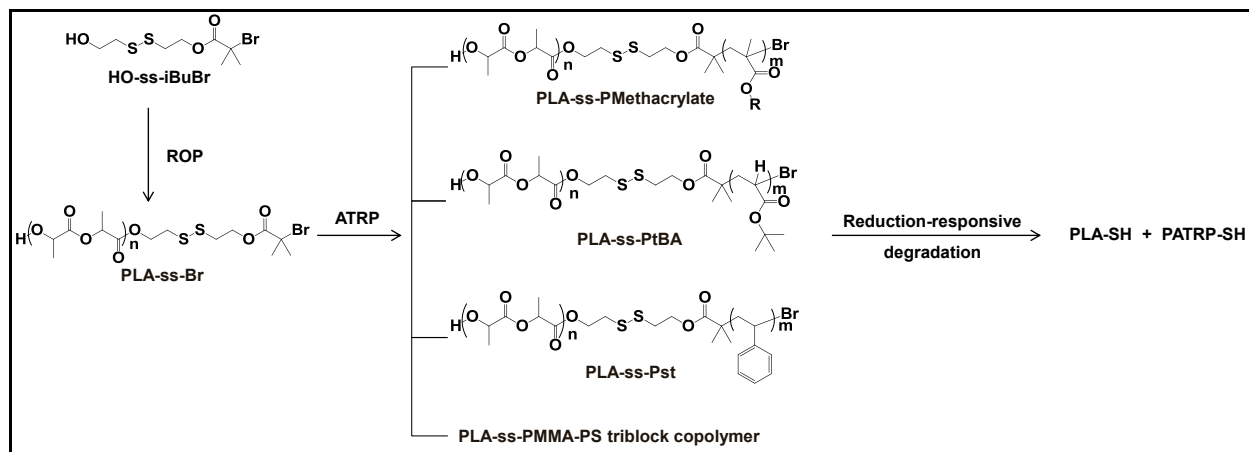
A new method to synthesize a variety of well-controlled polylactide (PLA)-based block copolymers having disulfide linkages at block junctions (PLA-ss-PATRPs) was investigated. The method employs a combination of ring opening polymerization (ROP) and atom transfer radical polymerization (ATRP) that initiates the synthesis of a new disulfide-labeled double-head initiator having both terminal OH and Br groups (HO-ss-iBuBr). The amount of tin catalyst and polymerization time significantly influenced the control of ROP initiated with HO-ss-iBuBr. A series of ATRP of various methacrylates as well as acrylate and styrene in the presence of the resulting PLA-ss-Br macroinitiators proceeded in a living manner. These well-controlled PLA-ss-PATRPs were further characterized for the thermal properties using differential scanning calorimetry (DSC) and thiol-responsive degradation upon the cleavage of disulfide linkages.

3.1 Introduction

In recent years, BCP micelles with stimuli-responsive properties have been extensively explored as effective building blocks in constructing smart and complex nanostructured materials for multifunctional applications.[122] In particular, degradation in response to external stimuli (named stimuli-responsive degradation, SRD) enables not only enhancing the release of encapsulated biomolecules[123] but also tuning the morphologies of self-assembled nanostructures.[124] These BCP nanomaterials are generally designed to incorporate cleavable linkages into block copolymers. They then degrade in response to external triggers such as low pH, light, or ultrasound, as well as reductive, oxidative, or enzymatic reactions, causing the nanomaterials to dissociate or disintegrate.[125]

Disulfide-thiol degradation has been utilized for the development of novel self-assembled micellar aggregates as enhanced/controlled delivery nanocarriers. This degradation platform is facilitated with the unique properties of disulfide linkages being cleaved to the corresponding thiols in response to reductive reactions either in the presence of reducing agents or thiol-disulfide exchange reaction.[126] Several approaches have been proposed to incorporate disulfide linkages into micellar nanocarrier cores as pendent side chains,[127] main chains of hydrophobic blocks,[64, 128] or *in-situ* crosslinks.[129] A recent approach involves the synthesis of sheddable BCPs having disulfide linkages at junctions of hydrophobic and hydrophilic blocks. These BCPs self-assemble in aqueous solution to form sheddable micelles with disulfides positioned at the interfaces of hydrophobic cores surrounded with hydrophilic coronas. Upon the cleavage of disulfides by reductive reactions, hydrophilic coronas are shed from hydrophobic cores, enhancing the release of encapsulated drugs and genes.[130] This approach has also been explored to develop highly-ordered nanoporous films of sheddable BCPs with photo-cleavable[131] and acid-labile linkages.[132] Several methods to prepare sheddable BCPs with disulfide junctions have been proposed, including coupling reaction of hydrophilic and hydrophobic polymers bearing terminal reactive groups[80, 133] and immobilization of initiating species on hydrophilic poly(ethylene oxide) (PEO).[134] Despite these advances, several drawbacks include the requirement for extra purification steps to remove excess homopolymers or the difficulties to introduce functional groups into the hydrophilic PEO block for further bioconjugation.

We have recently developed a new method that centers on the synthesis of a new disulfide-labeled double-head initiator having both terminal hydroxyl (-OH) and bromo (-Br) groups (HO-ss-iBuBr).[135] The initiator enables to proceed both ROP[136] and ATRP.[137] As a proof-of-concept approach, the method has utilized to synthesize sheddable micelles of biodegradable PLA-based BCPs with hydrophilic POEOMA (PLA-ss-POEOMA); POEOMA coronas were escaped from PLA cores by the cleavage of disulfide linkages at block junctions in response to thiols. Furthermore, the method has several features; they include no requirements for the removal of homopolymers and facile incorporation of functional groups through copolymerization with functional monomers during the ATRP.

In this chapter, we further investigated the applicability of the versatile method to synthesize a variety of well-controlled PLA-based BCPs having disulfide linkages at block junctions (PLA-ss-PATRPs) (Scheme 3.1). ROP of LA in the presence of HO-ss-iBuBr was systematically explored to better understand the important parameters that significantly influence the control of ROP: amount of tin catalyst and polymerization time. In the presence of well-defined PLA-ss-Br, the kinetics for ATRP of a broad range of methacrylates as well as t-butyl acrylate and styrene was examined using GPC and ^{1}H-NMR. For the well-defined PLA-ss-PATRPs, the thermal properties and thiol-responsive degradation upon the cleavage of disulfide linkages were studied.
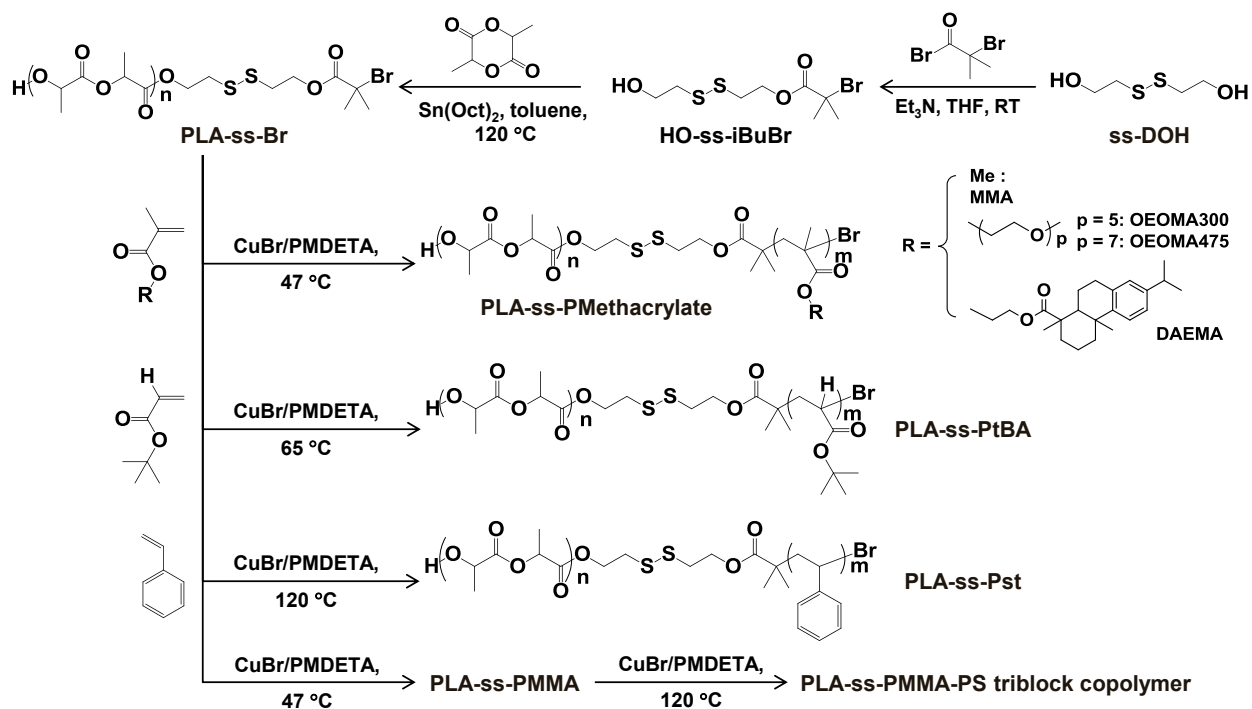
Scheme 3.1. Synthesis of PLA-ss-Br macroinitiator by ROP and a variety of well-controlled PLA-ss-PATRPs by ATRP.

3.2 Experimental section

3.2.1 Materials

2-Hydroxyethyl disulfide (ss-DOH), α-bromoisobutyryl bromide (Br-iBuBr), triethylamine (Et$_3$N), 3,6-dimethyl-1,4-dioxane-2,5-dione (DL-lactide, LA), tin(II) 2-ethylhexanoate (Sn(Oct)$_2$, 95%), copper(I) bromide (CuBr, >99.99%), and N,N,N',N'',N''-pentamethyldiethylenetriamine (PMDETA, >98%) from Aldrich and DL-dithiothreitol (DTT, 99%) from Acros Organics were purchased and used as received. Oligo(ethylene glycol) monomethyl ether methacrylate with MW = 475 g/mol and pendent EO units DP $\approx$ 7 (OEOMA475), OEOMA with MW = 300 g/mol and pendent EO units DP $\approx$ 5 (OEOMA300), methyl methacrylate (MMA), t-butyl acrylate (tBA), and styrene (St) from Aldrich were purified by passing it through a column filled with basic alumina to remove the inhibitors.

Dehydroabietic ethyl methacrylate (DAEMA) was synthesized and purified by Dr. Kejian as described in our previous paper.[138]

3.2.2 Instrumentation

^{1}H-NMR spectra were recorded using a 500 MHz Varian spectrometer. The CDCl$_3$ singlet at 7.26 ppm and DMSO-d_6 multiplet at 2.5 ppm were selected as the reference standards. Spectral features are tabulated in the following order: chemical shift (ppm); multiplicity (s - singlet, d - doublet, t - triplet, m - complex multiplet); number of protons; position of protons. Molecular weight and molecular weight distribution were determined by GPC with a Viscotek VE1122 pump and a refractive index (RI) detector. Two PolyAnalytik columns (PAS-103L and 106L, designed to determine molecular weight up to 2,000,000 g/mol) were used with THF as an eluent at 30 °C at a flow rate of 1 mL/min. Linear polystyrene (PSt) and poly(methyl methacrylate) (PMMA) standards from Fluka were used for calibration. Aliquots of polymer samples were dissolved in THF and the clear solutions were filtered using a 0.25 µm PTFE filter to remove any THF-insoluble species. A drop of anisole was added as a flow rate marker. Monomer conversion was determined using GPC for OEOMA and DAEMA as well as ^{1}H-NMR and gas chromatography (GC) for MMA, St, and tBA. GC experiments were carried on an Agilent 6890N GC equipped with a flame ionization detector and a capillary column (ValboBond VB-Wax, 30 m x 0.5 mm x 1.0 µm, Valco Instruments Ltd.). The initial temperature was 60 °C (2 min hold) and the final temperature of 180 °C (2 min hold) was reached at a heating rate of 20 °C/min. Thermal properties including T$_g$ of PLA-ss-Br and PLA-ss-PATRPs were measured with a TA Instruments DSC Q10 differential scanning calorimeter over a temperature range of -75 to 200 °C at a heating rate of 10 °C/min (cycles: heating from 25 to 200 °C (1st run), cooling to -75 °C, heating to 200 °C (2nd run), and cooling to 25 °C). The T$_g$ values were determined from the 2nd heating run.

3.2.3 Synthesis of 2-hydroxyethyl-2-(bromoisobutyryl)ethyl disulfide (HO-ss-iBuBr)

Br-iBuBr (9.84 g, 43.0 mmol) dissolved in THF (50 mL) was added drop-wise at 0 °C over 20 min to a solution consisting of ss-DOH (6.31 g, 40.9 mol), Et$_3$N (6.84 ml, 49.1 mmol), and THF (150 mL) purged with dry nitrogen for 15 min. The resulting mixture was stirred for 14 hrs at room temperature. White solids (Et$_3$N-HCl adducts) formed during the reaction were

removed by vacuum filtration. Filtrates were concentrated by a rotary evaporation and washed with aqueous acidic and basic solutions three times. The residue was extracted with ethyl acetate (50 ml) three times, and then dried with anhydrous Na_2SO_4. Solvents were removed by rotary evaporation and the product was purified by silica column chromatography with a mixture of ethyl acetate/hexane (3/7 v/v). The product was collected as the second of the total two bands off a silica gel column. The product was isolated by evaporation of solvents and further dried in a vacuum oven at room temperature for 12 hrs to form yellow oily residue. Yield = 6.05 g (49%). $R_f = 0.32$ on silica (3/7 ethyl acetate/hexane). ^{1}H-NMR ($CDCl_3$, ppm) 4.45 (t, 2H, -$\underline{CH_2}$OC(O)-), 3.9 (t, 2H, HO-$\underline{CH_2}$-), 3.0 (t, 2H, -SS-$\underline{CH_2}$-CH$_2$OC(O)-), 2.9 (t, 2H, HOCH$_2$-$\underline{CH_2}$-SS-), 1.95 (s, 6H, -C($\underline{CH_3})_2$Br). ^{13}C-NMR ($CDCl_3$, ppm) 30.4, 36.2, 41.0, 55.5, 59.9, 63.4, 171.2. Mass calculated for $C_8H_{19}BrNaO_3S_2$: 324.59382. Found: 324.95491.

3.2.4 Synthesis of PLA-ss-Br

A series of ROP of LA was conducted in the presence of HO-ss-iBuBr and $Sn(Oct)_2$ in toluene at 120 °C. The detailed procedure for PLA-2 with $[LA]_o/[HO\text{-}ss\text{-}iBuBr]_o/[Sn(Oct)_2]_o = 70/1/0.05$ is as follows; HO-ss-iBuBr (300.3 mg, 0.99 mmol), LA (10.0 g, 69.4 mmol), $Sn(Oct)_2$ (20.1 mg, 0.05 mmol), and toluene (6 mL) were added to a 25 mL Schlenk flask. The resulting mixture was deoxygenated by three freeze-pump-thaw cycles. The reaction flask was filled with nitrogen, thawed, and then immersed in an oil bath preheated to 120 °C to start the polymerization. After 3 hrs, the polymerization was stopped by cooling down to room temperature. The resulting homopolymers were precipitated from MeOH (note that LA is dissolved in MeOH). They were then isolated by vacuum filtration and further dried in a vacuum oven at room temperature overnight, resulting in white solids.

3.2.5 Synthesis of PLA-ss-PATRPs with disulfide junctions

A standard procedure for normal ATRP catalyzed with CuBr/PMDETA complex was carried out under various conditions to synthesize various PLA-ss-PATRPs. As an example, a detailed procedure for the synthesis of PLA-ss-PMMA is as follows; the dried, purified PLA-2 (1.0 g, 0.07 mmol), MMA (0.34 g, 3.4 mmol), PMDETA (7.0 µL, 0.03 mmol), and THF (0.42 mL) were added to a 10 mL Schlenk flask. The resulting mixture was deoxygenated by three freeze-pump-thaw cycles. The reaction flask was filled with nitrogen and CuBr (4.8 mg, 0.03

mmol) was then added to the frozen solution. The flask was sealed, purged with vacuum and backfilled with nitrogen once. The mixture was thawed and the flask was then immersed in an oil bath preheated to 47 °C to start the polymerization. Aliquots were withdrawn at different time intervals to analyze molecular weight by GPC and conversion by ^{1}H-NMR or GC. The polymerization was stopped by cooling and exposing the reaction mixture to air.

For the synthesis of other PLA-ss-polymethacrylates, similar conditions with CuBr/PMDETA at 47 °C were applied. For the synthesis of PLA-ss-PtBA, the purified PLA-2 (0.5 g, 0.04 mmol), tBA (0.25 g, 1.93 mmol), PMDETA (4.0 μL, 0.02 mmol), and CuBr (2.8 mg, 0.02 mmol) were used at 65 °C in THF (0.3 mL). For the synthesis of PLA-ss-PSt, the purified PLA-2 (1.0 g, 0.08 mmol), St (0.42 g, 4.03 mmol), PMDETA (8.4 μL, 0.04 mmol), and CuBr (5.8 mg, 0.04 mmol) were mixed with anisole (0.53 mL) at 120 °C.

The resulting PLA-ss-PATRPs were purified by the removal of residual copper species and unreacted monomers as follows; As-prepared green polymer solutions were passed through a column filled with basic aluminum oxide with THF as an eluent to remove copper species. The polymer solution was concentrated by rotary evaporation, and then precipitated from a large volume of hexane for most PLA-ss-PATRPs and MeOH for PLA-ss-PtBA. The precipitated polymers were filtered by vacuum filtration and residual solvent was further removed using a vacuum oven at room temperature overnight.

3.2.6 Synthesis of PLA-ss-PMMA-b-PSt triblock copolymer

Well-defined PLA-ss-PMMA-Br was prepared and purified as described above. For the consecutive ATRP of St, the dried, purified PLA-ss-PMMA-Br (0.4 g, 0.03 mmol), St (0.13 g, 1.29 mmol), PMDETA (2.7 μL, 0.013 mmol), and anisole (0.17 mL) were added to a 10 mL Schlenk flask. The resulting mixture was deoxygenated by three freeze-pump-thaw cycles. The reaction flask was filled with nitrogen and CuBr (1.8 mg, 0.013 mmol) was then added to the frozen solution. The flask was sealed, purged with vacuum and backfilled with nitrogen once. The mixture was thawed and the flask was then immersed in an oil bath preheated to 120 °C to start the polymerization. The polymerization was stopped after 3 hrs by cooling and exposing the reaction mixture to air.

3.2.7 Thiol-responsive degradation of PLA-ss-PATRPs in DMF

An aliquot of PLA-ss-PATRPs (50 mg) dissolved in DMF (10 mL) was mixed with a stock solution of DTT in DMF under magnetic stirring. The amount of DTT was defined to be 5 mole equivalents to disulfides of polymers. Aliquots of the mixtures were analyzed using GPC at given time intervals.

3.3 Results and Discussion

3.3.1 Synthesis of PLA-ss-Br

HO-ss-iBuBr, a double-head initiator labeled with a disulfide having terminal OH and Br groups, was synthesized previously by a carbodiimide coupling reaction of ss-DOH with 2-bromoisobutyric acid in the presence of dicyclohexyl carbodiimide.[135] In the experiments, a new procedure with the use of Br-iBuBr and Et_3N as a base resulted in a higher yield (49%).

In the presence of HO-ss-iBuBr, a series of ROP of LA catalyzed with $Sn(Oct)_2$ in toluene at 120 °C was carried out under various conditions. With the mole ratio of $[LA]_0/[HO\text{-ss-}iBuBr]_0 = 70/1$, several parameters including amount of $Sn(Oct)_2$ and polymerization time were varied to examine their effect on the course of ROP of LA. After purification by precipitation from MeOH, the purified PLA-ss-Br homopolymers were characterized using ^1H-NMR for degree of polymerization (DP) and by GPC calibrated with PSt standards for molecular weight and molecular weight distribution. Figure 3.1 shows an example of ^1H-NMR spectrum of PLA-ss-Br. A multiplet appeared at 5.2 ppm corresponds to methine protons in PLA and a singlet at 1.9 ppm corresponds to six methyl protons. From the integral ratio of the peaks $[(b/2)/(h/6)]$, the DP of PLA-ss-Br was determined to be 75. The results are summarized in Table 3.1.
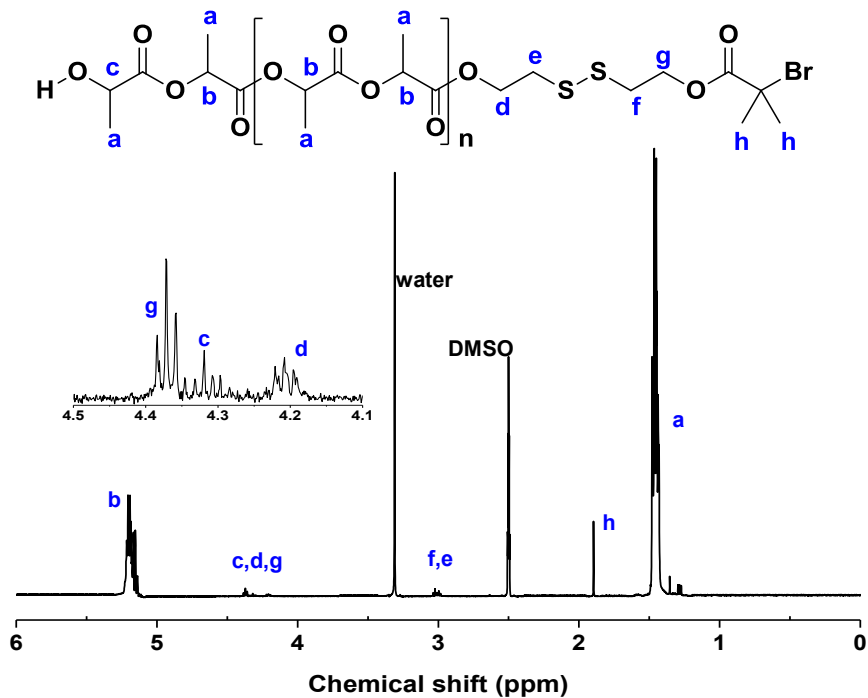
Figure 3.1. ^{1}H-NMR spectrum of PLA-ss-Br (PLA-2) in DMSO-d_6.

Table 3.1. Characteristics of a series of PLA-ss-Br homopolymers prepared by ROP of LA in toluene at 120 °C under different conditions.[a]

PLA	$[Sn(Oct)_2]_o$ /$[HO\text{-}ss\text{-}iBuBr]_o$	Time (hrs)	DP[b]	$M_{n,theo}$[b] (g/mol)	M_n[c] (g/mol)	M_w/M_n[c]	HMS[d] (%)
1	0.14	3	89	12,700	12,800	1.15	25.1
2	0.05	3	75	10,000	10,800	1.08	6.9
3	0.03	3	65	9,200	9,400	1.06	6.3
4	0.03	4	72	10,900	10,400	1.11	11.3
5	0.03	6	74	11,000	10,700	1.14	14.7

a. $[LA]_0/[HO\text{-}ss\text{-}iBuBr]_0 = 70/1$; LA/toluene = 1.9/1 wt/wt.

b. Determined by ^{1}H-NMR.

c. Determined by GPC calibrated with PSt standards.

d. Calculated by peak analysis using deconvolution method of GPC traces.

First, the amount of $Sn(Oct)_2$ defined as the mole ratio of $[Sn(Oct)_2]_0/[HO\text{-ss-iBuBr}]_0$ was varied. With a larger amount of $Sn(Oct)_2$ as the ratio of 0.14/1, PLA-1 had the DP = 89 by ^{1}H-NMR and M_n = 12,800 g/mol with M_w/M_n = 1.15 by GPC. When the $[Sn(Oct)_2]_0/[HO\text{-ss-}$ iBuBr$]_0$ decreased to 0.05 and further 0.03, the DP of PLA decreased to 75 (PLA-2) and to further 65 (PLA-3). These results are consistent with the results that the polymerization rate was enhanced with an increasing amount of $Sn(Oct)_2$ up to $[Sn(Oct)_2]_0/[initiator]_0 < 1$.[139] However, the GPC trace of PLA-1 exhibits bimodal distribution with a high molecular weight shoulder (HMS) (Figure 3.2a). From the peak analysis using deconvolution method, the high molecular weight species was estimated to be 25%. When the $[Sn(Oct)_2]_0/[HO\text{-ss-iBuBr}]_0$ decreased to 0.05, high molecular weight species significantly reduced to <7%. Next, the polymerization time increased from 3 to 6 hrs. The DP determined by ^{1}H-NMR increased from 65 to 74 (PLA-5) as well as the high molecular weight species increased from 6.3 to 14.7% (Figure 3.2b). The occurrence of the HMS is possibly attributed to unexpected side reactions. Overall, the ROP of LA under the conditions proceeded in a living character, yielding PLA-ss-Br polymers having narrow molecular weight distributions with $M_w/M_n < 1.15$. For further chain extension of PLA-ss-Br using ATRP, the recipe of PLA-2 was used to synthesize PLA-ss-Br precursors.
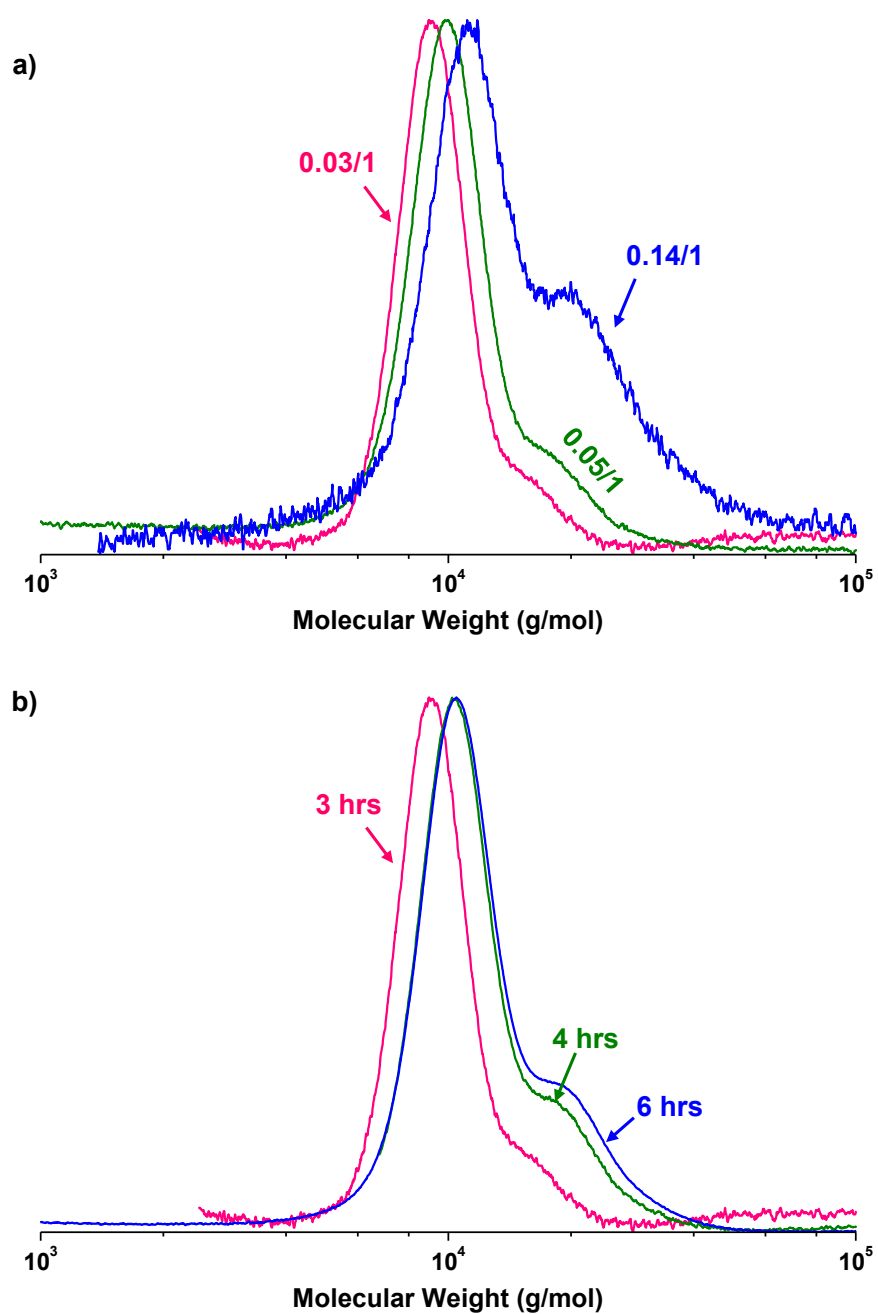
Figure 3.2. GPC traces of PLA-ss-Br prepared by ROP with various $[Sn(Oct)_2]_0/[HO\text{-}ss\text{-}iBuBr]_0$ for 3 h (a) and polymerization time with $[Sn(Oct)_2]_0/[HO\text{-}ss\text{-}iBuBr]_0 = 0.03/1$ (b).

3.3.2 Synthesis of various PLA-ss-PATRPs with disulfide junctions

A series of PLA-based BCPs with varying (co)polymers were synthesized by a normal ATRP catalyzed with CuBr/ligand complex in the presence of PLA-ss-Br macroinitiator (PLA-2, Table 3.1) in organic solvents. The monomers used here include various methacrylates including OEOMA300, OEOMA475, MMA, and a rosin-derived DAEMA, as well as tBA and St. The results are summarized in Table 3.2.

Table 3.2. Characteristics of a series of PLA-ss-PATRPs prepared by ATRP in the presence of PLA-ss-Br.[a]

PLA-ss-PATRPs	Solvent	Temp (°C)	Time (hrs)	Conv[a]	$M_{n,theo}$[b] (g/mol)	M_n[c] (g/mol)	M_w/M_n[c]
PLA-ss-POEOMA475	THF	47	1.5	0.92	32,700	18,300	1.15
PLA-ss-POEOMA300	THF	47	1.5	0.91	24,400	16,400	1.28
PLA-ss-PMMA	THF	47	1.5	0.93	19,500	15,300	1.22
PLA-ss-PDAEMA	THF	47	2.0	0.67	26,300	15,300	1.21
PLA-ss-PSt	Anisole	120	2.0	0.66	15,900	12,700	1.22
PLA-ss-PtBA	THF	65	5.0	0.93	19,000	16,400	1.20
PLA-ss-PMMA-PSt	Anisole	120	3.0	0.55	18,300	15,400	1.23

a. Determined by GPC for OEOMA and DAEMA, ^{1}H-NMR for MMA and St, and GC for tBA.

b. Determined by ^{1}H-NMR.

c. Determined by GPC calibrated with PMMA standards, except for PLAss-PSt, PLA-ss-PtBA, and PLA-ss-PDAEMA using PSt standards.

The normal ATRP of methacrylates in the presence of CuBr/PMDETA complex was first examined in THF at 47 °C. As seen in Figure 3.3a, the ATRP of four methacrylates shows first-order kinetics, indicating a constant concentration of active centers during the polymerization. For OEOMA monomers and MMA, the polymerization rate was fast; monomer conversion reached 90% in 1.5 hrs. For the reproducible ATRP of DAEMA, however, the rate was relatively

slower; the conversion reached 67% in 2 hrs. The slow polymerization of DAEMA in the presence of even more active CuBr/Me$_6$TREN complex was described in our previous report.[138a] Compared to other methacrylates, such a slower polymerization of DAEMA is plausibly because of its bulky side chains. For all methacrylate polymerizations, molecular weight increased linearly with conversion and molecular weight distribution was as low as $M_w/M_n < 1.25$ (Figure 3.3b). Figure 3.4 shows the typical NMR signals at 3.3 ppm (singlet) corresponding to pendent methoxy protons for PLA-ss-POEOMAs, at 3.5 ppm (singlet) corresponding to methoxy protons for PLA-ss-PMMA, and at 6.7-7.1 ppm corresponding to aromatic protons for PLA-ss-PDAEMA. The GPC and ^{1}H-NMR results suggest that the normal ATRP of methacrylates in the presence of PLA-ss-Br proceeded in a living fashion, yielding well-controlled PLA-ss-polymethacrylates with $M_w/M_n < 1.25$ up to 90% conversion.
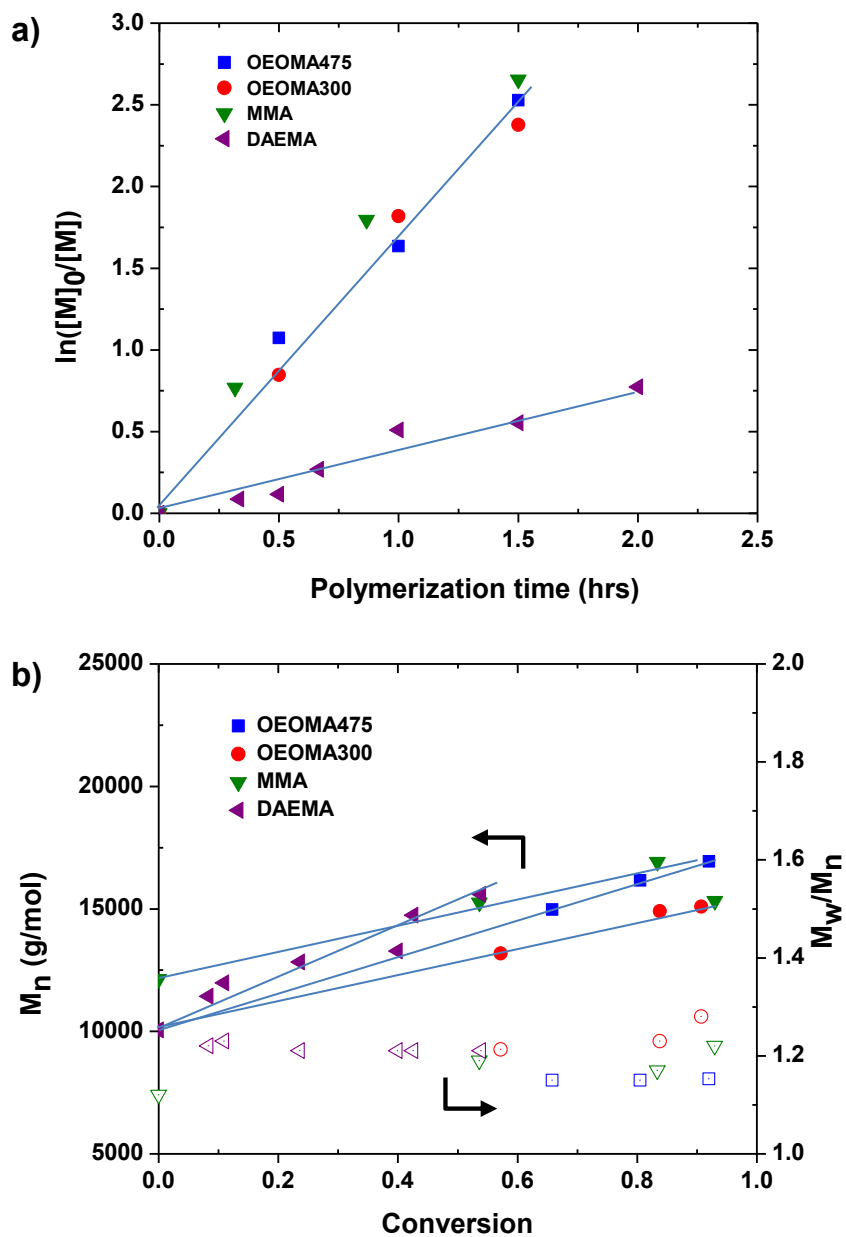
Figure 3.3 For ATRP of methacrylates including OEOMA300, OEOMA475, MMA, and DAEMA in the presence of PLA-ss-Br in THF at 47 °C, first-order kinetic plots over time (a) and evolution of molecular weight and molecular weight distribution over conversion (b). Conditions: [methacrylate]$_0$/[PLA-ss-Br]$_0$/[CuBr/PMDETA]$_0$ = 50/1/0.5; methacrylate/THF = 1.5/1 wt/wt. The solid lines in (a) and (b) are linear fits.
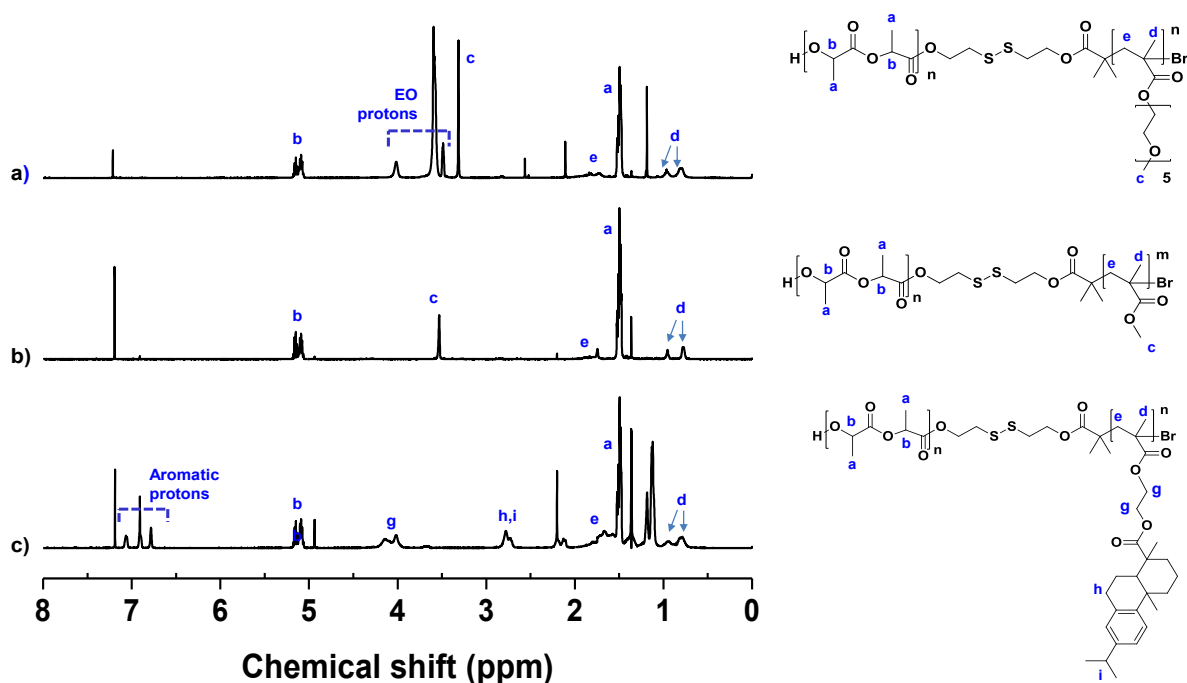
Figure 3.4. ^{1}H-NMR spectra of PLA-ss-polymethacrylates including POEOMA300 (a), PMMA (b), and PDAEMA (c) in CDCl$_3$.

ATRP of St in the presence of PLA-ss-Br and CuBr/PMDETA complex was carried out in anisole at 120 °C. High temperature was required, because the polymerization of St is generally slow than that of methacrylates. As seen in Figure 3.5a, monomer conversion increased with time, reaching >60% in 2 hrs. The polymerization proceeded in a living character; first-order kinetics, linear increase in molecular weight over conversion, and narrow molecular weight distribution as low as M_w/M_n < 1.25 (Figure 3.5b). However, molecular weights determined by GPC calibrated with PSt standards were much smaller than theoretically estimated ones; the difference is presumably attributed to the different hydrodynamic volume of PLA-ss-PSt BCPs from PSt homopolymers. ^{1}H-NMR spectrum shows peaks at 6.3 – 7.2 ppm corresponding to aromatic protons in phenyl rings of PSt blocks, confirming the successful synthesis of well-controlled PLA-ss-PSt by chain extension of PLA-ss-Br with PSt by the ATRP (Figure 3.6).
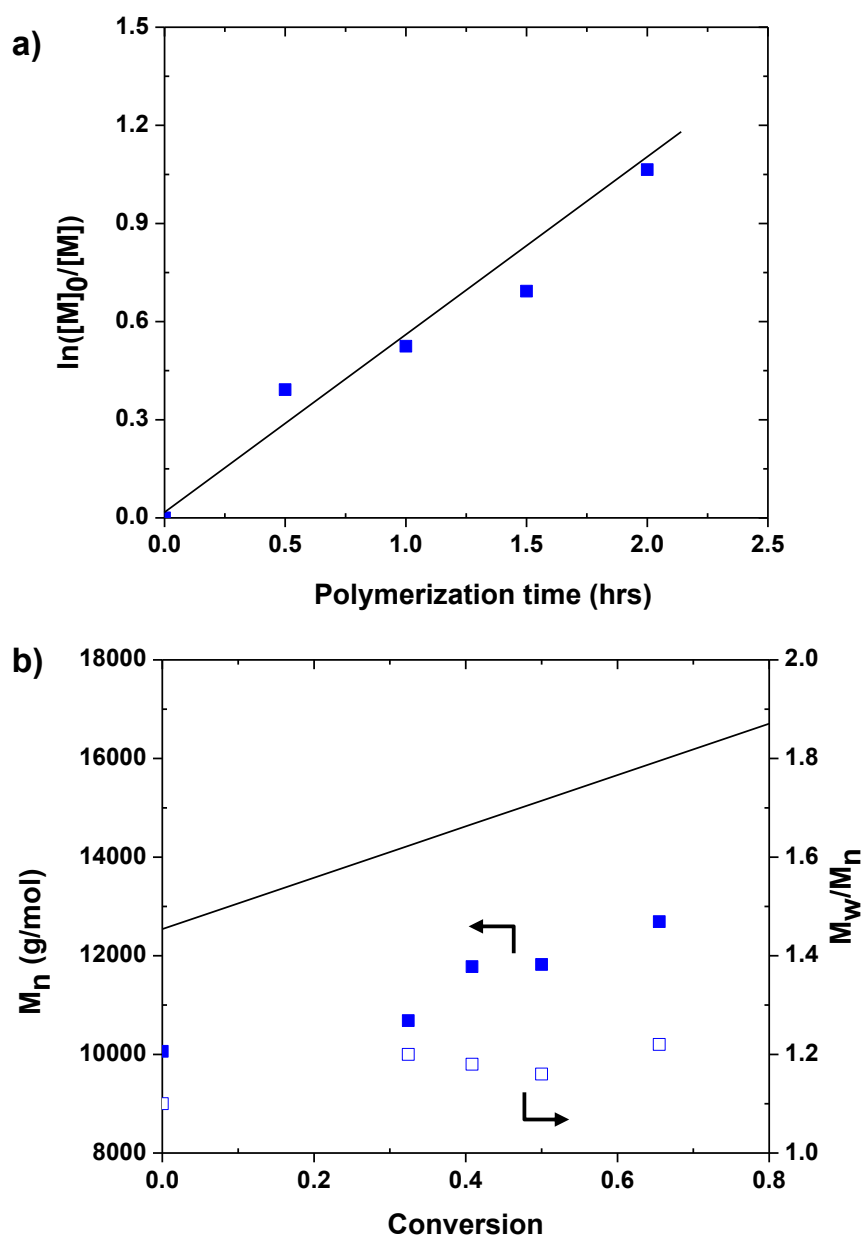
Figure 3.5. First-order kinetic plot (a) and evolution of molecular weight and molecular weight distribution with conversion (b) for ATRP of St in the presence of PLA-ss-Br in anisole at 120 °C. Conditions: $[St]_0/[PLA-ss-Br]_0/[CuBr/PMDETA]_0 = 50/1/0.5$; St/anisole = 0.8/1 wt/wt. The solid line is a linear fit in a) and the theoretically predicted molecular weight over conversion in (b).
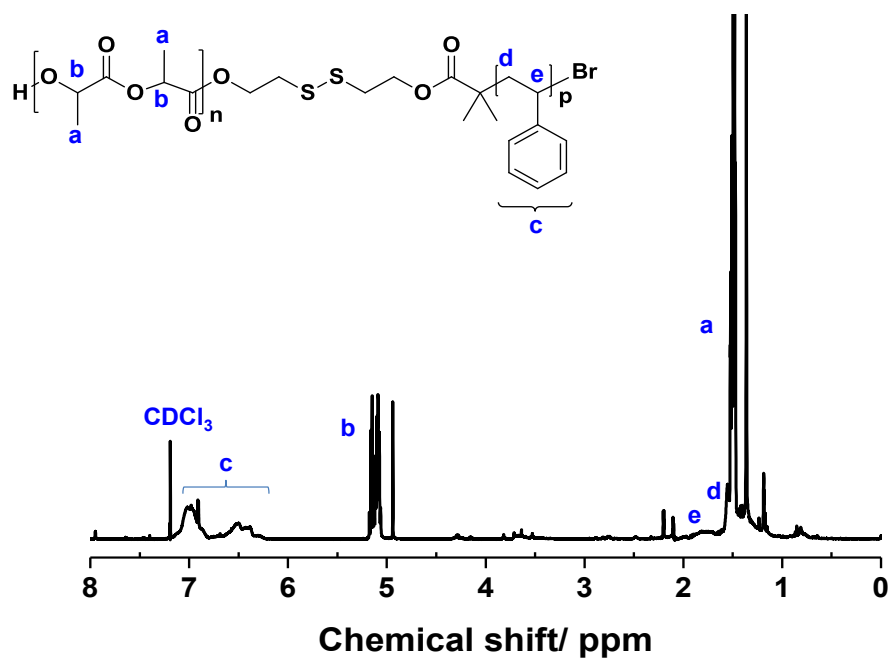
Figure 3.6. ^{1}H-NMR spectrum of PLA-ss-PSt in CDCl$_3$.

ATRP of tBA in the presence of PLA-ss-Br and CuBr/PMDETA complex was carried out in THF at 65 °C. Using GC, monomer conversion was determined to be 93% after 5 hrs. The evolution of GPC trace to high molecular weight region, with M_n = 16,400 g/mol and M_w/M_n = 1.20 (Figure 3.7) and ^{1}H-NMR results (Figure 3.8) suggest the successful synthesis of well-controlled PLA-ss-PtBA.

Figure 3.7. GPC traces of PLA-ss-PtBA, compared with PLA-ss-Br precursor.

Figure 3.8. ^{1}H-NMR spectrum of PLA-ss-PtBA in CDCl$_3$.

With the success in ATRP of MMA and St, a consecutive ATRP of MMA and St was conducted to synthesize a triblock copolymer of PLA-ss-PMMA-b-PSt. In the presence of PLA-ss-Br with M_n = 9,600 g/mol and M_w/M_n = 1.22, ATRP of MMA was carried out at 47 °C in THF for 25min. After purification, ATRP of St was carried out in the presence of PLA-ss-PMMA-Br as a macroinitiator at 120 °C in anisole for 3 hrs. The GPC and GC results indicate the evolution of GPC trace to high molecular weight region, with M_n = 11,800 g/mol and M_w/M_n = 1.2 at conversion = 0.60 for PLA-ss-PMMA-Br and M_n = 15,400 g/mol and M_w/M_n = 1.23 at conversion = 0.55 for PLA-ss-PMMA-b-PSt (Figure 3.9). ^{1}H-NMR spectrum shows a typical peak at 3.6 ppm corresponding to methoxy protons in PMMA block and peaks at 6.3 – 7.2 ppm corresponding to aromatic protons of PSt blocks, suggesting the successful synthesis of well-controlled PLA-ss-PMMA-b-PSt triblock copolymer (Figure 3.10).
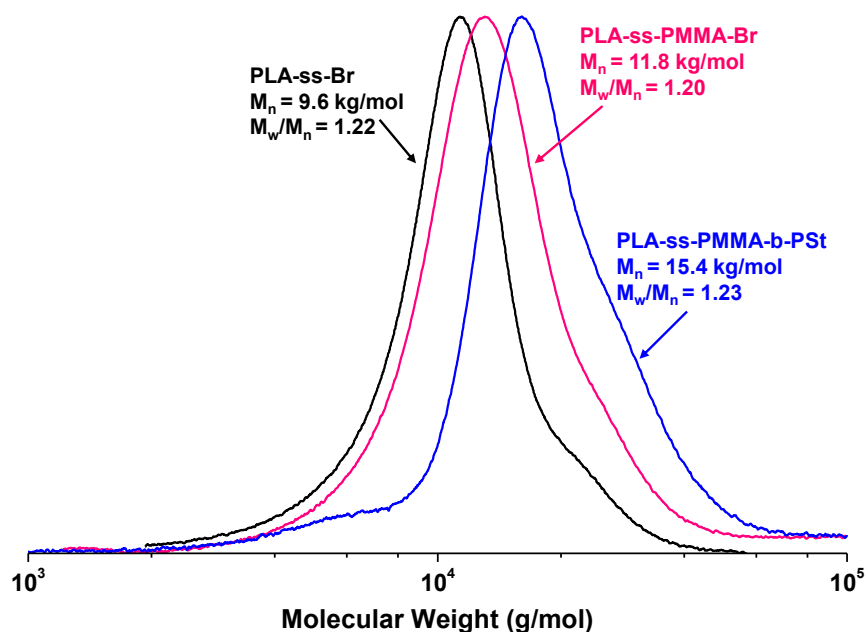
Figure 3.9. GPC traces of PLA-ss-Br, PLA-ss-PMMA-Br, and PLA-ss-PMMA-b-PSt.
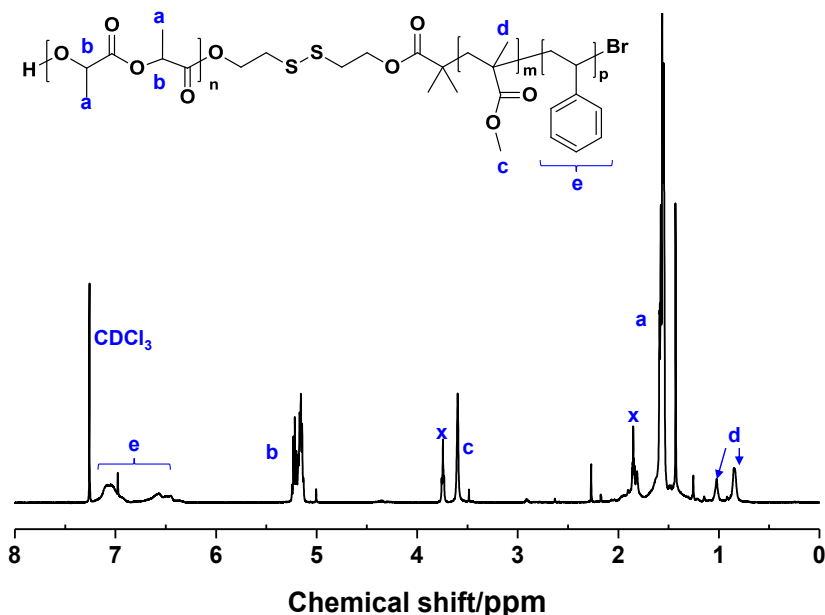
Figure 3.10. ¹H-NMR spectrum of PLA-ss-PMMA-b-PSt in CDCl₃. x denotes a trace of THF.

3.3.3 Thermal analysis of PLA-ss-PATRPs using DSC

DSC was used to characterize thermal properties and glass transition temperature (T_g) of selected PLA-ss-PATRPs. Figure 3.11 shows the DSC diagrams of PLA-ss-Br, PLA-ss-PMMA, PLA-ss-PSt, and PLA-ss-PDAEMA. PLA-ss-Br homopolymer had a strong glass transition at T_g = 38.8 °C with no melting transition, suggesting that PLA-ss-Br is amorphous. PLA-ss-PMMA BCP exhibits only one T_g which appeared at 53.7 °C, suggesting that the amorphous PLA block is miscible with the PMMA block. This result is consistent with that reported for miscible blends of amorphous PLA with PMMA homopolymers.[140] PLA-ss-PSt block copolymer also exhibits only one glass transition at T_g = 46.5 °C. However, several reports describe immiscible homopolymer blends of amorphous PLA and PSt that exhibit two glass transitions in the DSC diagrams. In addition, the transition of PSt is relatively weak compared with that of PLA; thus, only one glass transition corresponding to PLA is detected for immiscible blends of PLA/PSt containing less than 25 wt % of PSt.[141] In our experiment, PLA-ss-PSt BCP contains <22 wt % of PSt block, suggesting that PLA block is not miscible with PSt block, although PLA-ss-PSt has only one glass transition. For PLA-ss-PDAEMA, two T_g values appeared at 48.6 and 86.7 °C.

The T_g = 48.6 °C corresponding to PLA block is higher than PLA-ss-Br (38.9 °C) and the T_g = 86.7 °C to PDAEMA block is lower than reported value (>90 °C)[138a] of PDAEMA homopolymer.
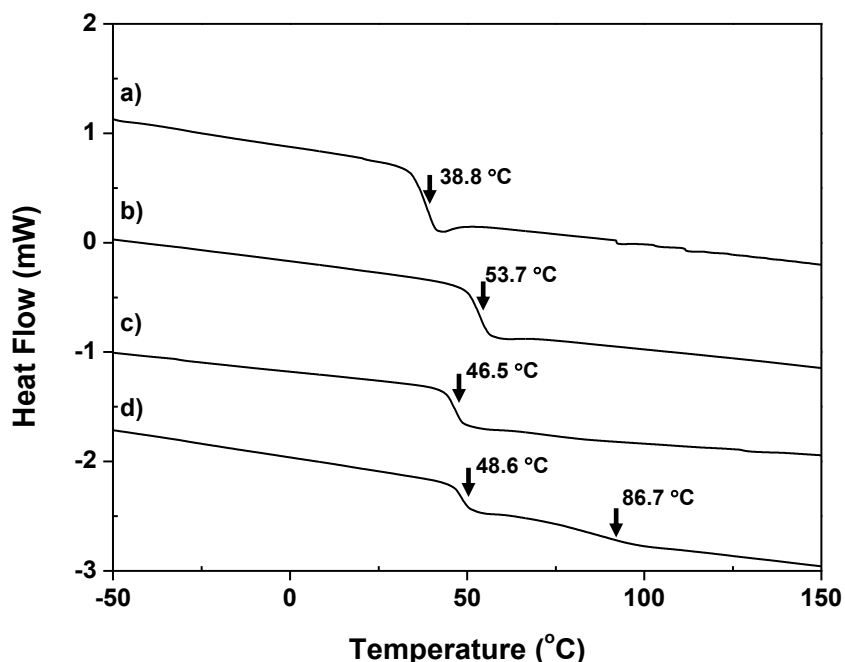
Figure 3.11. DSC diagrams of PLA-ss-Br (a), PLA-ss-PMMA (b), PLA-ss-PSt (c), and PLA-ss-PDAEMA (d).

3.3.4 Reductive degradation of PLA-ss-PATRPs

The resulting PLA-ss-PATRPs contain disulfide linkages at block junctions that can be cleaved in response to thiols through thiol-disulfide exchange reaction (Scheme 3.2). In the experiments, GPC was used to follow the degradation of PLA-ss-PATRPs in the presence of DTT in DMF at room temperature. PLA-ss-PMMA was first examined with different amounts of DTT, which is defined as the mole equivalent ratio of DTT/disulfide = 5/1. As seen in Figure 3.12a, molecular weight decreased from M_n = 15,100 to 11,200 g/mol in the presence of 1 mole equivalent DTT and further decreased to 9,100 g/mol with 5 mole equivalent DTT. This result suggests that the cleavage of disulfide linkages is enhanced with an increasing amount of

reducing agents.[142] Similar result was observed for PLA-ss-PDAEMA whose molecular weight decreased from M_n = 16,300 g/mol to 9,400 g/mol in the presence of 5 mole equivalent DTT (Figure 3.12b).
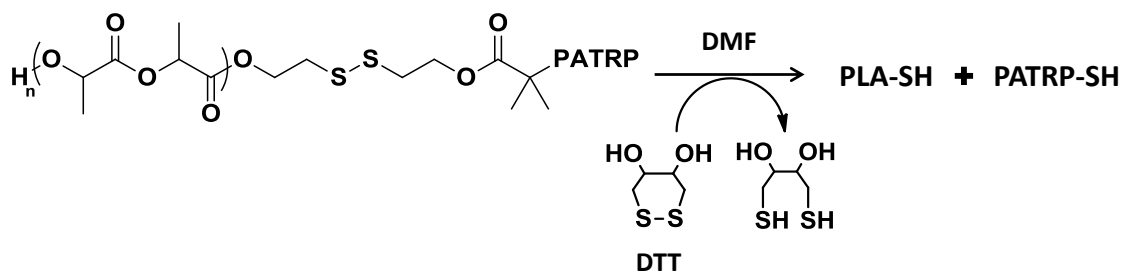
Scheme 3.2. Thiol-responsive cleavage of disulfide linkages at block junction in the presence of DTT.
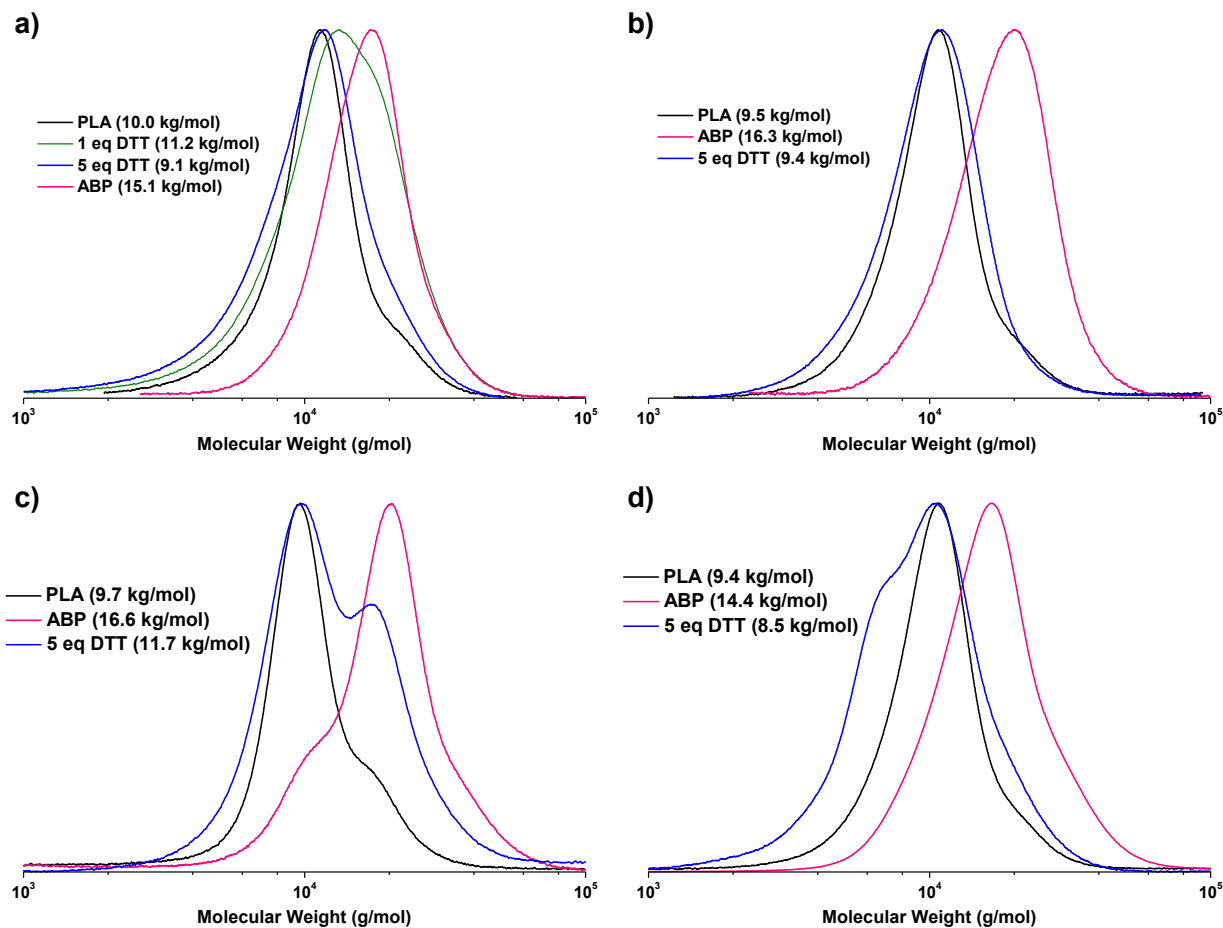
Figure 3.12. Overlaid GPC traces before and 15 hrs after being mixed with DTT for PLA-ss-PMMA (a), PLA-ss-PDAEMA (b), PLA-ss-POEOMA300 (c), and PLA-ss-PSt (d) in DMF. Note that molecular weights of BCPs used for degradation experiments were determined after purification.

An interesting result is observed when PLA-ss-POEOMA300 was mixed with 5 mole equivalent DTT. As seen in Figure 3.12c, the GPC trace was shifted to lower molecular weight region and the molecular weight decreased from M_n = 16,600 g/mol to 11,700 g/mol. Different from the above two BPCs, the GPC trace of the degraded polymers shows bimodal distribution. Peak analysis using a deconvolution method suggests 42% low molecular weight species presumably corresponding to the cleaved PLA block and 58% high molecular weight species corresponding to the cleaved POEOMA300 block (Figure 3.13a). This analysis is consistent with the theoretically calculated $M_{n,theo}$ = 10,800 g/mol for PLA block and 8,700 g/mol for POEOMA300 block (DP = 29), suggesting 55 wt% PLA block in PLA-ss-POEOMA300 at

conversion = 0.55. However, the GPC peak for the cleaved POEOMA300 is positioned in higher molecular weight region than that for the cleaved PLA block. This is presumably due to the larger hydrodynamic volume of POEOMA300 than PLA in THF. For PLA-ss-PSt with M_n = 14,400 g/mol in the presence of DTT, the GPC trace of degraded products is also bimodal (Figure 3.12d). The low molecular weight species could be attributed to the presence of cleaved PSt. Based on estimated $M_{n,theo}$ = 4,000 g/mol for PSt block (DP = 39) and 12,400 g/mol for PLA block, PSt block can be estimated to be 24 wt% (Figure 3.13b).
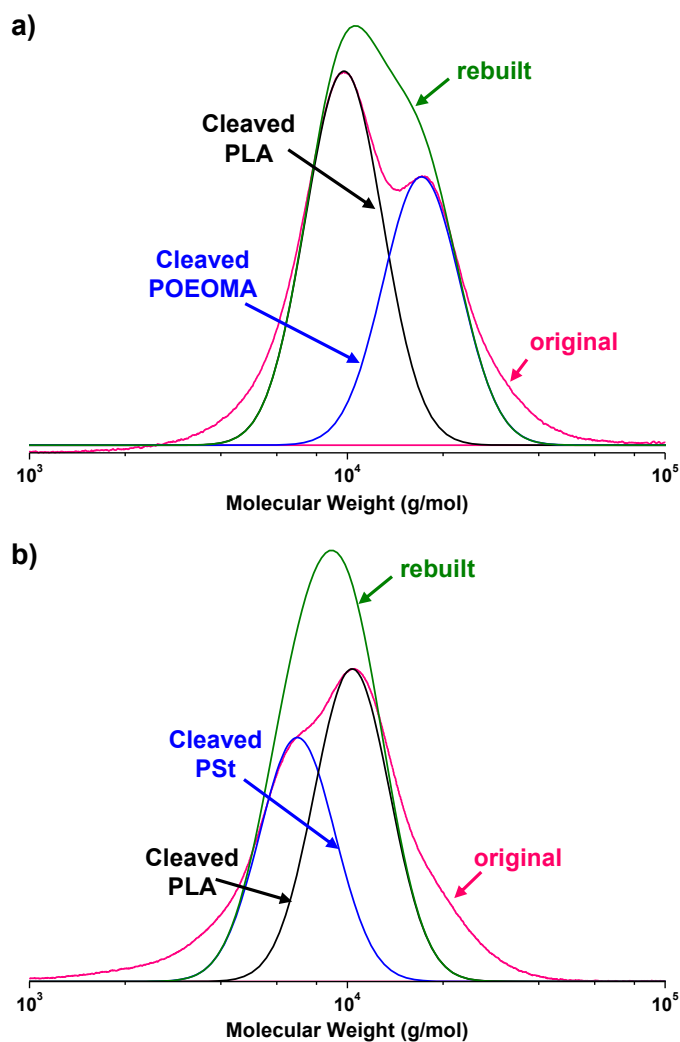
Figure 3.13. Peak analysis by deconvolution method for GPC trace of PLA-ss-POEOAM300 (a) and PLA-ss-PSt (b).

49

3.4 Conclusion

A new method employing a combined ROP and ATRP was further examined to synthesize various PLA-ss-PATRPs having disulfides at block junctions. ROP of LA was well-controlled with narrow molecular weight distribution of PLA-ss-Br ($M_w/M_n < 1.15$). With an increasing amount of Sn(Oct)$_2$ and polymerization time, the amount of high molecular weight species yielded by side coupling reactions increased. ATRP of methacrylates, tBA, and St proceeded in a living manner with first-order kinetics, linear increase in molecular weight over conversion, and low $M_w/M_n < 1.2$, yielding well-controlled PLA-ss-PATRPs, confirmed by ^{1}H-NMR and GPC. Thermal analysis results suggest that PLA block is miscible with PMMA, exhibiting one T_g, while it is phase-separated from PDAEMA. In the response to DTT, PLA-ss-PATRPs degraded to the corresponding thiols including PLA-SH and PATRP-SH upon the cleavage of disulfide junctions. It is anticipated that these significant results can be utilized for further development of multifunctional nanomaterials as micelles and as films with stimuli-responsive degradation.

Chapter 4

Reductively-sheddable cationic nanocarriers

for dual chemotherapy and gene therapy with enhanced release
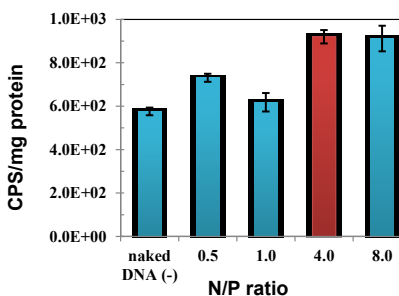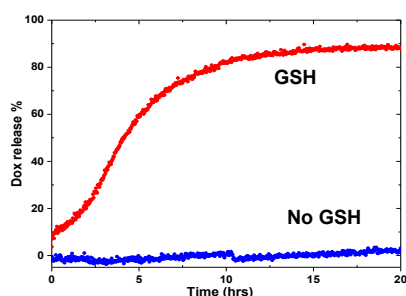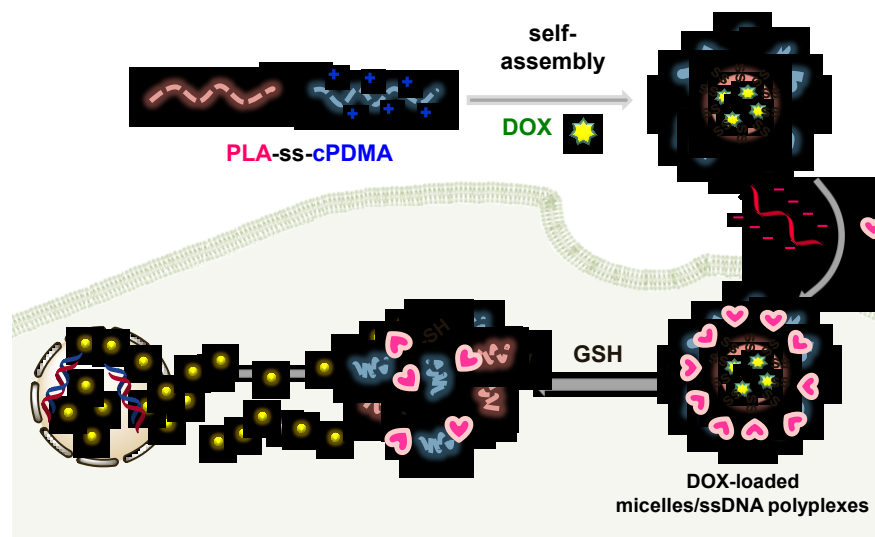
The development of a versatile strategy to synthesize cationic nanocarriers capable of co-delivery and enhanced release of drugs and oligonucleotides is promising for synergic dual chemotherapy and gene therapy. Chapter 4 reports a novel cationic amphiphilic diblock copolymer having a single reduction-responsive disulfide linkage at a junction between a FDA-approved polylactide (PLA) block and a cationic methacrylate block (C-ssABP). The amphiphilic design of the C-ssABP enables the formation of cationic micellar aggregates possessing hydrophobic PLA cores, encapsulating anticancer drugs; cationic coronas, ensuring

complementary complexation with negatively-charged oligonucleotides through electrostatic interactions; and disulfides at interfaces, leading to enhanced release of both encapsulated drugs and complexed oligonucleotides. The reduction-responsive intracellular trafficking results from flow cytometry, confocal laser scanning microscopy, and cell viability, as well as *in vitro* gene transfection assay suggest that C-ssABP offers versatility as an effective nanocarrier platform for dual chemotherapy and gene therapy.

4.1 Introduction

ABP-based self-assembled micelles have been extensively explored as effective candidates of polymer-based nanocarriers in pharmaceutical science.[143] Well-designed ABP-based micelles consist of hydrophobic cores enabling encapsulation of hydrophobic therapeutics to deliver targeted sites. PLA and its copolymers have been considered as effective building blocks in constructing hydrophobic cores. This is due to their unique features being biocompatible, FDA-approved for clinical use, and biodegradable by enzymatic reaction or hydrolysis under physiological conditions.[136, 144] To promote their applicability toward biomedical applications, an introduction of dynamic covalent linkages, particularly disulfide linkages, into PLA-based ABPs and their self-assembled structures has been proposed.[29a, 69b, 76, 145] The reductive cleavage of the disulfide linkages caused the disintegration of PLA-based nanocarriers, exhibiting the enhanced release of encapsulated anticancer drugs. Furthermore, hydrophobic PLA cores are engineered with hydrophilic surfaces to minimize opsonisation, leading to prolonged circulation in the blood.[146] Typical hydrophilic polymers that have been used include PEG[147] and polymethacrylates.[148] Besides these neutral sheaths, ionic shells can also be appealing because therapeutic biomolecules having relatively high molecular weight such as nucleic acids, proteins, and polysaccharides are ionic compounds (either cationic or anionic).[149] In particular, nanocarriers with positive charges (cationic nanocarriers) facilitate the delivery of anionic nucleic acids (DNA, RNA, and chemically modified oligonucleotides) though electrostatic interactions.[150]

Gene therapy including gene silencing mostly utilizes nonviral vectors based on positively-charged cationic polymers that grant nucleic acids with protection against enzymatic degradation. They form polyplexes with negatively-charged phosphate groups of nucleic acids through ionic complexation. After internalization inside targeted cells, the nucleic acids can escape from endosomes and transfer to the nuclei; such endosomal escape that leads to effective gene transfection is facilitated by proton-sponge or pH buffering effect inside endosomes (called endosomal escape).[151] Of several cationic polymers that have been extensively explored as gene carriers, poly(N,N-dimethylaminoethyl methacrylate) (PDMA) has shown its relatively lower cytotoxicity driven by tertiary amine.[152] The quaternized PDMA (cPDMA) can imbibe nucleic acids with protection against enzymatic degradation as they form polyplexes through ionic

complexation with negatively charged phosphate groups of nucleic acids. Further, the PDMA block is easily incorporated into the block copolymers through various controlled radical polymerization methods as well as converted to the corresponding quaternized cationic block. In order to enhance nucleic acid transfection for the success of nucleic acid-based therapies, disulfide reduction chemistry has been explored. Two typical approaches based on the location of disulfide linkages in cationic (co)polymers include reduction-responsive main-chain degradation and PEG deshedding. For the reduction-responsive main-chain degradation, disulfides are formulated in polycation backbones. This approach enhances endosomal escape inside cells while minimizing cytotoxicity as well as increasing transfection efficiency.[153] For the reduction-responsive PEG deshedding, disulfides are positioned at block junctions between polycation backbones and PEG blocks. This approach is desired to circumvent what is known as PEG dilemma, thus enhancing both circulation time in the blood and transfection efficiency.[154]

Herein, we report on novel PLA-based cationic micelles self-assembled from cationic PLA-ss-cPDMA ABP (C-ssABP) for development of reduction-responsive co-delivery and enhanced intracellular release of encapsulated drugs in hydrophobic PLA cores and oligonucleotides in cationic coronas (Scheme 4.1). The cationic ABP was synthesized by a combination of ROP, ATRP, and post-functionalization through quaternization. The single disulfide linkages are positioned at block junctions in C-ssABP; thus self-assembled micelles had the disulfides located at interfaces between PLA cores/drugs and cPDMA coronas/DNA. Different from the conventional methods previously mentioned to circumvent the PEG dilemma, here the reductive cleavage of the interfacial disulfide linkages resulted in shedding cPDMA coronas, causing the destabilization of the integrity of micellar aggregates, thus leading to both enhanced release of drugs and prompted endosomal escape of oligonucleotides. Intracellular release of encapsulated DOX and DNA transfection were confirmed by *in vitro* results from FC, CLSM, and cell viability assay as well as gene transfection assay.
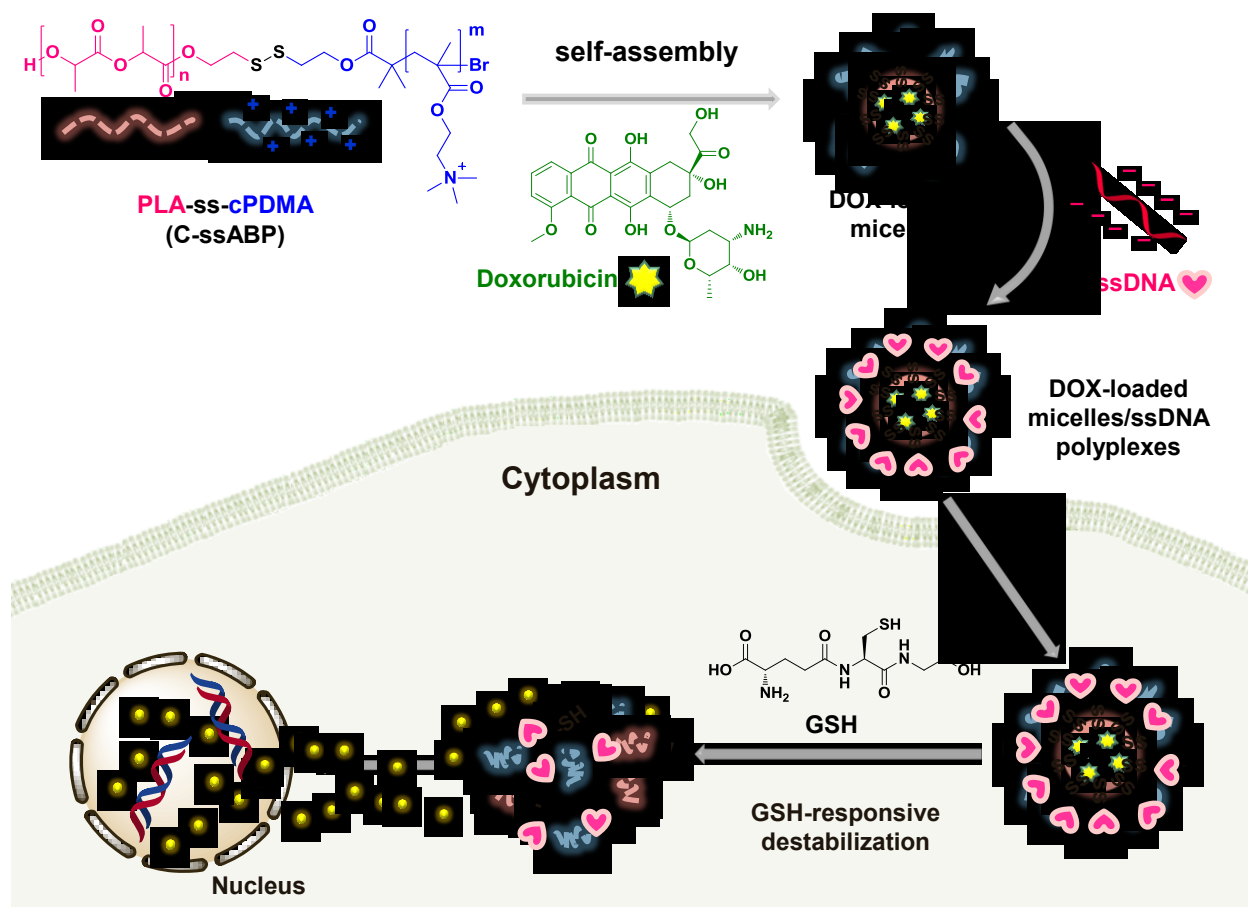
Scheme 4.1. Preparation of cationic C-ss-ABP (PLA-ss-cPDMA) diblock copolymer, and its self-assembled doxorubicin-loaded micelles/ssDNA polyplexes for reduction-responsive co-delivery with enhanced release of of drugs and genes.

4.2 Experimental section

4.2.1 Materials

3,6-Dimethyl-1,4-dioxane-2,5-dione (DL-lactide, LA), tin(II) 2-ethylhexanoate (Sn(Oct)$_2$, 95%), copper(I) bromide (CuBr, >99.99%), *N,N,N′,N″,N″*-pentamethyldiethylenetriamine (PMDETA, >98%), iodomethane (MeI), L-glutathione reduced (GSH), and doxorubicin hydrochloride (DOX, -NH$_3^+$Cl$^-$ salt form, >98%) from Aldrich, DL-dithiothreitol (DTT, 99%) from Acros Organics, and 5'-*O*-dimethoxytrityl-2′-deoxyribonucleoside-3′-*O*-(β-cyanoethyl-*N,N*-diisopropyl)phosphoramidites and protected 2′-deoxyribonucleoside- CPG from Glen

Research (Sterling, Virginia) were purchased and used as received. N,N-dimethylaminoethyl methacrylate (DMA, >98%) purchased from Aldrich was purified by passing it through a column filled with basic alumina to remove the inhibitors. HO-ss-iBuBr was synthesized according to our previous publication.[155]

4.2.2 Instrumentation and analysis

^{1}H-NMR spectra were recorded using a 500 MHz Varian spectrometer. The CDCl$_3$ singlet at 7.26 ppm, DMSO-d_6 multiplet at 2.5 ppm, and DMF-d_7 singlet at 8.03 ppm were selected as the reference standards. Molecular weight and molecular weight distribution were determined by GPC. An Agilent GPC was equipped with a 1260 Infinity Isocratic Pump and a RI detector. Two Agilent PLgel mixed-C and mixed-D columns were used with DMF containing 0.1 mol% LiBr at 50 °C at a flow rate of 1.0 mL/min. Linear poly(methyl methacrylate) standards from Fluka were used for calibration. Aliquots of polymer samples were dissolved in DMF/LiBr. The clear solutions were filtered using a 0.25 μm PTFE filter to remove any solvent-insoluble species. A drop of anisole was added as a flow rate marker. Monomer conversion was determined using ^{1}H-NMR.

4.2.2.1 Dynamic light scattering (DLS)

The size of micelles in hydrodynamic diameter by volume was measured by DLS at a fixed scattering angle of 175° at 25 °C with a Malvern Instruments Nano S ZEN1600 equipped with a 633 nm He-Ne gas laser. UV/Vis spectra were recorded on an Agilent Cary 60 UV/Vis spectrometer using a 1 cm wide quartz cuvette.

4.2.2.2 Transmission Electron Microscope (TEM) images

TEM images were taken using a Philips Tecnai 12 TEM, operated at 120 kV and equipped with a thermionic LaB6 filament. An AMT V601 DVC camera with point to point resolution and line resolution of 0.34 nm and 0.20 nm respectively was used to capture images at 2048 by 2048 pixels. To prepare specimens, the micellar dispersions were dropped onto copper TEM grids (400 mesh, carbon coated), blotted and then allowed to air dry at room temperature.

4.2.3 Synthesis of ssDNA

ssDNA were assembled using an Applied Biosystems Model 3400 synthesizer on a 1 µmole scale employing standard β-cyanoethylphosphoramidite cycles supplied by the manufacturer. The oligomer-derivatized CPG beads were transferred from the reaction column to screw cap microfuge tubes fitted with teflon lined caps and the oligomer released from the support and protecting groups removed by treatment with a mixture of concentrated ammonium hydroxide/EtOH (0.3/0.1 v/v) for 4 hrs at 55 ºC. The crude oligonucleotide were transferred and concentrated in a speedvac concentrator followed by purification from pre-terminated products by strong anion exchange HPLC using a Dionex DNAPAC PA-100 column (0.4 cm x 25 cm) purchased from Dionex Corp, (Sunnyvale, CA) with a linear gradient of 0–50% buffer B over 30 min (buffer A: 100 mM Tris HCl, pH 7.5, 10% acetonitrile and buffer B: 100 mM Tris HCl, pH 7.5, 10% acetonitrile, 1 M NaCl) at 40 °C. The column was monitored at 260 nm for analytical runs or 280 nm for preparative runs. The purified oligomer was desalted using C-18 SEP PAK cartridges (Waters Inc.) and quantified using a Varian CARY Model 3E spectrophotometer.

4.2.4 Synthesis of PLA-ss-Br using ROP

HO-ss-iBuBr (300.3 mg, 0.99 mmol), LA (10.0 g, 69.4 mmol), Sn(Oct)$_2$ (20.1 mg, 0.05 mmol), and toluene (6 mL) were added to a 25 mL Schlenk flask. The resulting mixture was deoxygenated four times by freeze-pump-thaw cycles. The reaction flask was filled with nitrogen, thawed, and then immersed in an oil bath preheated to 120 °C to start the polymerization. After 2.5 hrs, the polymerization was stopped by cooling down to room temperature. The resulting PLA homopolymers were precipitated from MeOH and dried in a vacuum oven at room temperature for >12 hrs.

4.2.5 Synthesis of PLA-ss-PDMA (ssABP) using ATRP

The purified, dried PLA-ss-Br (1.0 g, 87 µmol), DMA (0.68 g, 4.34 mmol), PMDETA (9.05 µL, 0.04 mmol), and THF (1.07 mL) were added to a 10 ml Schlenk flask. The resulting mixture was deoxygenated three times by freeze-pump-thaw cycles. The reaction flask was filled with nitrogen and CuBr (6.2 mg, 0.04 mmol) was then added to the frozen solution. The flask was closed, evacuated, and backfilled with nitrogen two times. The mixture was thawed and the flask was then immersed in an oil bath preheated to 47 °C to start the polymerization. The

polymerization was stopped by cooling down and exposing the reaction mixture to air. For purification, as-prepared green polymer solutions were passed through a column filled with basic aluminum oxide with THF as an eluent to remove copper species. The polymer solution was concentrated by rotary evaporation and precipitated from hexane (500 ml) under stirring for 12 hrs. The precipitates were filtered by vacuum filtration and residual solvents were further removed in a vacuum oven at room temperature for 12 hrs.

4.2.6 Quaternization of ssABP to synthesize C-ssABP

The purified, dried ssABP (0.9 g, 51 μmol) was dissolved in THF (10 mL) and stirred for 10 min at room temperature. After drop-wise addition of MeI (0.3 g, 2.1 mmole), the resulting mixture was stirred for 14 hrs. The formed yellow solids were isolated by vacuum filtration and further dried in a vacuum oven at room temperature for 12 hrs.

4.2.7 Reductive cleavage of disulfide linkages of ssABP in DMF

An aliquot of dried, purified ssABP (50 mg) was mixed with DTT (2.1 mg, 13.4 μmol) in DMF (10 mL) under stirring at room temperature. After 20 hrs, aliquots were taken to analyze molecular weight distribution of degraded products using GPC.

4.2.8 Aqueous micellization of C-ssABP using a dialysis method

A solution of aliquot of the purified, dried C-ssABP (10.3 mg) in DMF (4 mL) was mixed with water (6 mL). The resulting mixture was stirred for 2 hrs, and then dialyzed in a dialysis tubing (MWCO = 12,000 g/mol) against water for 3 days to remove DMF. The outer water (800 mL) was changed once a day, yielding colloidally-stable micellar aggregates in aqueous solution at 0.7 mg/mL concentration.

4.2.9 Reductive-destabilization of aqueous C-ssABP micelles

Aliquots of aqueous micellar dispersion (0.74 mg/mL, 2 mL) were mixed with GSH (6.1 mg, 20 μmol, 10 mM) under stirring. After 19 hrs, aliquots were taken to analyze their size distributions using DLS.

4.2.10 Gel electrophoresis

Aliquots of ssDNA (20 pmol) were labelled with ^{32}P at 5′-OH with gamma ^{32}P ATP and PNK. Labelled ssDNA (10 pmol) were mixed with unlabelled ssDNA (3990 pmol), and then mixture was dried to adjust the concentration to be 4000 pmol. The resulting mixture was then re-suspended in water to give a total of 40 μL. A series of C-ssABP/ssDNA polyplexes were prepared at N/P ratios of 0, 0.1, 0.5, 1, 2, 4, 8, and 16. Electrophoretic gel mobility assays was used to study the binding isotherm of ssDNA to cationic micelles. All samples were run on a 1% agarose gel for 30 min at 100 V and binding was monitored using a phosphorimager. The final concentration of ssDNA per well was 100 pmol.

4.2.11 Preparation and characterization of C-ssABP/ssDNA polyplexes

An aqueous stock solution of sterile ssDNA was prepared. To prepare a series of aqueous polyplexes at various ratios of ssDNA to C-ssABP, the different volumes of the aqueous C-ssABP stock solution were mixed with the equal volume of the aqueous ssDNA stock solution. The resulting mixtures were vortexed for 20 sec, and then incubated at room temperature for 30 min prior to use. They were characterized for size by DLS and zeta potential using a Brookhaven ZetaPlus in phosphate buffered saline (PBS) solution at pH 7.3.

4.2.12 Preparation of DOX-loaded micelles

Similar to the procedure for aqueous micellization, water (10 mL) was added drop-wise to an organic solution consisting of the purified, dried C-ssABP (20 mg), DOX (2 mg), and Et$_3$N (1.44 μL, 3 molar equivalents to DOX) in DMF (2 mL). The resulting dispersion was dialyzed over water (800 mL) for 19 hrs, yielding DOX-loaded micellar dispersion at 1.9 mg/mL. To determine a loading level of DOX, aliquots of the DOX-loaded micellar dispersion (1 mL) were dried using rotary evaporator. Residues were dissolved in DMF (3 mL) to form clear solutions. Their UV/Vis spectra were recorded, and DOX loading was calculated by the weight ratio of loaded DOX to dried polymers. To prepare DOX-loaded polyplexes, DOX-loaded micelles were mixed with ssDNA in PBS and vortexed for 30 min at room temperature.

4.2.13 GSH-triggered release of DOX from DOX-loaded micelles

An aliquot of DOX-loaded micellar dispersion (3 mL, 1.9 mg/mL) was transferred into a dialysis tubing (MWCO = 3,500 g/mol) and immersed in aqueous PBS (50 mL) as a control and 10 mM aqueous GSH buffered with PBS under stirring. The absorbance of DOX in outer water (50 mL) was recorded at 2 min interval using a UV/Vis spectrometer equipped with an external probe at $\lambda = 497$ nm. For quantitative analysis, DOX (74.3 μg, equivalent to DOX encapsulated in 3 mL DOX-loaded micelles) was dissolved in 10 mM aqueous GSH buffered with PBS (50 mL) and its UV/Vis spectrum was recorded.

4.2.14 Cell culture

HeLa cancer cells were cultured in DMEM (Dulbecco's modified Eagle's medium) containing 10% FBS (fetal bovine serum) and 1% antibiotics (50 units/mL penicillin and 50 units/mL streptomycin) at 37 °C in a humidified atmosphere containing 5% CO_2.

4.2.15 Cell viability using MTT assay

HeLa cells were plated at 5 x 10^5 cells per well into a 96-well plate and incubated for 24 hrs in DMEM (100 μL) containing 10 % FBS and 1 % antibiotics. They were then incubated with various concentrations of micellar dispersions of C-ssABP for 48 hrs. Blank controls without micelles (cells only) were run simultaneously as control. Cell viability was measured using CellTiter 96 Non-Radioactive Cell Proliferation Assay kit (MTT, Promega) according to the manufacturer's protocol. Briefly, 3-(4,5-dimethylthiazol-2-yl)-2,5-diphenyltetrazolium bromide (MTT) solutions (15 μL) was added into each well. After 4 hrs incubation, the medium containing unreacted MTT was carefully removed. DMSO (100 μL) was added into each well in order to dissolve the formed formazan blue crystals, and then the absorbance at $\lambda = 570$ nm was recorded using Powerwave HT Microplate Reader (Bio-Tek). Each concentration was 12-replicated. Cell viability was calculated as the percent ratio of absorbance of mixtures with micelles to control (cells only). A similar procedure was used for cell viability of polyplexes and DOX-loaded micelles.

4.2.16 Flow cytometry (FC)

HeLa cells were plated at 2×10^5 cells/ well into a 6-well plate and incubated hrs in DMEM (2 mL) at 37 °C. After 24 hrs, cells were treated with DOX-loaded micelles (116 μL for DOX = 2.3 μg/mL) and DOX-loaded polyplexes (200 μL for DOX = 2.3 μg/mL)at 37 °C for 10 hrs. After culture medium was removed, cells were washed with PBS buffer three times and then treated with trypsin. The suspended cells were diluted in DMEM (500 μL) for flow cytometry measurements. Resulting data was analyzed by means of a BD FACSCANTO II flow cytometer and BD FACSDiva software.

4.2.17 Confocal laser scanning microscopy (CLSM)

HeLa cells plated at 2×10^5 cells/ well into a 6-well plate and incubated for 24 hrs in DMEM (2 mL) were treated with DOX-loaded micelles and DOX-loaded polyplexes (DOX = 2.3 μg/mL) at 37 °C for 10 hrs. After culture medium was removed, cells were washed with PBS buffer three times. After the removal of supernatants, the cells were fixed with cold methanol (-20 °C) for 20 min at 4 °C. The slides were rinsed with PBS buffer for five times and TBST (tris-buffered saline Tween-20) for three times. Cells were stained with 2-(4-amidinophenyl)-1H-indole-6-carboxamidine (DAPI). The fluorescence images were obtained using a LSM 510 Meta/Axiovert 200 (Carl Zeiss, Jena, Germany).

4.2.18 *In vitro* gene transfection assay

The luciferase gene reporter assay was used to evaluate the efficiency of C-ssABP/ssDNA complexes to induce gene expression in HeLa cells. For transfection, HeLa cells were placed at 5×10^5 cells per well into a 6-well plate and incubated in DMEM (1 mL) supplemented with 10% FBS and 1% penicillin–streptomycin for 18 hrs prior to transfection. After old media were replaced with fresh ones, aliquots of C-ssABP/ssDNA polyplexes at various N/P ratios (0.5, 1, 4, 8, containing 2.5 μg DNA/well) were added to each well and incubated for 4 hrs at 37 °C. After the culture media being replaced with fresh ones (1 mL), the cells were incubated for another 48 hrs. The culture medium was removed and then the cells were washed with PBS (1 mL) twice. Cell lysis buffer (1 mL, Pierce, Rockford, IL) was then added to each well to lyse the cells. The cell plate was shaked at a moderate speed for 15 min. Lysed cells (20 μL) were transferred to 96-well plate and mixed with 1X D-luciferin solution (50

μL, Pierce, Rockford, IL) for luciferase expression on a Wallac Victor 1420 multilabel counter (Perkin-Elmer Life Sciences, Boston, Mass.). For the determination of protein level, BCA assay with lysate cells was performed according to the manufacturer's protocol (Pierce® BCA Assay Kit). Transfection of each polyplex was tested four times, and the results are given as mean ± SD of counts per second (CPS) normalized to protein concentration according to the BCA assay.

4.3 Results and Discussion

4.3.1 Synthesis of C-ssABP

Figure 4.1a illustrates our approach to synthesize well-controlled C-ssABP having single disulfide linkages at the junctions of a hydrophobic PLA block and a cationic cPDMA block. Figure 4.1b shows ^{1}H -NMR spectra.
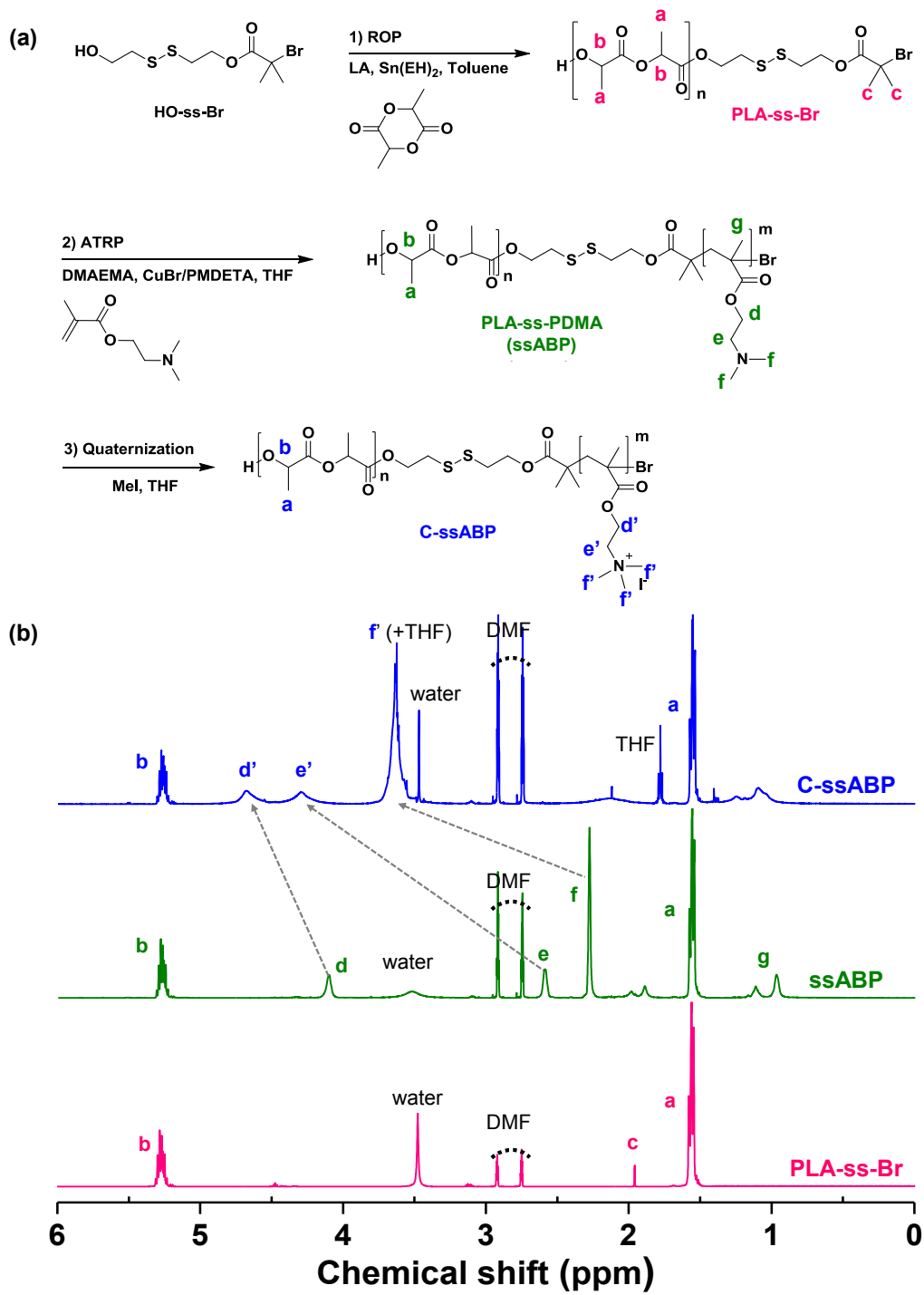
Figure 4.1. Synthetic route to cationic C-ssABP by a combination of ROP, ATRP, and quaternization (a) and ^{1}H-NMR spectra of PLA-ss-Br, ssABP, and C-ssABP in DMF-d_6 (b).

The first step is the synthesis of well-controlled PLA-ss-Br homopolymers with narrow molecular weight distribution by ROP of LA catalyzed with $Sn(Oct)_2$ in the presence of HO-ss-iBuBr in toluene at 120 °C. The conditions include $[LA]_0/[HO\text{-ss-iBuBr}]_0/[Sn(Oct)_2]_0 = 70/1/0.05$ with LA/toluene = 1.9/1 wt/wt. The detailed procedure was described in our previous report.[155] The resulting PLA-ss-Br homopolymer had the number average molecular weight, M_n = 12,900 g/mol and M_w/M_n = 1.09 by GPC (Figure 4.2) as well as the DP of PLA = 70 from the integral ratio of the peaks $[(b/2)/(c/6)]$ by ^{1}H-NMR. The second step is the synthesis of ssABP by conventional ATRP of DMA. The ATRP was conducted in the presence of PLA-ss-Br macroinitiator and catalyzed with CuBr/PMDETA active complex in THF at 47 °C under $[DMA]_0/[\text{PLA-ss-Br}]_0/[CuBr/PMDETA]_0 = 50/1/0.5$; DMA/THF = 0.8/1 wt/wt. After purification, GPC results indicate M_n = 16,700 g/mol and M_w/M_n = 1.13 (Figure 4.2). The ^{1}H-NMR spectrum shows two peaks at 4.2 ppm (d) and 2.6 ppm (e) corresponding to four methylene protons in pendant chains of DMA as well as a broad singlet at 2.3 ppm (f) corresponding to six methyl protons in t-amine groups. From the integral ratio of the peaks $[(d/2)/(b/2)]$ and the DP of PLA = 70, the DP of PDMA block was determined to be 45. The third step is the quaternization of ssABPs with excess MeI in THF to C-ssABPs. The yellow solids formed were characterized by ^{1}H-NMR. The peaks at 4.6 (d′) and 4.3 ppm (e′) corresponding to four methylene protons in side chains of cPDMA blocks as well as the peak at 3.6 ppm (f′) to nine methyl protons are clearly shifted as a result of quaternization. These results suggest the successful synthesis of well-defined cationic C-ssABP. Note that a few reports describe the synthesis of C-ssABP with no SRD concept.[156]
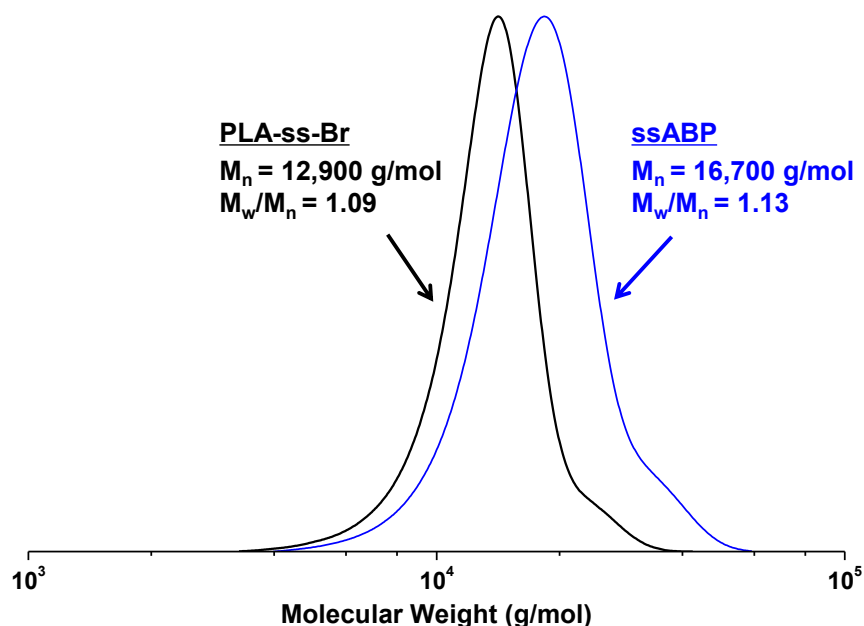
Figure 4.2. GPC traces of PLA-ss-Br and ssABP. Conditions for ATRP: $[DMA]_0/[PLA-ss-Br]_0/[CuBr/PMDETA]_0 = 50/1/0.5$; DMA/THF = 0.8/1wt/wt.

4.3.2 Aqueous assembly and disassembly of C-ssABP

The C-ssABP is amphiphilic and thus self-assembles to form cationic micellar aggregates consisting of hydrophobic PLA cores surrounded with cationic coronas. To prepare aqueous micellar aggregates through a dialysis method, a mixture of C-ssABP dissolved in DMF was dialyzed over fresh water for 3 days. The resulting micellar aggregates at 0.7 mg/mL were characterized for the size and morphology using DLS and TEM. As seen in Figure 4.3a (left), the DLS results indicate the monomodal distribution of micelles with an average diameter = 91.0 ± 6.0 nm on average from five freshly-prepared samples. TEM images show spherical micelles with a diameter to be 21.7 ± 4.4 nm, which is smaller by ≈70 nm than that determined by DLS. Since the smaller micelle size determined by TEM than by DLS is attributed to the dehydrated state of the micelles,[157] these results suggest that the micelles possess relatively long coronas.
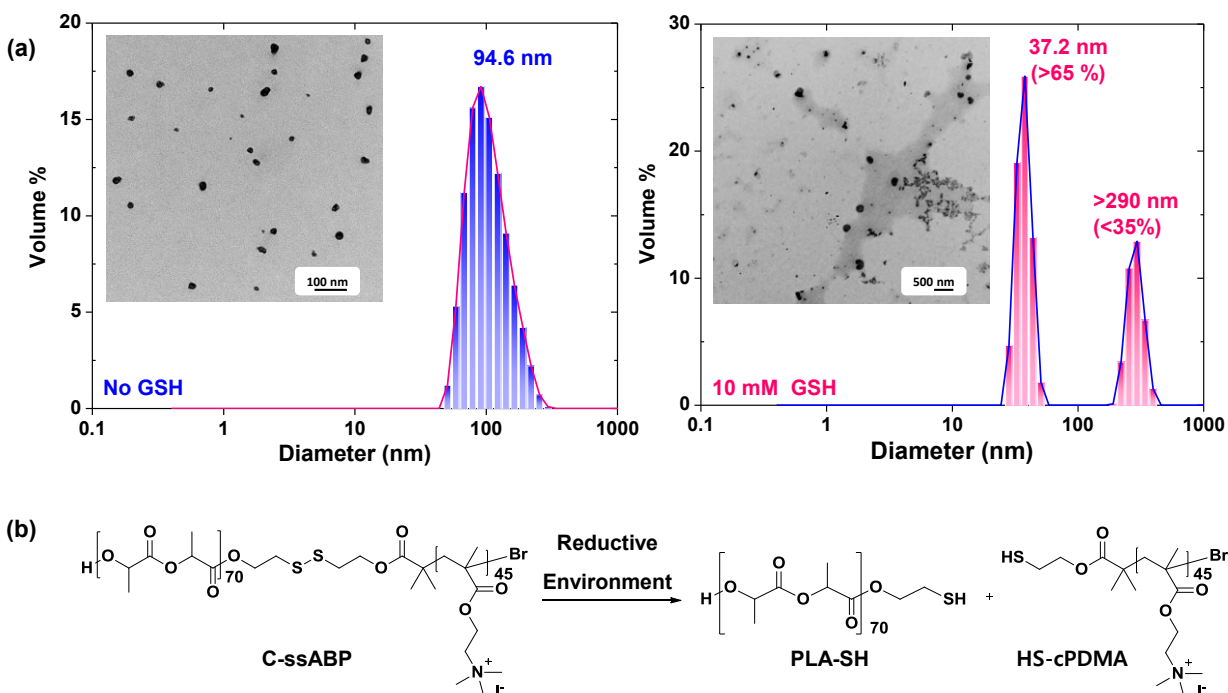
Figure 4.3. DLS diagrams and TEM images (insets) of C-ssABP micelles at 0.7 mg/mL before (left) and after (right) treatment with 10 mM GSH (a) and schematic illustration of reductive cleavage of disulfide linkages at block junctions of C-ssABP (b).

The C-ssABP is designed to have a disulfide linkage at block junction; thus its self-assembled micellar aggregates contain disulfide linkages positioned at interfaces between cores and cationic coronas. In response to reductive reactions, the size distribution became bimodal with the occurrence of large aggregates (diameter >250 nm) (Figure 4.3a (right)). This size change is attributed to the destabilization of micelles upon the cleavage of disulfide linkages at interfaces, as suggested from other sheddable micelles.[80, 130b, 133c, 154b] Such reduction-responsive cleavage of disulfide linkages at block junctions in the presence of excess DTT generates the corresponding thiols including PLA-SH and HS-cPDMA (Figure 4.3b).

4.3.3 C-ssABP/DNA complexation and characterization

The cationic coronas of C-ssABP micelles enable the electrostatic interactions with anionic phosphates of DNA molecules, leading to the formation of polyplexes. ssDNA with a sequence of 5′-GAT CAC TGA CTA CGC TAC-3′ was synthesized by Dr. Anne Noronha and

further used as a model oligonucleotide for complexation with cationic micelles. A series of polyplexes were prepared by mixing C-ssABP micelles with ssDNA at different ratios of N/P (amine/phosphate) of 0-16. Note that larger N/P ratio has more cationic micelles. First, agarose gel electrophoresis (conducted by Jack Cheong) was used to further examine polymer-DNA complexation. As shown in Figure 4.4a, an increasing amount of amine groups in the complex intensified the interactions of cationic coronas with phosphate groups of ssDNA. Compared with the ssDNA only (as denoted to N/P ratio = 0/1), a significant complexation of cationic micelles with ssDNA occurred at the N/P ratio of 2/1-4/1. Similar results are observed for other cationic vectors.[158]
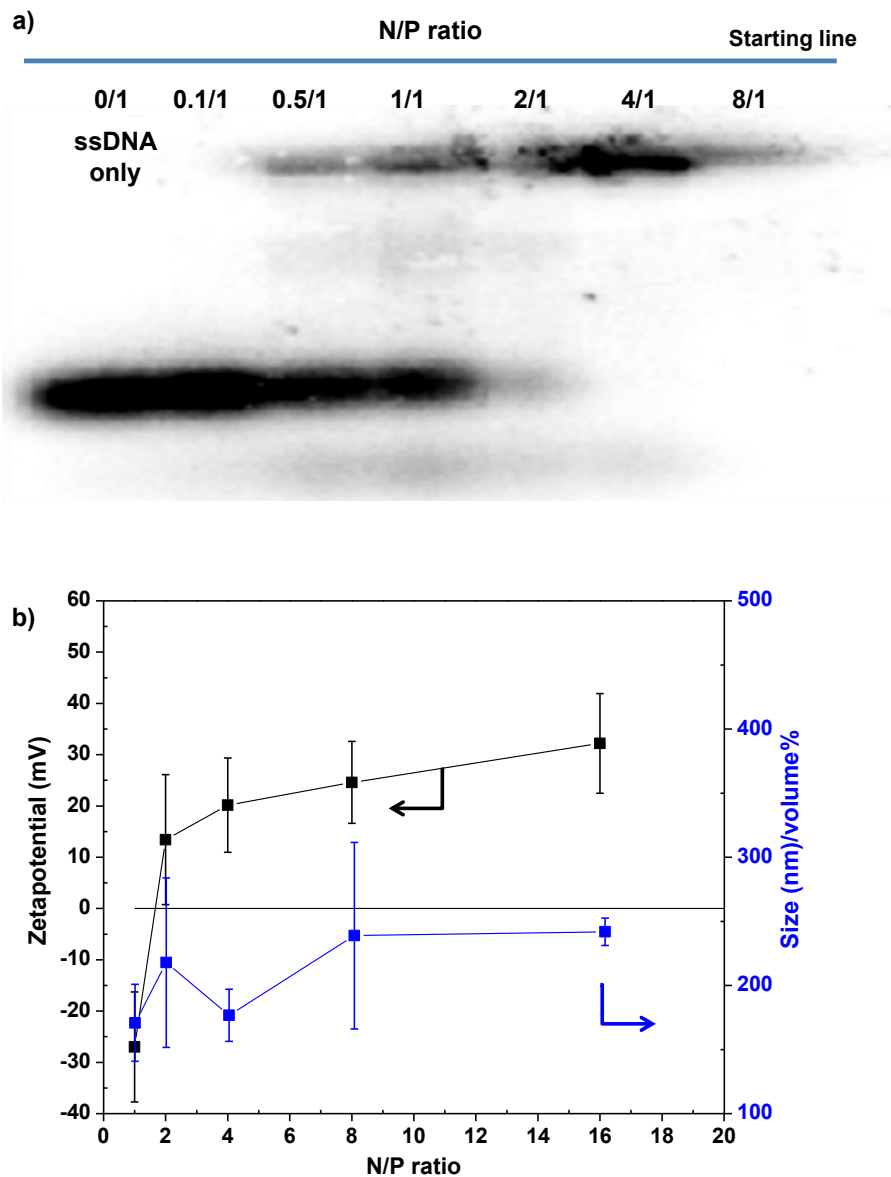
Figure 4.4. Electrophoretic mobility and binding efficiency of ^{32}P-labelled ssDNA (a) and evolution of ζ-potential and diameter by volume% (b) in polyplexes formed by C-ssABP micelles at different N/P ratios of 0.5/1 – 16/1.

Further, the C-ssABP/ssDNA polyplexes were characterized for surface charge using ζ-potential measurements and size using DLS (Figure 4.4b). ζ-potential was -28 mV for naked ssDNA, which is attributed to anionic phosphates. With an increasing N/P ratio (i.e. amount of cationic micelles), ζ-potential increased to positive values; which is presumably due to the

increase of cationic charges in the C-ssABP/DNA complexes. More interestingly, ζ-potential sharply jumped from negative to positive $\zeta = +25$ mV at the N/P ratio = 2/1, crossing $\zeta = 0$ mV (neutral surface) between the N/P ratio = 1/1-2/1. Similar trend is observed for the evolution of size over the increasing N/P ratio. These results are similar to the gel electrophoresis above, indicating the formation of stable C-ssABP/ssDNA complexes starting from the N/P ratio = 2/1.

4.3.4 *In vitro* cytotoxicity using MTT assay

The viability of HeLa cells in the presence of cationic micelles of C-ssABP and their polyplexes with ssDNA at N/P ratio = 4/1 was evaluated using a MTT colorimetric assay. Figure 4.5 shows that HeLa cell viability was >75% up to 200 µg/mL for both cationic micelles and polyplexes. When their concentrations increased to 400 µg/mL, HeLa cell viability decreased gradually to <60%. The decrease in HeLa viability is explained by high concentration of cationic charges of C-ssABP and their polyplexes which were exposed to the cells. Interestingly, HeLa viability is not significantly different in the presence of micelles and their polyplexes.
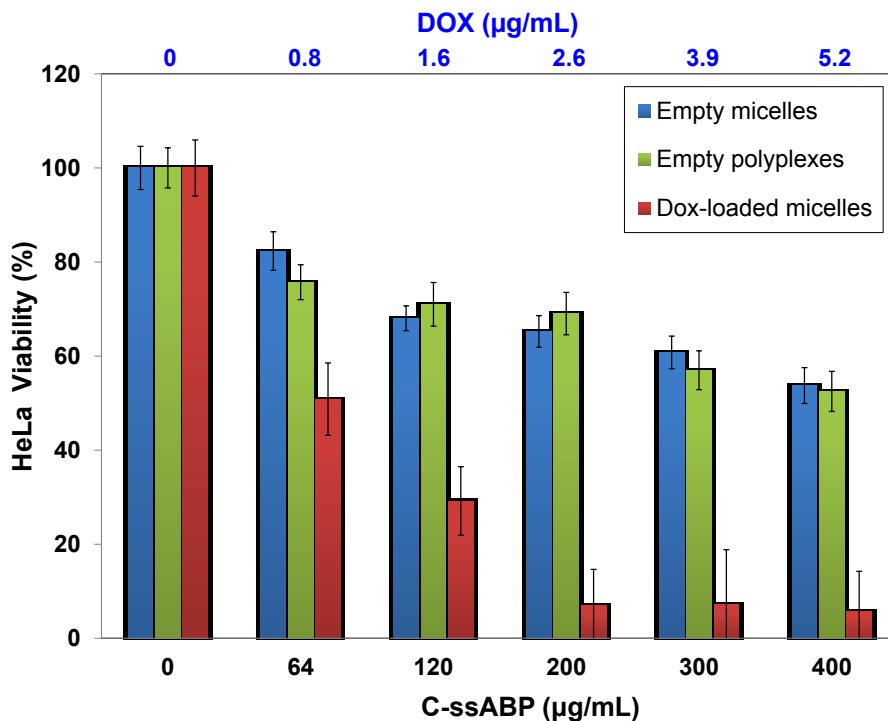
Figure 4.5. Viability of HeLa cells incubated for 48 hrs determined by MTT assay. Data are presented as the average ± SD (n = 12).

4.3.5 Loading and GSH-triggered release of DOX from DOX-loaded micelles

To assess the cationic C-ssABP micelles as a tumor-targeting drug delivery nanocarrier exhibiting enhanced reduction-responsive drug release, DOX was encapsulated in hydrophobic PLA cores using the dialysis method. Free DOX and DMF were removed by intensive dialysis over PBS for >19 hrs, yielding DOX-loaded micelles at 1.9 mg/mL. Figure 4.6 shows a typical UV/Vis spectrum of DOX-loaded micelles in DMF. Using the Beer-Lambert equation with the absorbance at λ_{max} = 480 nm and the extinction coefficient (ε) = 11,700 M^{-1} cm^{-1} in DMF reported in our previous publication,[72] the loading level of DOX was determined to be 1.3%.
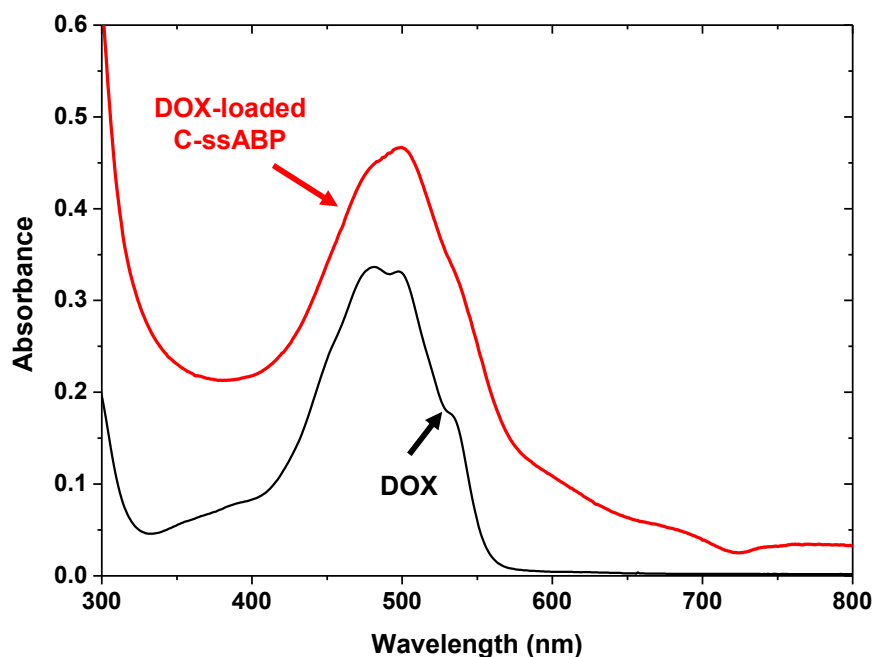
Figure 4.6. A typical UV/Vis spectrum of DOX-loaded C-ssABP in DMF.

The release of DOX from DOX-loaded micelles upon the cleavage of disulfide linkages at micellar interfaces was investigated. An aliquot of DOX-loaded micellar dispersion in dialysis tubing was placed in 10 mM aqueous GSH solution buffered with PBS and aqueous PBS as a control (Figure 4.7). In the absence of GSH, no significant release of DOX was observed because DOX is presumably confined in small micellar cores. In the presence of 10 mM GSH, however, DOX-loaded micelles degrade to the corresponding thiols (PLA-SH and HS-cPDMA), causing

the enhanced release of encapsulated DOX to aqueous solution. In fact, >80% DOX was released from the micelles within 10 hrs. Similar release profile of DOX from other sheddable micelles consisting of diblock copolymers with disulfides at block junctions in the presence of GSH is reported.[80, 130b, 154b]
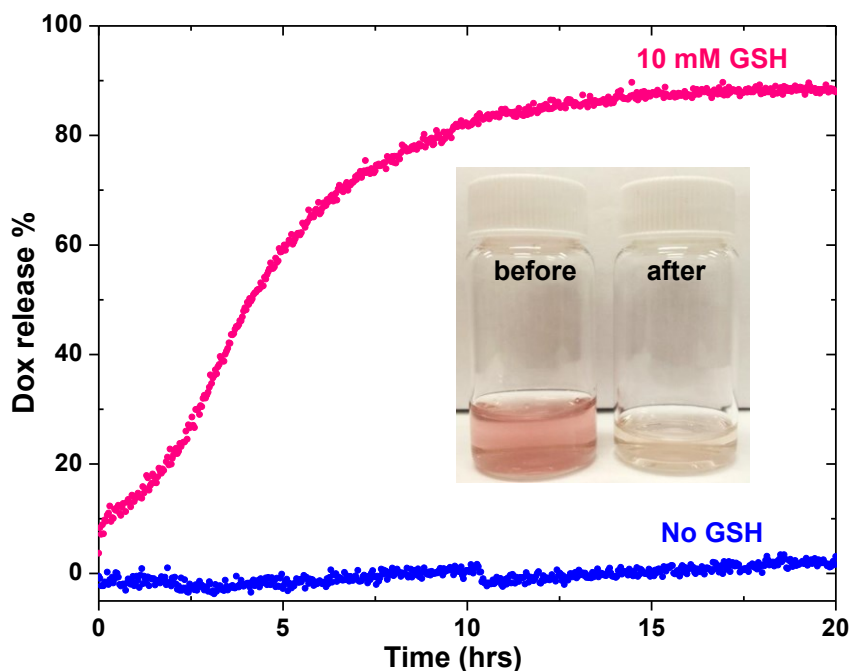
Figure 4.7. Release of DOX from DOX-loaded micelles in 10 mM aqueous GSH solution buffered with PBS, and aqueous PBS as a control. Inset: digital images of DOX-loaded micellar dispersion before and after GSH-triggered release of DOX.

4.3.6 Antitumor activity and intracellular trafficking

Given these promising results, the C-ssABP micelles were evaluated as effective intracellular drug delivery nanocarriers. The viability of HeLa cells incubated with DOX-loaded C-ssABP micelles was also examined. As seen in Figure 4.5, the viability significantly decreased with an increasing amount of DOX encapsulated in cationic micelles. Compared to empty micelles and polyplexes with no DOX, DOX-loaded micelles exhibited great inhibition of cell proliferation. In addition, the HeLa viability in the presence of DOX-loaded micelles appears to be competitive to

that with free DOX reported elsewhere.[72, 159] For example, the concentration of DOX at which the HeLa viability is ≈50% is 0.8-1.6 μg/mL for free DOX and DOX-loaded C-ssABP micelles. Further, intracellular trafficking of DOX from DOX-loaded micelles were examined using flow cytometry and CLSM. Figure 4.8a shows the flow cytometric histogram of HeLa cells incubated with DOX-loaded micelles and DOX-loaded polyplexes. Compared with HeLa cells only as a control, their histograms presented a noticeable shift in the direction of high fluorescence intensity. No significant difference between DOX-loaded micelles and DOX-loaded polyplexes is observed. Figure 4.8b shows CLSM images of HeLa cells incubated with DOX-loaded micelles and DOX-loaded polyplexes for 10 hrs. HeLa nuclei were stained with DAPI. Obviously, HeLa cells incubated with both DOX-loaded micelles and DOX-loaded polyplexes displayed strong DOX fluorescence in their nuclei. These results from both flow cytometry and CLSM confirm that DOX-loaded C-ssABP micelles and polyplexes are able to deliver and release DOX into the nuclei of cancer cells.
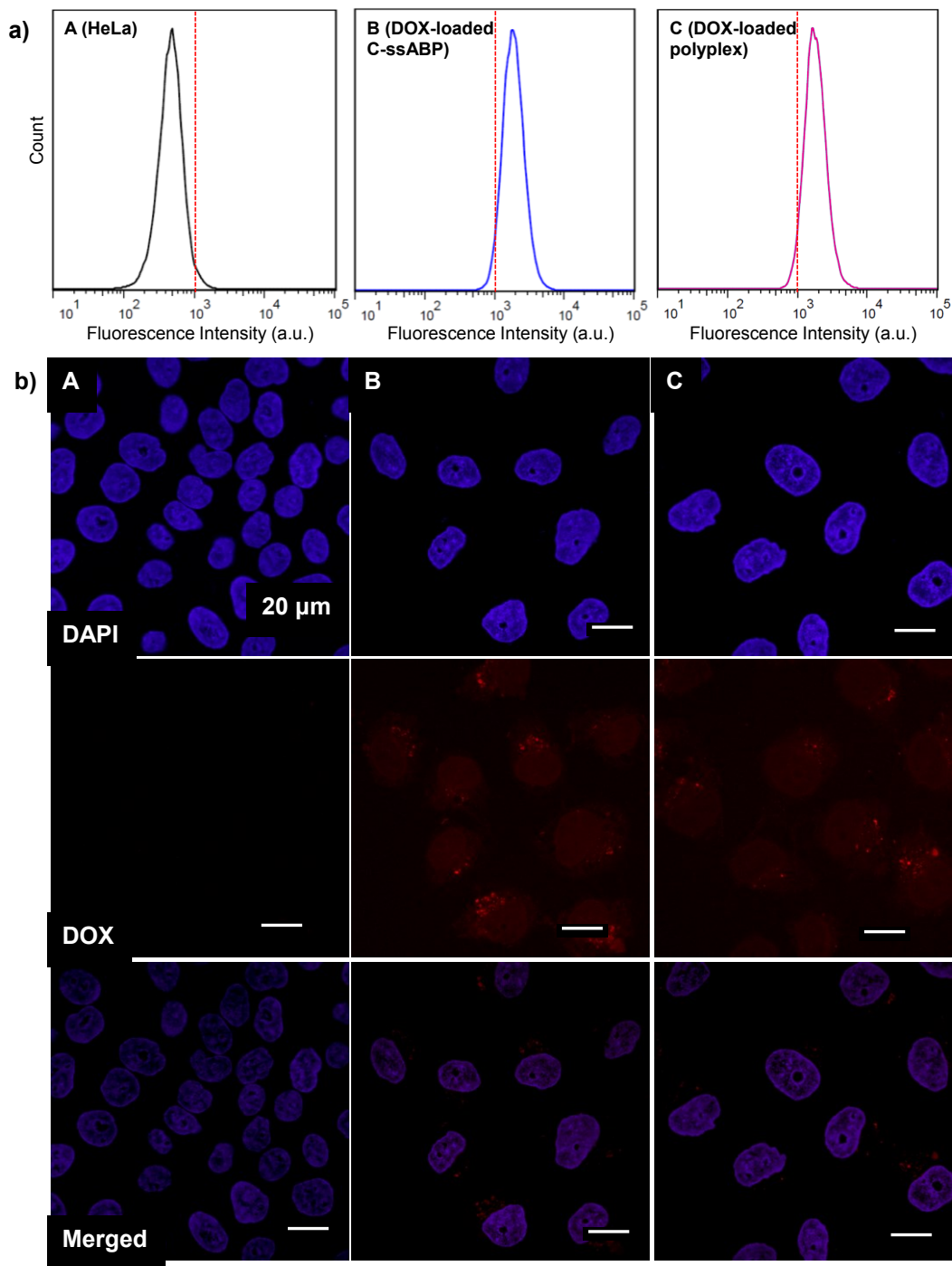
Figure 4.8. Flow cytometric histograms of HeLa cells only and incubated with DOX-loaded micelles and DOX-loaded polyplexes of C-ssABP for 10 hrs (a) and CLSM images (scale bar = 20µm) of HeLa cells only (left), incubated with DOX-loaded micelles (center), and DOX-loaded polyplexes (right) for 10 hrs (b).

4.3.7 *In vitro* gene transfection activity

In vitro gene transfection efficiency of C-ssABP/ssDNA complexes was evaluated using luciferase as a reporter gene in HeLa cells. Figure 4.9 shows the transfection efficiency of polyplexes at different N/P ratio from 0 (ssDNA only) to 8. Free DNA did not mediate significant luciferase expression, while transfection efficiency of polyplexes increased with an increasing amount of cationic micelles and reached a plateau at N/P ratio = 4. These results illustrate the N/P-dependent gene silencing activity of the polyplexes as previously observed for other polyplex formulations.[160]
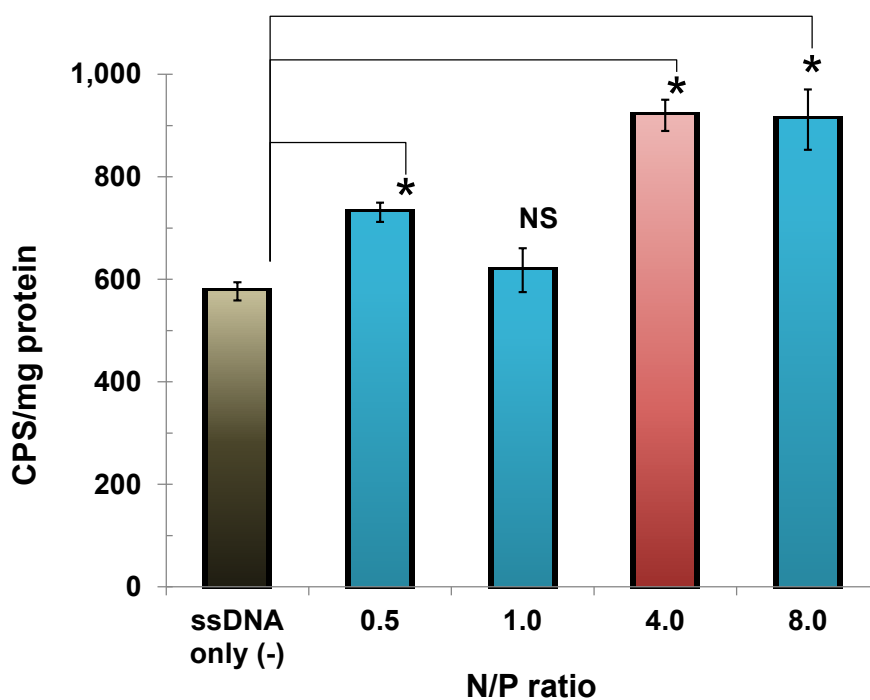
Figure 4.9. Luciferase expression in HeLa cells incubated with C-ssABP/ssDNA polyplexes at different N/P ratios, compared with naked DNA as negative control. Transgene expression was evaluated as counts per second per mg of protein. Data are shown as mean ± SD (n = 4; Student's t-test, *p < 0.001); NS-not significant.

74

4.4 Conclusion

Well-defined cationic C-ssABP was synthesized by a combination of ROP, ATRP, and followed by quaternization of pendant N,N-dimethylamino groups. The C-ssABP self-assembled to form aqueous micelles with diameter of 90 nm having disulfides at interfaces of hydrophobic PLA cores and cationic coronas. The positively-charged coronas were electrostatically interacted with negatively-charged ssDNA to form C-ssABP micelles/ssDNA polyplexes at the optimal N/P ratio = 2/1-4/1, confirmed by agarose gel electrophoresis and zeta potential measurements. MTT assay revealed >70% cell viability up to 200 μg/mL for both cationic micelles and polyplexes. Further, hydrophobic PLA cores enabled the encapsulation of anticancer drugs for targeted drug delivery. Reductive cleavage of disulfide linkages at interfaces resulted in the disassembly of cationic micelles and DOX-loaded micelles as well as polyplexes, leading to controlled/enhanced release of both anticancer therapeutics and oligonucleotides in cancer cells. The results from cell viability, flow cytometry, and CLSM as well as *in vitro* gene transfection assay suggest that the new C-ssABP possesses a great potential as an effective ABP-nanocarrier platform for co-delivery of drugs and oligonucleotides.

Chapter 5

Glutathione-triggered disassembly of dual disulfide located degradable nanocarriers of polylactide-based block copolymers for rapid drug release
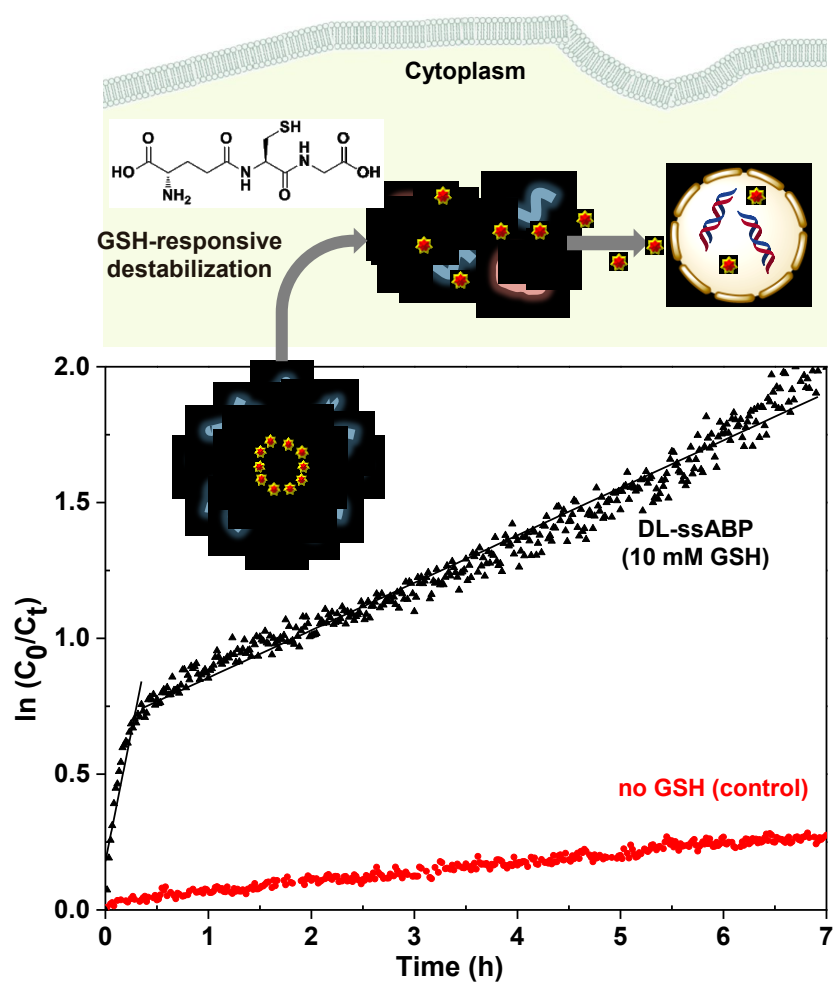
Reduction-responsive degradation based on disulfide-thiol chemistry is highly desirable in the development of self-assembled block copolymer nanocarriers for multifunctional polymer-based drug delivery applications. Most conventional approaches involve the incorporation of disulfide linkages at a single location. Chapter 5 reports a new dual disulfide located degradable polylactide (PLA)-based block copolymer (DL-ssABP) synthesized by a combination method of

ring opening polymerization, facile coupling reactions, and controlled radical polymerization. The amphiphilic design of the DL-ssABP enables the formation of self-assembled micelles having disulfides positioned in both the hydrophobic PLA core and the core/corona interface. The reductive response to glutathione as a cellular trigger results in the cleavage of disulfide linkages at the interface shedding hydrophilic coronas as well as the PLA core causing disintegration of PLA cores. Such dual disulfide degradation process leads to a synergistically enhanced release of encapsulated anticancer drugs in cellular environments. These results, combined with flow cytometry and confocal laser scanning microscopy (CLSM) as well as cell viability measurements, suggest that DL-ssABP offers versatility in tumor-targeting controlled/enhanced drug delivery applications.

5.1 Introduction

Polymer-based drug delivery systems, particularly self-assembled micelles based on block copolymers have drawn a significant attention as promising candidates for tumor-targeting drug delivery applications.[143] Well-defined micellar nanocarriers having optimal sizes (50 - 150 nm in diameter) can minimize renal clearance by kidney filtration as well as prevent their extravasation into healthy cells that is common to small drugs. The nanocarriers formulated with hydrophilic neutral surface coatings exhibit a prolonged blood circulation.[12, 161] Tumors are characterized with rapidly-grown vasculatures with irregularly-aligned endothelial cells which facilitates extravasation (enhanced permeation) of drug-carrying micelles into tumors. Furthermore, their insufficient lymphatic drainage allows for these micelles to be retained inside solid tumors (retention). This process is known as the enhanced permeation and retention (EPR) effect (or passive targeting).[162] These features offer micellar nanocarriers to minimize undesired side effects and maximize drug efficacy. After internalized into cancer cells through endocytosis, nanocarriers undergo sustainable release of anticancer drugs inside cells.[163]

A classical model of drug release involves a diffusion-controlled mechanism which requires overcoming hydrophobic-hydrophobic interactions between drug molecules and micellar core-forming polymers. It is a facile mechanism, whereas it is uncontrolled and slow.[164] One of the promising methods is the incorporation of dynamic covalent bonds (i.e. cleavable linkages) in the design and development of block copolymers and their nanostructures. When needed, the cleavable linkages are cleaved in response to external stimuli, causing degradation or destabilization of the micelles. This stimuli-responsive degradation (SRD) can enhance the release of encapsulated drugs as well as facilitate the removal of empty vehicles after drug release.[165] Several stimuli-responsive cleavable linkages have been explored, including acid-labile,[166] photo-cleavable groups,[131c, 167] and polypeptides.[168] In particular, disulfides are cleaved to the corresponding thiols in response to reductive reactions.[126b, 169] In biological systems, glutathione (GSH, a tripeptide containing cysteine having a pendant thiol) is found at millimolar concentrations (2-10 mM) in intracellular compartments, while its concentration is much smaller in extracellular milieu (<20 μM).[170] Such large redox potential between intracellular and extracellular compartments as well as enhanced concentration in cancer cells renders GSH as an effective cellular trigger that can cleave disulfide linkages in

micellar nanocarriers through disulfide-thiol exchange reactions.[171] Due to such unique features, block copolymer based micelle exhibiting redox-responsive degradation system has been considered as a promising platform for tumor-targeting drug delivery applications.[172]

Several approaches have been reported for the synthesis of disulfide-containing block copolymers and their self-assembled nanostructures. Most approaches involve the incorporation of different densities of disulfide linkages positioned at a single location, either in backbone of the polymer chains as single[128b, 145, 173] and multiple groups,[64, 85c, 128a, 174] as pendant chains,[72, 127, 175] as crosslinkers,[129b, 129d, 159, 176] or at block junctions.[29a, 133b, 133c, 134a, 154b, 176d, 177] A new multi-location SRD strategy has recently been explored to develop effective reduction-responsive nanocarriers.[178] They possess disulfide linkages in dual locations, namely in the micellar core, the interlayered corona, and the interface between hydrophobic core and corona. The preliminary results suggest that this strategy enables the accelerated release of encapsulated anticancer drugs in response to reductive reductions at both sites.[69a, 179]

In this chapter, we have explored the promising multi-location SRD strategy to develop novel dual-located disulfide degradable polylactide (PLA)-based block copolymers (DL-ssABPs) and their self-assembled micelles as effective intracellular drug delivery nanocarriers exhibiting rapid reduction-responsive drug release. Compared to conventional hydrophobic polymethacrylate-containing pendant disulfide linkages,[69a] PLA is a typical class of aliphatic polyesters and is biocompatible, biodegradable by hydrolysis and enzymatic reactions, and FDA-approved for clinical use.[136, 180] As illustrated in Scheme 5.1, the DL-ssABP triblock copolymer consists of a hydrophobic central PLA block and two hydrophilic polymethacrylate blocks containing pendant oligo(ethylene oxide) (POEOMA). This copolymer has a single disulfide bond in the middle of the hydrophobic block and two disulfide linkages at block junctions, resulting POEOMA-ss-(PLA-ss-PLA)-ss-POEOMA triblock copolymer. The DL-ssABP self-assembled to form colloidally-stable micelles having disulfides located at both the hydrophobic PLA core and the PLA/POEOMA interface. These disulfide linkages were cleaved in response to GSH (a cellular trigger), shedding the POEOMA coronas from the PLA cores as well as causing disintegration of the PLA cores. The degradation of DL-ssABP micelles enabled the enhanced release of encapsulated anticancer drugs. The results from flow cytometry and confocal laser scanning microscopy (CLSM) measurements as well as cell viability measurements indicate that

rapid DOX release from DOX-loaded micelles triggered by higher intracellular GSH concentration resulted in enhanced inhibition of the cellular proliferation after cell internalization.
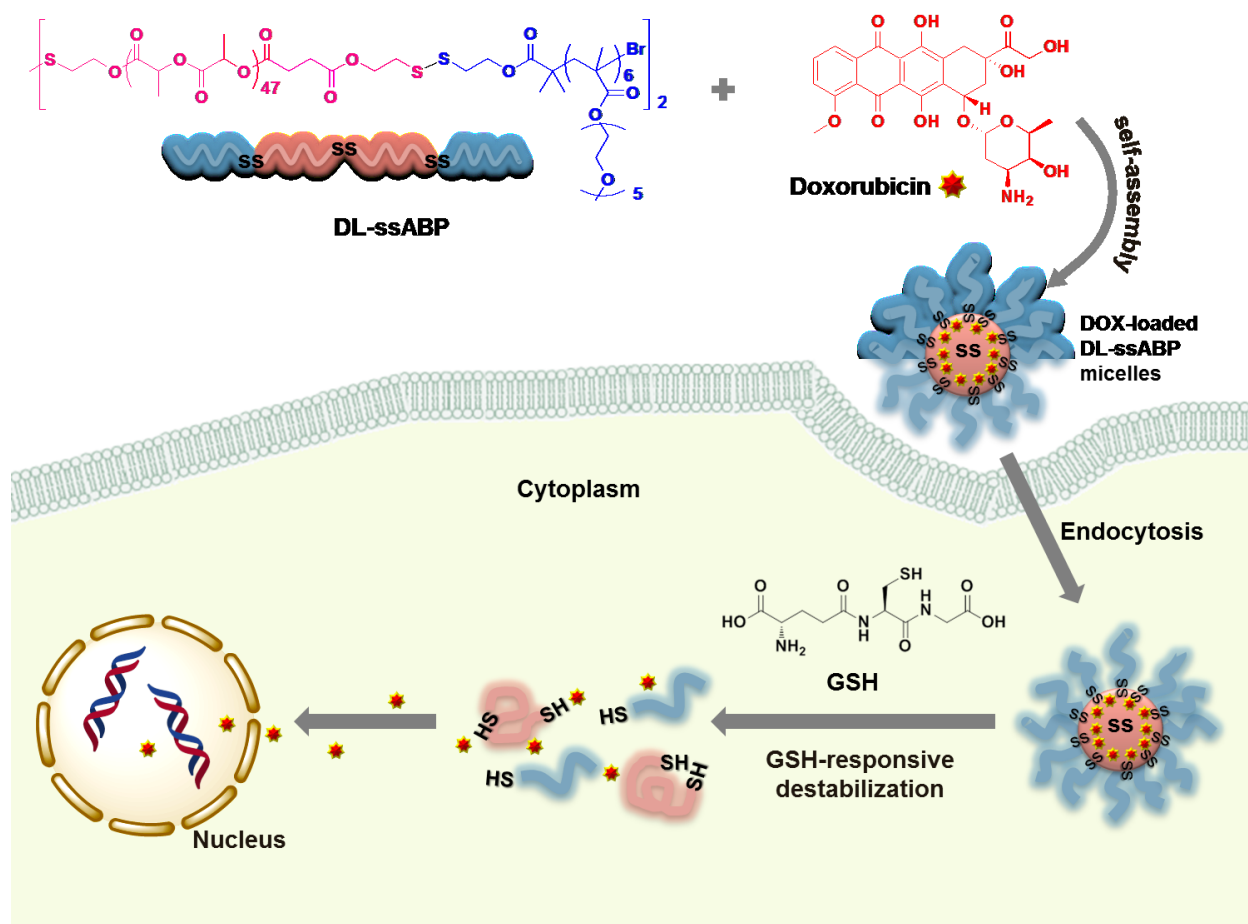
Scheme 5.1. Preparation and illustration of a dual location disulfide degradable DL-ssABP [POEOMA-ss-(PLA-ss-PLA)-ss-POEOMA] triblock copolymer, and its self-assembled doxorubicin-loaded micelles as effective intracellular drug delivery nanocarriers.

5.2 Experimental section

5.2.1 Materials

3,6-Dimethyl-1,4-dioxane-2,5-dione (DL-lactide, LA), 2-hydroxyethyl disulfide (ss-DOH), tin(II) 2-ethylhexanoate (Sn(Oct)$_2$, 95%), succinic anhydride (SA, 99%), triethylamine

(Et$_3$N), N,N′-dicyclohexylcarbodiimide (DCC), 4-(N,N-dimethylamino)pyridine (DMAP), copper(I) bromide (CuBr, >99.99%), N,N,N′,N″,N″-pentamethyldiethylenetriamine (PMDETA, >98%), glutathione (GSH, a reduced form), Nile Red (NR), and doxorubicin hydrochloride (DOX, -NH$_3^+$Cl$^-$ forms, >98%) from Aldrich and DL-dithiothreitol (DTT, 99%) from Acros Organics were purchased and used as received. Oligo(ethylene oxide) monomethyl ether methacrylate (OEOMA) with MW = 300 g/mol and pendent EO units ≈5 was purchased from Aldrich and was purified by passing through a column filled with basic alumina to remove the inhibitors. 2-Hydroxyethyl-2′-(bromoisobutyryl)ethyl disulfide (HO-ss-iBuBr) was synthesized according to our previous publication.[155]

5.2.2 Instrumentation

^{1}H-NMR spectra were recorded using a 500 MHz Varian spectrometer. The CDCl$_3$ singlet at 7.26 ppm was selected as the reference standard. Molecular weight and molecular weight distribution were determined by gel permeation chromatography (GPC). An Agilent GPC was equipped with a 1260 Infinity Isocratic Pump and a RI detector. Two Agilent PLgel mixed-C and mixed-D columns were used with DMF containing 0.1 mol% LiBr at 50 °C at a flow rate of 1.0 mL/min. Linear poly(methyl methacrylate) standards from Fluka were used for calibration. Aliquots of the polymer samples were dissolved in DMF/LiBr. The clear solutions were filtered using a 0.25 μm PTFE filter to remove any solvent-insoluble species. A drop of anisole was added as a flow rate marker. Carboxylation, esterification, and monomer conversion were determined using ^{1}H-NMR. The size of micelles in hydrodynamic diameter by volume was measured by dynamic light scattering (DLS) at a fixed scattering angle of 175° at 25 °C with a Malvern Instruments Nano S ZEN1600 equipped with a 633 nm He-Ne gas laser. Fluorescence spectra on a Varian Cary Eclipse Fluorescence spectrometer and UV/Vis spectra on an Agilent Cary 60 UV/Vis spectrometer were recorded using a 1 cm wide quartz cuvette.

5.2.2.1 Transmission Electron Microscopy (TEM).

TEM images were obtained using a Philips Tecnai 12 TEM, operated at 120 kV and equipped with a thermionic LaB6 filament. An AMT V601 DVC camera with point to point resolution and line resolution of 0.34 nm and 0.20 nm respectively was used to capture images at

2048 by 2048 pixels. To prepare specimens, the micellar dispersions were dropped onto copper TEM grids (400 mesh, carbon coated), blotted and then allowed to air dry at room temperature.

5.2.3 Synthesis of ss(PLA-OH)$_2$

ss-DOH (0.11 g, 0.69 mmol), LA (10.0 g, 69.4 mmol), Sn(Oct)$_2$ (19.7 mg, 0.05 mmol), and toluene (6.7 mL) were added to a 10 mL Schlenk flask. The resulting mixture was deoxygenated by four freeze-pump-thaw cycles. The reaction flask was filled with nitrogen, thawed, and then immersed in an oil bath preheated at 120 °C to start the polymerization. After 2.5 hrs, the polymerization was stopped and cooled to room temperature. The resulting homopolymers were precipitated from cold MeOH (note that LA is soluble in MeOH). They were then isolated by vacuum filtration and further dried in a vacuum oven at room temperature overnight, resulting in white solid. Molecular weight (GPC-DMF/LiBr): M_n = 20,400 g/mol and M_w/M_n = 1.10.

5.2.4 Carboxylation to ss(PLA-COOH)$_2$

A clear solution consisting of the purified, dried ss(PLA-OH)$_2$ (2.5 g, 0.17 mmol) and Et$_3$N (1.04 g, 8.53 mmol) in anhydrous tetrahydrofuran (THF, 40 mL) was mixed with a solution of succinic anhydride (0.85 g, 8.53 mmol) in THF (10 mL) at 0 °C and then kept at room temperature for 12 hrs. The reaction mixture was filtered to remove the white solids that formed, and then the resulting homopolymers were purified by precipitation from 0.1 M aqueous HCl solution.

5.2.5 Esterification to ss(PLA-ss-Br)$_2$.

A mixture of ss(PLA-COOH)$_2$ (1.0 g, 71.9 μmol), HO-ss-iBuBr (65 mg, 0.22 mmol), DMAP (8.79 mg, 71.9 μmol), and dichloromethane (DCM, 9 mL) was mixed with a solution of DCC (0.16 g, 0.79 mmol) in DCM (1 mL) and stirred at room temperature for 12 hrs. The N,N′-dicyclohexylurea (DCU) that formed as a by-product was removed by vacuum filtration. Solvent was evaporated and the product was purified by precipitation from cold MeOH. The resulting white solids were dried in a vacuum oven at 35 °C for 15 hrs.

5.2.6 Synthesis of DL-ssABP.

ss(PLA-ss-Br)$_2$ (0.5 g, 0.036 mmol), OEOMA (0.22 g, 0.73 mmol), PMDETA (3.8 μL, 0.03 mmol), and THF (0.69 mL) were added to a 10 mL Schlenk flask. The resulting mixture was deoxygenated by three freeze-pump thaw cycles. The reaction flask was filled with nitrogen and CuBr (2.6 mg, 0.02 mmol) was added to the frozen solution. The flask was sealed, purged with vacuum and backfilled with nitrogen once. The mixture was thawed and the flask was then immersed in an oil bath preheated to 47 °C to start the polymerization. After 2 hrs, the polymerization was stopped by cooling and exposing the reaction mixture to air.

For purification, the as-prepared polymer solution was diluted with THF and passed through a basic alumina column to remove residual copper species. The solvent was removed under rotary evaporation at room temperature, and the polymer was isolated by precipitation from hexane, then dried under vacuum at room temperature for 15 hrs.

5.2.7 Reductive cleavage of disulfide linkages of DL-ssABP in DMF.

An aliquot of the dried, purified DL-ssABP (50 mg) was mixed with DTT (2.1 mg, 13.4 μmol) in DMF (10 mL) under stirring at room temperature. Aliquots were taken periodically to analyze molecular weight distribution of degraded products using GPC.

5.2.8 Aqueous micellization of DL-ssABP using solvent evaporation method.

Water (10 mL) was added drop-wise to a solution consisting of the purified, dried DL-ssABP (12.5 mg) dissolved in THF (1 mL). The resulting dispersion was stirred at room temperature for 24 hrs to form colloidally-stable micellar aggregates in aqueous solution at 1.2 mg/mL.

5.2.9 Determination of critical micellar concentration (CMC) using a Nile Red (NR) probe.

A stock solution of Nile Red (NR) in THF at 1 mg/mL and a stock solution of DL-ssABP in THF at 1 mg/mL were prepared. Water (10 mL) was added drop-wise into a series of mixtures consisting of the same amount of the stock solution of NR (0.5 mL, 0.5 mg NR) and various amounts of the stock solution of DL-ssABP in 20 mL vials. The resulting dispersions were stirred for 24 hrs to evaporate THF. The dispersions were then filtered using 0.45 μm PES filters to remove excess NR. A series of NR-loaded micelles at various concentrations of DL-ssABP

ranging from 5x10^{-6} to 0.4 mg/mL were formed. Their fluorescence spectra were recorded at λ_{max} = 600 nm.

5.2.10 Reductive-destabilization of aqueous DL-ssABP micelles.

Aliquots of aqueous micellar dispersion (1.2 mg/mL, 2 mL) were mixed with 10 mM GSH (6.1 mg, 20 µmol) under stirring. Aliquots were taken periodically to follow a change in size distribution by DLS.

5.2.11 Preparation of DOX-loaded micelles.

Water (10 mL) was drop-wise added to a solution consisting of the purified, dried DL-ssABP (20 mg), DOX (2 mg), and Et$_3$N (1.44 µL, 3 molar equivalents to DOX) in DMF (2 mL). The resulting dispersion was transferred into a dialysis tubing (MWCO = 3,500 g/mol) and dialyzed over water (800 mL) for 48 hrs, yielding DOX-loaded micelles in water at 1.1 mg/mL. To determine the loading level of DOX, aliquots of the DOX-loaded micellar dispersion (1 mL) were mixed with DMF (5 mL) and their UV/Vis spectra were recorded at λ_{ex} = 480 nm. DOX loading was calculated by the weight ratio of loaded DOX to dried polymers.

5.2.12 GSH-triggered release of DOX from aqueous DOX-loaded micelles.

An aliquot of DOX-loaded micellar dispersion (3 mL, 1.1 mg/mL) was transferred into a dialysis tubing (MWCO = 12,000 g/mol) and immersed in aqueous PBS solution (50 mL) as a control and 10 mM aqueous GSH buffered with PBS solution under stirring. The absorbance of DOX in outer water (50 mL) was recorded at 2 min interval using a UV/Vis spectrometer equipped with an external probe at λ = 497 nm. For quantitative analysis, DOX (38.9 µg, equivalent to DOX encapsulated in 3 mL DOX-loaded micelles) was dissolved in 10 mM aqueous GSH buffered with PBS solution (50 mL) and its UV/Vis spectrum was recorded.

5.2.13 Cell culture.

HeLa cancer cells were cultured in DMEM (Dulbecco's modified Eagle's medium) containing 10% FBS (fetal bovine serum) and 1% antibiotics (50 units/mL penicillin and 50 units/mL streptomycin) at 37 °C in a humidified atmosphere containing 5% CO_2.

5.2.14 Flow cytometry.

HeLa cells were plated at 5×10^5 cells/ well into a 6-well plate and incubated in DMEM (2 mL) at 37 °C. After 24 hrs, cells were treated with DOX-loaded DL-ssABP micelles (223.9 µL, DOX = 2.2 µg/mL) at 37 °C for 16 hrs. After the culture medium was removed, the cells were washed with PBS solution and treated with trypsin. The cells were suspended in DMEM (500 µL) for flow cytometry measurements. Data analysis was performed by means of a BD FACSCANTO II flow cytometer and BD FACSDiva software.

5.2.15 Confocal laser scanning microscopy (CLSM).

HeLa cells plated at 2×10^5 cells/ well into a 6-well plate and incubated for 24 hrs in DMEM (2 mL) were treated with DOX-loaded micelles (DOX = 2.2 µg/mL) at 37 °C for 16 hrs. After culture medium was removed, cells were washed with PBS buffer three times. After the removal of supernatants, the cells were fixed with cold methanol (-20 °C) for 20 min at 4 °C. The slides were rinsed five times with PBS solution and three times with TBST (tris-buffered saline Tween-20). Cells were stained with 2-(4-amidinophenyl)-1H-indole-6-carboxamidine (DAPI). The fluorescence images were obtained using a LSM 510 Meta/Axiovert 200 (Carl Zeiss, Jena, Germany).

5.2.16 Cell viability using MTT assay.

HeLa cells were plated at 5×10^5 cells per well into a 96-well plate and incubated for 24 hrs in DMEM (100 µL) containing 10 % FBS and 1 % antibiotics. Then, they were incubated with various concentrations of empty (DOX-free), free DOX, and DOX-loaded micelles of DL-ssABP for 48 hrs. Blank controls without micelles (cells only) were run simultaneously as control. Cell viability was measured using CellTiter 96 Non-Radioactive Cell Proliferation Assay kit (MTT, Promega) according to the manufacturer's protocol. Briefly, 3-(4,5-dimethylthiazol-2-yl)-2,5-diphenyltetrazolium bromide (MTT) solutions (15 µL) was added into each well. After 4 hrs incubation, the medium containing unreacted MTT was carefully removed. DMSO (100 µL) was added into each well in order to dissolve the formed formazan purple crystals, and then the absorbance at $\lambda = 570$ nm was recorded using Powerwave HT Microplate Reader (Bio-Tek). Each concentration was 12-replicated. Cell viability was calculated as the percent ratio of absorbance of mixtures with micelles to control (cells only).

5.3 Results and Discussion

5.3.1 Synthesis and reduction-responsive degradation of DL-ssABP.

Scheme 5.2 illustrates our approach to synthesize POEOMA-ss-PLA-ss-PLA-ss-POEOMA having disulfide linkages positioned both in the middle of triblock copolymer and at the block junctions.
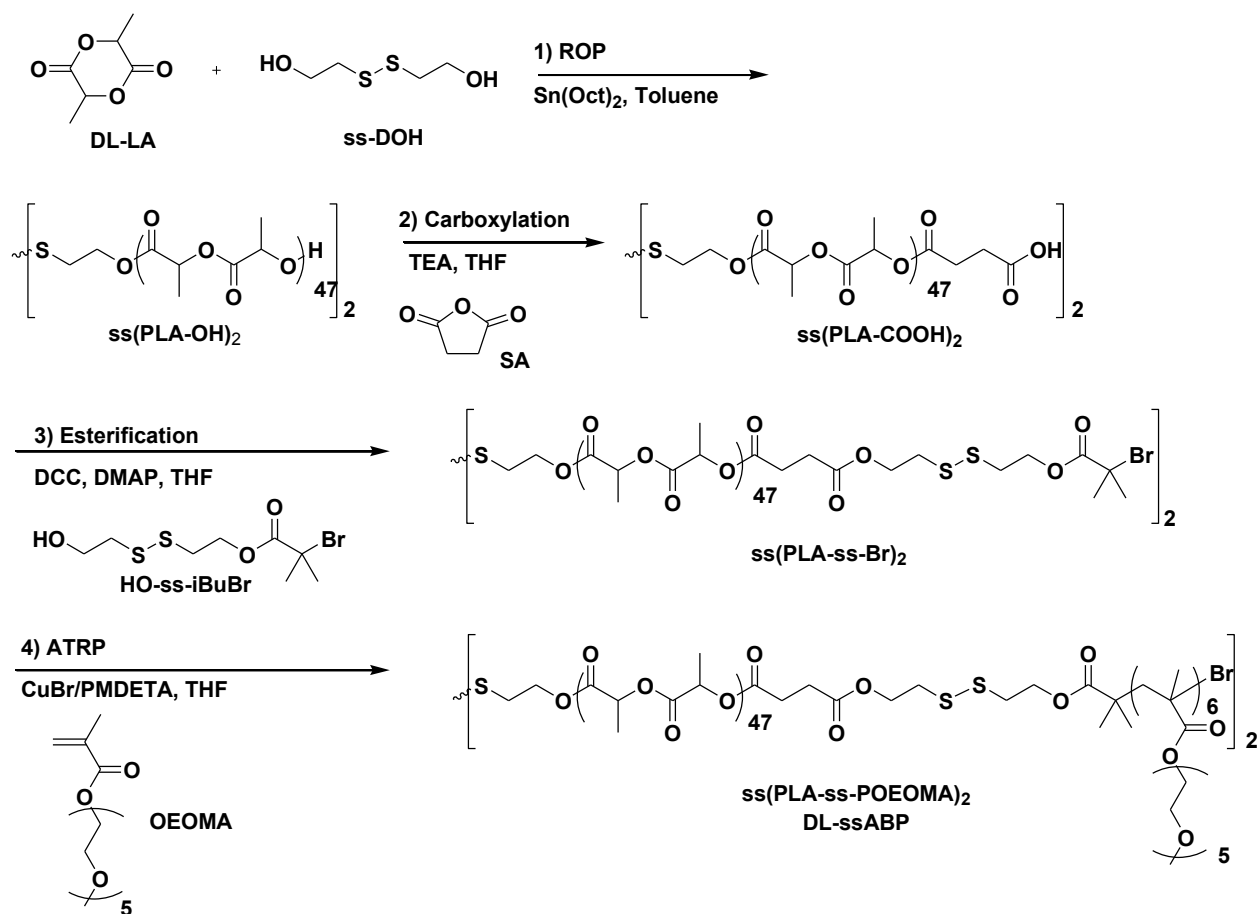
Scheme 5.2. Synthesis of a reduction-responsive dual location disulfide degradable DL-ssABP triblock copolymer by a combination of ring opening polymerization, coupling reactions, and atom transfer radical polymerization.

The first step is the synthesis of well-controlled ss(PLA-OH)$_2$ by ring opening polymerization (ROP) of LA initiated with ss-DOH at 120 °C in toluene. The detailed procedure is described in our previous report.[145] Here, the resulting ss(PLA-OH)$_2$ had a number average

molecular weight, M_n = 20,400 g/mol with M_w/M_n = 1.10 determined by gel permeation chromatography (GPC) (Figure 5.1) and a degree of polymerization (DP) = 94 determined by ^{1}H-NMR (Figure 5.2a). The second step is the carboxylation of ss(PLA-OH)$_2$ with excess SA in anhydrous THF, converting the ss(PLA-OH)$_2$ to ss(PLA-COOH)$_2$. ^{1}H-NMR was used to follow the reaction conversion. As seen in Figure 5.2b, the multiplet at 4.3-4.4 ppm (e) corresponding to terminal methine protons in the backbone of PLA chains disappeared, while the peaks at 2.6-2.8 ppm (f, g), corresponding to methylene protons of succinic moiety, appeared as a consequence of the carboxylation. From the integral ratio of peaks [(b/2)/{(f+g)/4}], the conversion was calculated to be >95%. The third step is the esterification of the purified, dried ss(PLA-COOH)$_2$ by a facile carbodiimide coupling reaction with a double-head initiator (HO-ss-iBuBr), yielding a brominated ss(PLA-ss-Br)$_2$. As seen in Figure 5.2c, a singlet at 1.95 ppm (l) corresponding to six methyl protons in terminal iBuBr moieties appeared as a result of the successful bromination. From the integral ratio of peaks [(b/2)/(l/6)], the conversion was also calculated to be >98%.
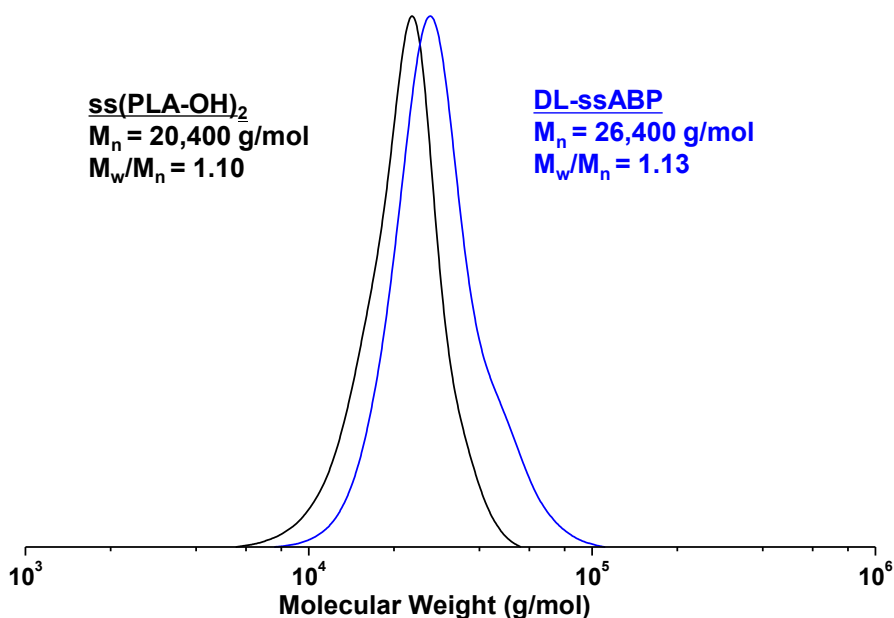
Figure 5.1. GPC traces of DL-ssABP, compared with ss(PLA-OH)$_2$ precursor.
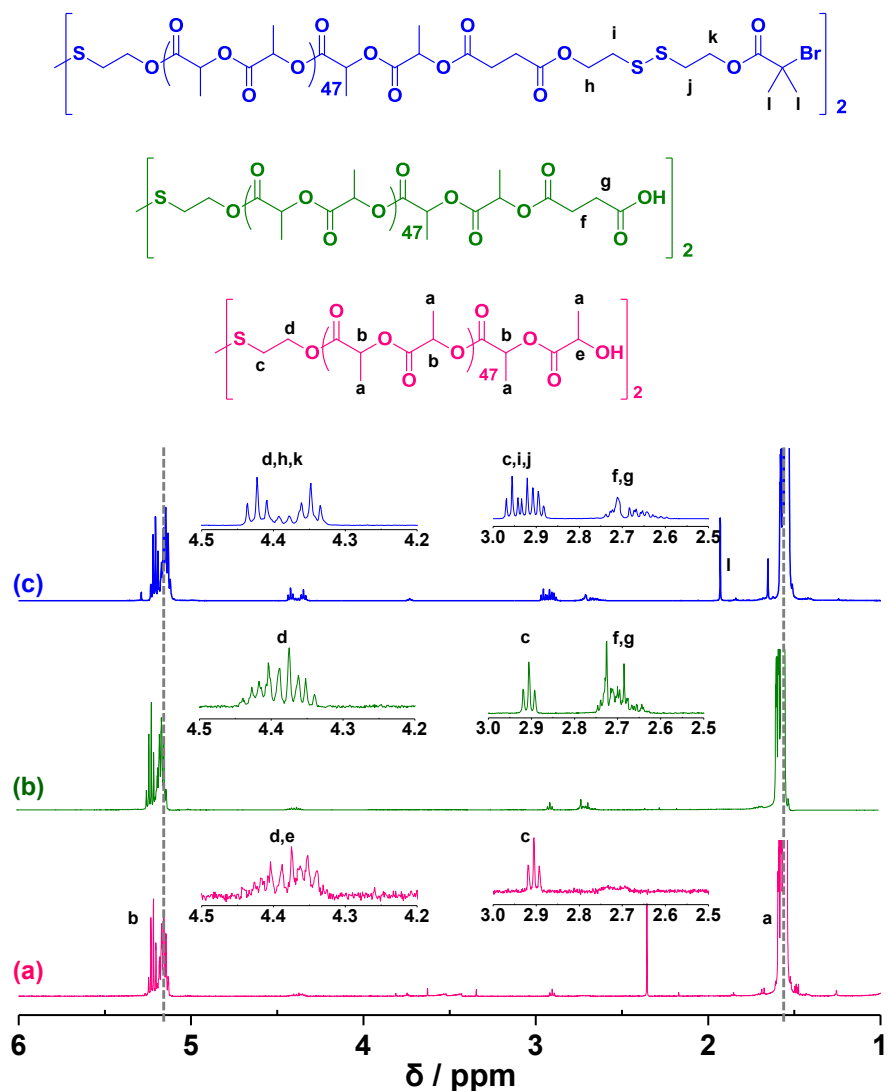
Figure 5.2. ^{1}H-NMR spectra of ss(PLA-OH)$_2$ (a), ss(PLA-COOH)$_2$ (b), and ss(PLA-ss-Br)$_2$ (c) in CDCl$_3$.

The last step is the chain extension of ss(PLA-ss-Br)$_2$ with water-soluble POEOMA using atom transfer radical polymerization (ATRP).[137] The ATRP conditions include [OEOMA]$_0$/[ss(PLA-ss-Br)$_2$]$_0$/[CuBr/PMDETA]$_0$ = 20/1/0.5 in THF at 47 °C. After 2 hrs, conversion from OEOMA to POEOMA was determined to be 60 % using ^{1}H-NMR. The resulting DL-ssABP triblock copolymer had M_n =26,400 g/mol with M_w/M_n = 1.13 by GPC (Figure 5.1). ^{1}H-NMR indicates the DP of POEOMA block = 12 calculated from the integral ratio of the peaks [(b/2)/(p/3)] (Figure 5.3). These results suggest the successful synthesis of

well-defined POEOMA$_6$-ss-(PLA$_{47}$-ss-PLA$_{47}$)-ss-POEOMA$_6$ triblock copolymers with disulfide linkages in the middle of the hydrophobic block and at block junctions.
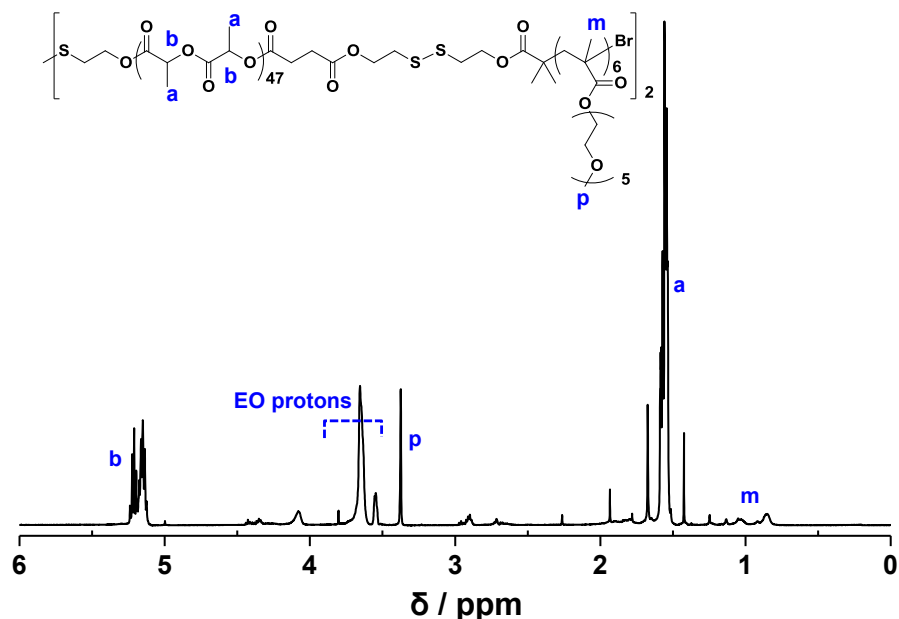
Figure 5.3. ^{1}H-NMR spectrum of DL-ssABP in CDCl$_3$. Conditions for ATRP: [OEOMA]$_0$/[ss(PLA-ss-Br)$_2$]$_0$/[CuBr/PMDETA]$_0$ = 20/1/0.5; OEOMA/THF = 0.4/1 wt/wt in THF at 47 °C.

The resulting DL-ssABP contains a single disulfide linkage in the middle of the triblock copolymer and two disulfides at block junctions. Figure 5.4a illustrates the reduction-responsive cleavage of the three disulfide linkages in DL-ssABP to the corresponding thiols; HS-PLA-SH and POEOMA-SH. Aliquots of DL-ssABP were mixed with DTT (5 mole equivalent to disulfides) in DMF as a homogeneous solution under stirring and GPC was used to follow the cleavage of the disulfide linkages. As seen in Figure 5.4b, the GPC trace of DL-ssABP is shifted to low molecular weight region following treatment with DTT. Molecular weight decreased with incubation time and reached a plateau after 2 hrs, as a result of the cleavage of disulfide linkages at dual locations (Figure 5.5).
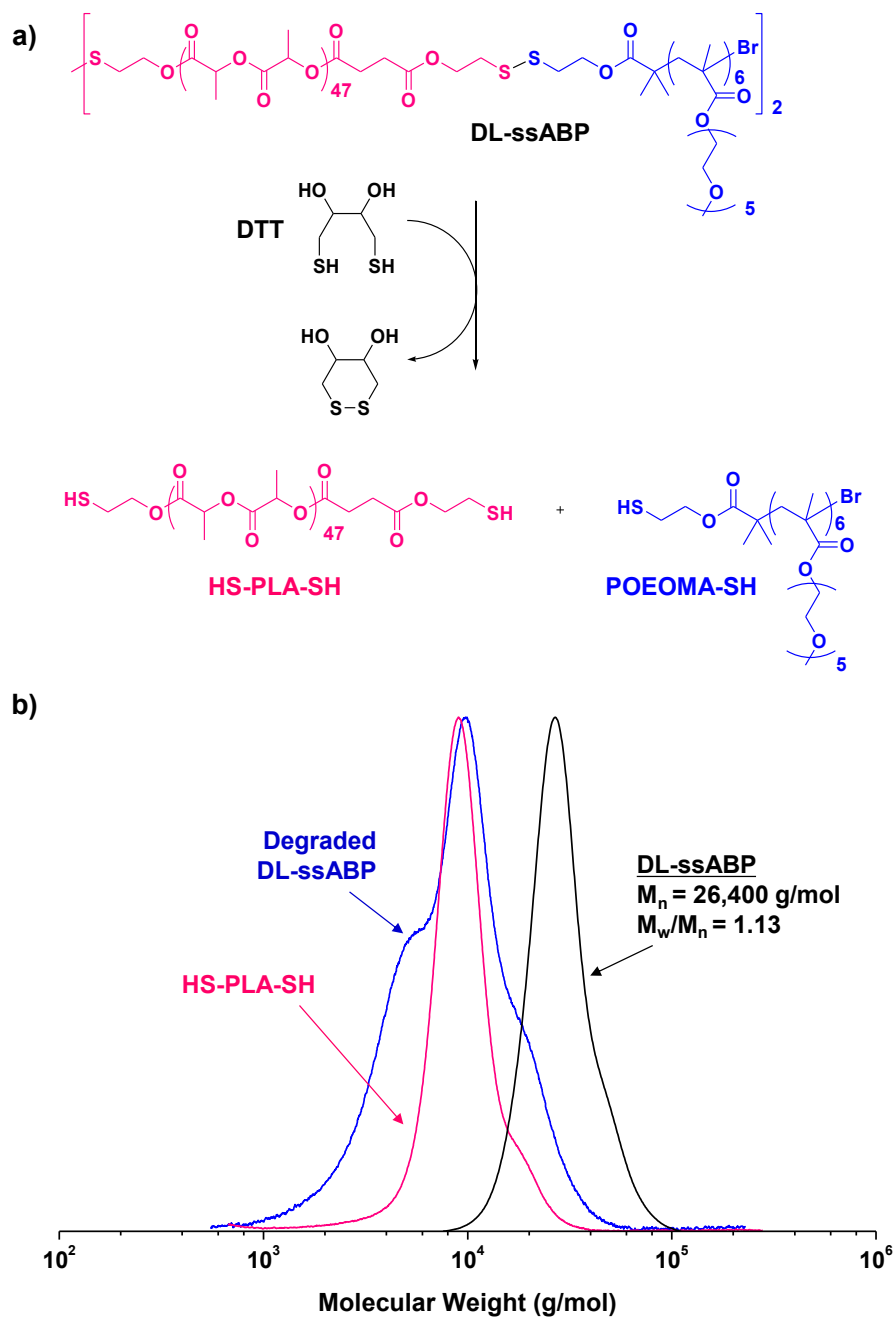
Figure 5.4. Reduction-responsive cleavage of disulfides of DL-ssABP in the presence of DTT (a) and GPC trace of degraded DL-ssABP after treatment with DTT in DMF, compared with DL-ssABP and HS-PLA-SH (b). Note that HS-PLA-SH is a degraded product of ss(PLA-ss-Br)$_2$ upon reductive cleavage of the disulfide linkages in DMF containing excess DTT for 2 hrs.
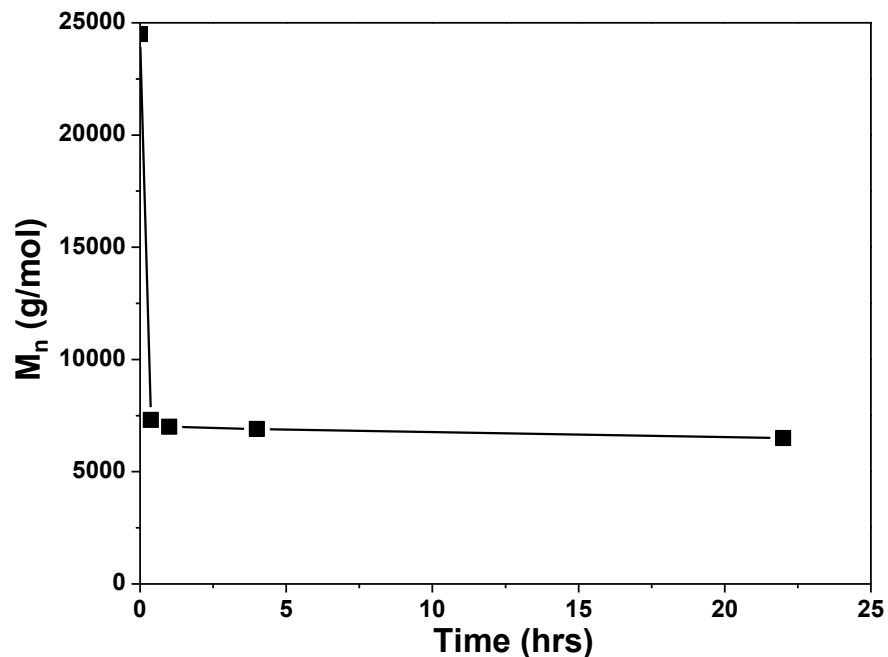
Figure 5.5. Evolution of molecular weights of DL-ssABP mixed with DTT (5 mole equivalents to disulfide linkages) over incubation time.

5.3.2 Aqueous micellization and disassembly of DL-ssABP.

The resulting DL-ssABP is amphiphilic, consisting of a hydrophobic PLA middle block and hydrophilic POEOMA blocks. Its CMC was first determined using fluorescence spectroscopy with a NR probe.[181] A series of mixtures consisting of the same amount of NR in various concentration of DL-ssABP ranging from $5x10^{-6}$ to 0.4 mg/mL in aqueous solution were prepared. After the removal of THF by evaporation and excess NR by filtration (0.45 µm PES filter), their fluorescence spectra were recorded (Figure 5.6a). The method is based on the fact that the fluorescence intensity of NR increases when more NR is entrapped in hydrophobic PLA core, while it decreases in water due to low solubility of NR in water. From the linear regressions of fluorescence intensity at λ_{max} = 600 nm, the CMC of DL-ssABP was determined to be 43 µg/mL (Figure 5.6b).
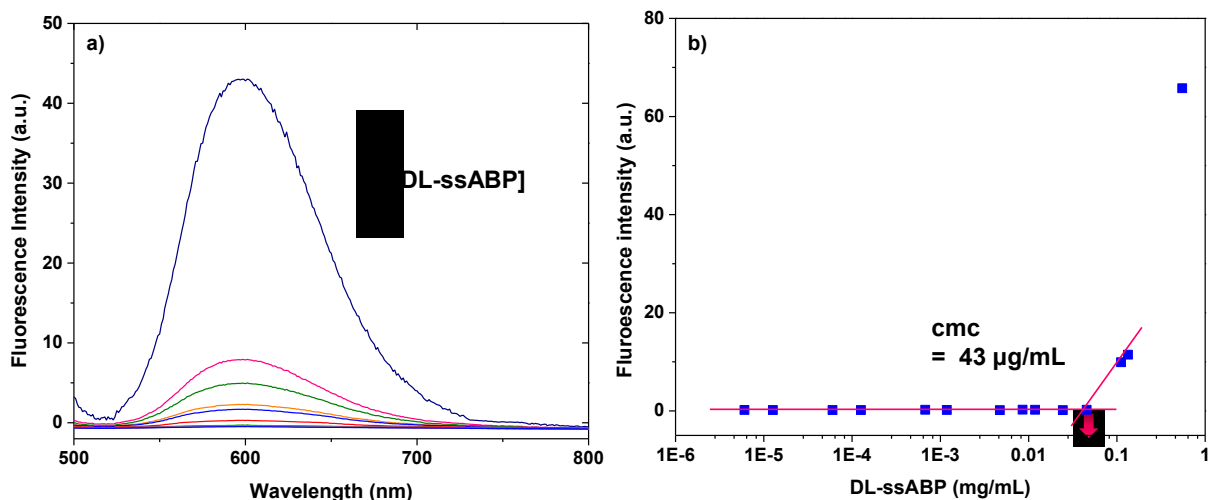
Figure 5.6. Overlaid fluorescence spectra of Nile Red at various concentrations of DL-ssABP (a) and evolution of fluorescence intensity at 600 nm over concentrations of DL-ssABP to determine CMC (b).

At concentrations above the CMC, DL-ssABP self-assembles through aqueous micellization to form micellar aggregates consisting of hydrophobic PLA cores surrounded with hydrophilic POEOMA coronas. For example, aqueous self-assembled aggregates were prepared using a solvent evaporation method at a concentration of 1.2 mg/mL and their size and morphology were examined using DLS and TEM. DLS results indicate a hydrodynamic diameter of ≈55 nm with a monomodal size distribution (Figure 5.7a). TEM images indicate an average diameter of 30.4 ± 6.5 nm with relative broad size distribution (Figure 5.7b), which is smaller than the size determined by DLS. The difference in micelle sizes between DLS and TEM can be attributed to the dehydrated state of the micelles.[157]

The self-assembled DL-ssABP micelles are composed of disulfide linkages in the dual locations positioned in the PLA cores and PLA/POEOMA interfaces. These disulfide linkages can be cleaved in response to reductive reactions, causing destabilization (or disassembly) of micelles. As seen in Figure 5.7c and 5.7d, both DLS and TEM results indicate the increase in micelle size with multimodal distribution in the presence of 10 mM GSH (a cellular reducing agent) after 20 hrs. The occurrence of aggregation is attributed to both hydrophobicity of cleaved HS-PLA-SH chains and amphiphilicity of cleaved POEOMA-SH chains generated upon the cleavage of disulfide linkages in the dual locations. Similar results about the occurrence of

aggregation in the presence of reducing agents have been reported for polyester-based block copolymer micelles having multiple disulfide linkages positioned in the main chains.[174a]
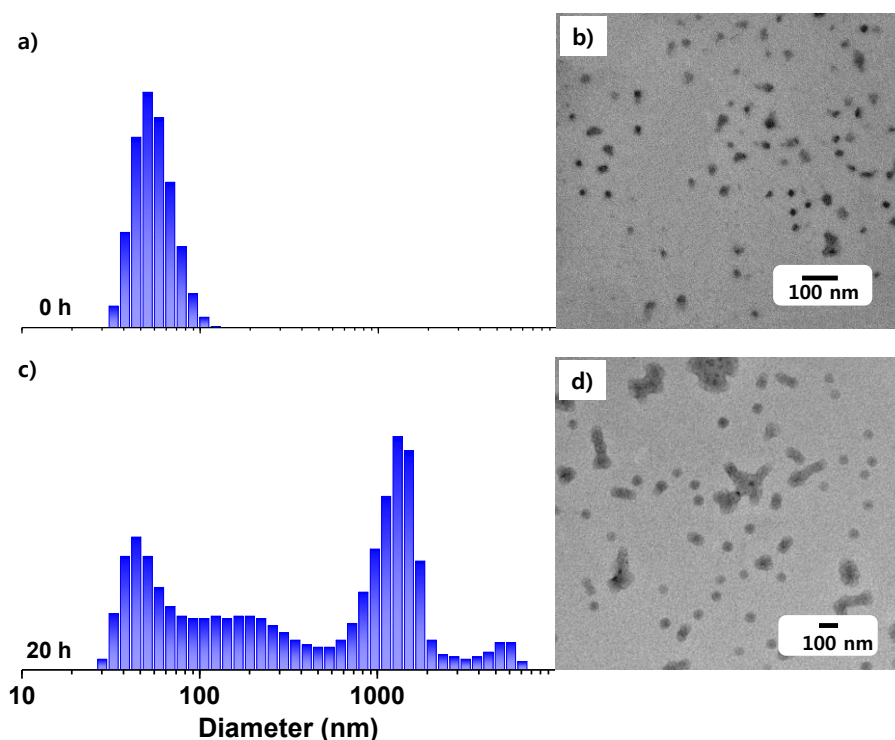
Figure 5.7. DLS diagrams (a, c) and TEM images (b, d) of DL-ssABP micelles before (a, b) and after (c, d) treatment with 10 mM GSH at 1.2 mg/mL.

5.3.3 Loading and GSH-triggered DOX release.

The resulting DL-ssABP based micelles were evaluated for enhanced release of encapsulated anticancer drugs in the presence of GSH. To prepare DOX-loaded micelles using a dialysis method, an aliquot of DOX ($NH_3^+Cl^-$ forms) was pretreated with Et_3N (3 mole equivalents) in DMF for deprotonation in order to increase its solubility in the hydrophobic micellar core. The organic mixture was transferred into a dialysis tubing and then dialyzed in water over two days to remove DMF and free (not encapsulated) DOX. Using UV/Vis spectroscopy with the pre-determined extinction coefficient of DOX = 12,400 $M^{-1}cm^{-1}$ in a mixture of water/DMF = 1/5 v/v at λ = 497 nm,[179] the loading level of DOX was determined to be 2.2 ± 0.5 wt% at the initial ratio of DOX/polymer = 1/10 wt/wt.

Next, GSH-responsive release of DOX from DOX-loaded micelles was examined in the absence (control) and presence of 10 mM GSH in PBS solution. DOX can diffuse through the dialysis tubing after GSH-triggered release from DOX-loaded micelles. Its UV absorbance corresponding to accumulation of released DOX in the outer solution was monitored over time using a UV spectrometer equipped with an external probe at $\lambda = 497$ nm. As compared in Figure 5.8, the DOX release from DL-ssABP micelles was faster in the presence of 10 mM GSH than without GSH. For example, within 5 hrs, the release reached >80 % in the presence of 10 mM GSH, while <20% in the absence of GSH. Further, the apparent diffusion coefficient of DOX from DL-ssABP micelles was calculated to be 1.89/h within 30 min, which is much larger than 0.17/h, showing an early burst release of encapsulated DOX (around 60 %) in the presence of GSH. The enhanced and early burst release is presumably attributed to the reductive cleavage of disulfide linkages in dual locations as at both the micellar cores and the interfaces. In comparison to monocleavable micelles having single disulfides in the middle of triblock copolymers, the model release kinetics of our system is significantly more rapid.[128b, 128e, 145]
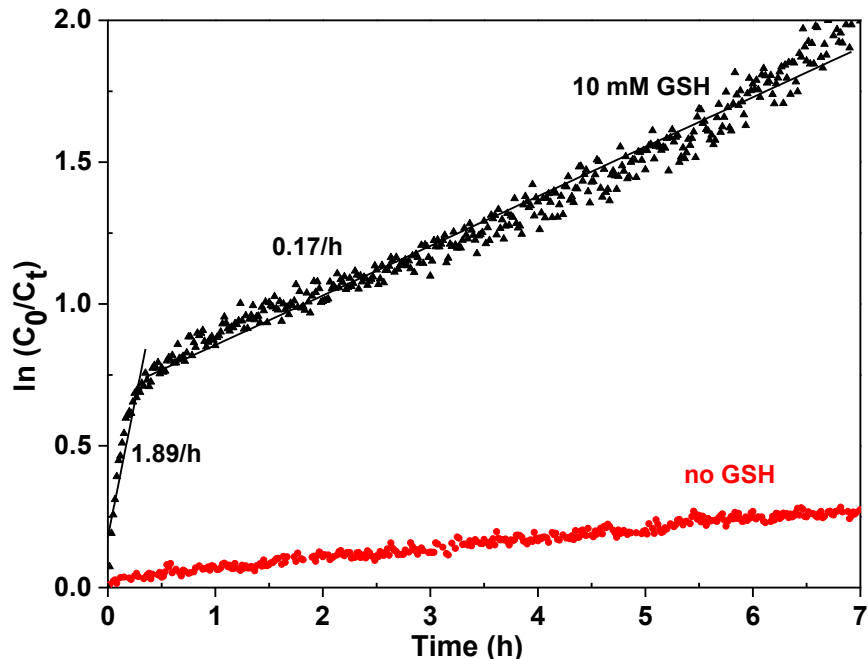
Figure 5.8. Enhanced release of DOX from DOX-loaded DL-ssABP micelles in the absence (control) and presence of 10 mM GSH. The apparent diffusion coefficients of DOX released from DOX-loaded micelles are calculated from the slopes obtained by fitting the data to a linear regression.

5.3.4 Intracellular release and antitumor activity.

Given a promising result, the DL-ssABP-based micelles were evaluated as effective intracellular drug delivery nanocarriers. Intracellular trafficking of DOX from DOX-loaded DL-ssABP micelles were examined using flow cytometry and CLSM. Figure 5.9a shows the flow cytometric histogram of HeLa cells incubated with DOX-loaded micelles and free DOX. Note that the amount of free DOX was designed to be the same as that encapsulated in DOX-loaded micelles. Compared with HeLa cells only as a control, their histograms presented a noticeable shift in the direction of high fluorescence intensity. Figure 5.9b shows CLSM images of HeLa cells with and without DOX-loaded micelles and free DOX for 16 hrs. HeLa nuclei were stained with DAPI. Obviously, HeLa cells incubated with DOX-loaded DL-ssABP micelles displayed strong DOX fluorescence in their nuclei. These results from both flow cytometry and CLSM confirm that DOX-loaded DL-ssABP micelles are able to delivery and release DOX into the nuclei of cancer cells. Compared to the images from free DOX which is brighter, the images from DOX-loaded micelles suggest that GSH-responsive DOX release may delay an access to targeted nuclei. In biological systems, cellular GSH-OEt can penetrate cellular membranes and rapidly reach a high intracellular concentration of GSH.[182] Several reports investigated that the pre-treatment of cancer cells with GSH-OEt enhance cellular GSH levels. In other words, compared with no pre-treatment, the intracellular DOX release results suggest that DOX could be released from DOX-loaded micelles after uptake.[72, 128a, 134a, 176d]
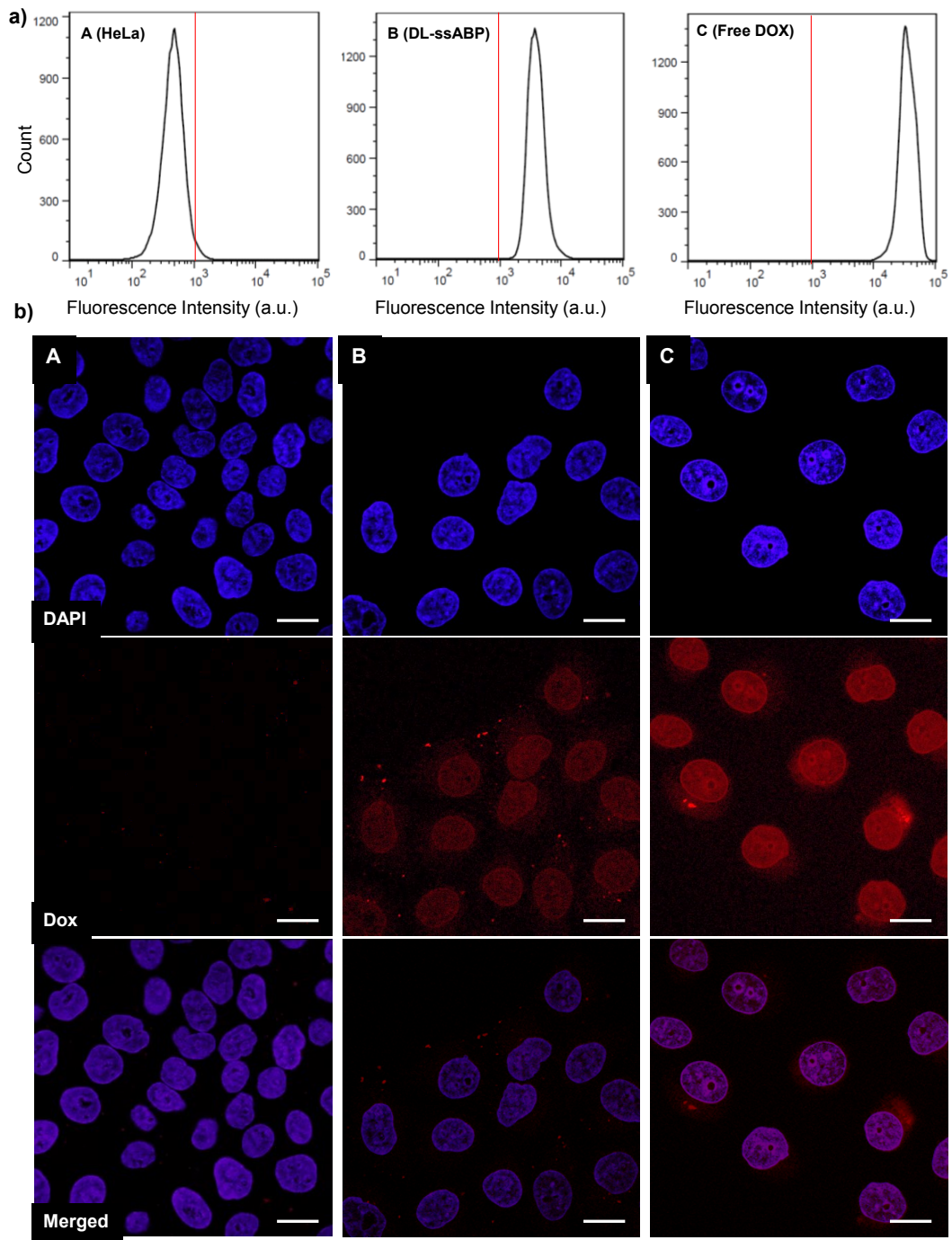
Figure 5.9. Flow cytometric histograms (a) and CLSM images (b) of HeLa cells only (A) and incubated with DOX-loaded DL-ssABP micelles (B), and free DOX (C) for 16 hrs. Scale bar = 20 μm.

In vitro cytotoxicity of DOX-free (empty) and DOX-loaded micelles based on DL-ssABP was compared with free DOX as a control using a MTT colorimetric assay. As seen in Figure 5.10a, empty micelles exhibited >90 % of HeLa cell viability, suggesting non-cytotoxicity of DL-ssABP micelles at concentrations up to 500 μg/mL. In the presence of DOX-loaded micelles, however, the HeLa cell viability decreased with an increasing concentration of DOX-encapsulated micelles (Figure 5.10b). For example, the viability was <50% at 1.4 μg/mL, which is competitive or lower than the reported other block copolymer-based nanocarriers to HeLa cells.[128a, 133c, 159] It further decreased to <5% at 15 μg/mL.[183] This decrease in HeLa cell viability suggests the inhibition of cellular proliferation due to the effective and rapid release of DOX from DL-ssABP platform. This is a consequence from the degradation of dual-located disulfide linkages in response to intracellular GSH inside cancer cells. Compared with DOX-loaded micelles, the HeLa cell viability in the presence of free DOX is lower at the same concentrations. These results are consistent with those obtained from flow cytometry and CLSM described above.
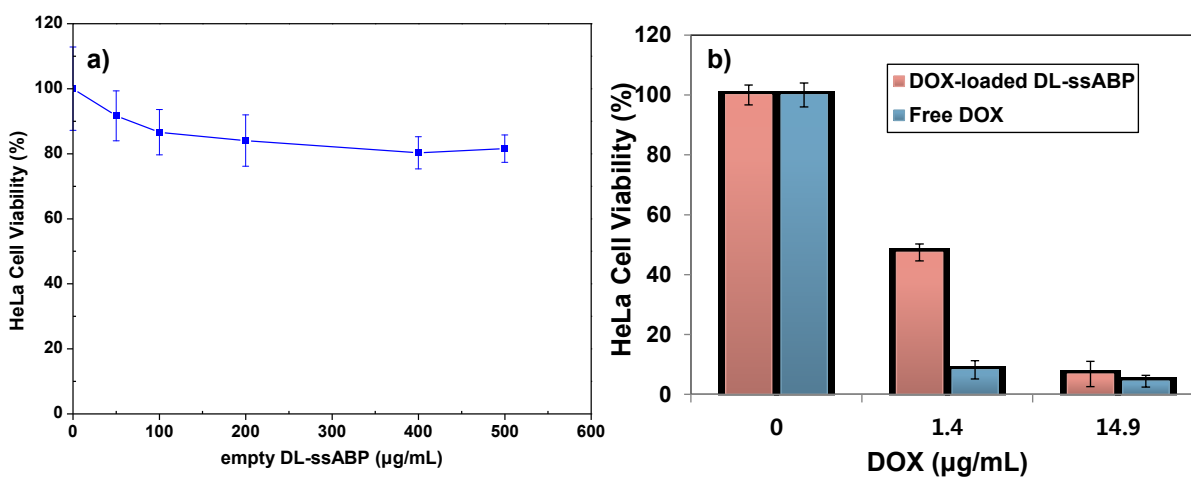
Figure 5.10. Viability of HeLa cells incubated with different amounts of empty (Dox-free) micelles (a) and free DOX and DOX-loaded micelles (b) for 48 hrs determined by MTT assay. Data are presented as the average ± standard deviation (n = 12).

5.4 Conclusion

Novel PLA-based DL-ssABPs having both a single disulfide in the middle of hydrophobic PLA block and two disulfides at PLA/hydrophilic POEOMA block junctions were synthesized by a combination method of well-defined organic and polymeric syntheses including ROP, facile coupling reactions, and ATRP. The DL-ssABP and its precursors prepared in each synthetic step, as well as the degraded products generated by the cleavage of the disulfides positioned in dual locations were well-characterized their molecular composition by ^{1}H-NMR and molecular weights by GPC. Above the CMC, 43 µg/mol, the DL-ssABP self-assembled to form colloidally-stable micellar aggregates having disulfides in dual locations; in the hydrophobic core and at the PLA/POEOMA interface. After the cleavage of dual-located disulfide linkages in response to GSH cellular trigger, sheddable POEOMA coronas were released from the PLA core as well as disintegrated the hydrophobic PLA core, causing destabilization of the micelles. Such a disassembly enabled the early burst and then a sustained enhanced release of encapsulated anticancer drugs. These results, combined with the intracellular release of anticancer drugs confirmed by CLSM, flow cytometry, and MTT viability, suggest that the dual-located location disulfide degradation strategy accelerated the release of encapsulated model drugs from the micelles.

Chapter 6

Air-spun PLA nanofibers modified with reductively-sheddable hydrophilic surfaces for vascular tissue engineering : synthesis and surface modification
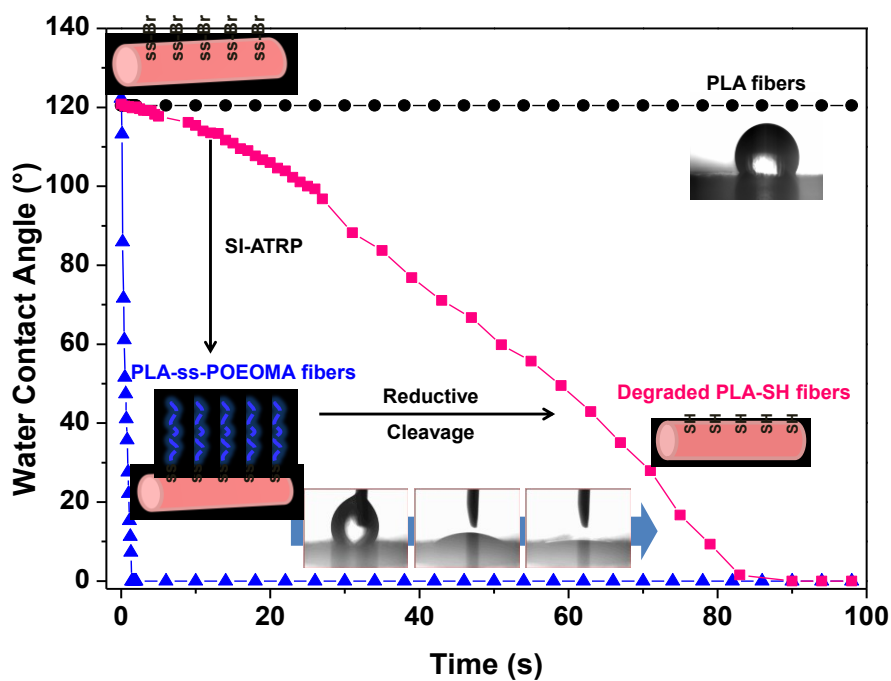
Polylactide is a class of promising biomaterials that hold a great promise for various biological and biomedical applications, particularly, vascular tissue engineering as fibrous mesh to coat inside vascular prosthesis. However, their hydrophobic surface to non-specific interactions and limited ability to further modification are challenging. Chapter 6 reports the development of new air-spun PLA nanofibers modified with hydrophilic surfaces exhibiting reduction response. Surface-initiated atom transfer radical polymerization allows for grafting pendant oligo(ethylene oxide)-containing polymethacrylate (POEOMA) from PLA air-spun fibers labeled with disulfide linkages. The resulting POEOMA-g-PLA fibers exhibit enhanced

thermal stability and improved surface properties, as well as thiol-responsive shedding of hydrophilic POEOMA by the cleavage of disulfide linkages in response to reductive reactions, thus tuning the surface properties.

This chapter is reproduced the article published in *Macromolecular rapid communications*, **2014**, *35*(4)*, 447-453 with permission from the publisher.

6.1 Introduction

Polylactide (PLA), along with polycaprolactone and polyglycolide, is a class of hydrophobic aliphatic polyesters based on hydroxyalkanoic acids.[136, 180b] These polyesters are biocompatible, biodegradable by enzymatic reactions or hydrolysis in physiological conditions, and used in FDA-approved medical devices. They also exhibit low immunogenicity and good mechanical properties. Being facilitated with these biological properties, PLA and their copolymers are processed to various formats;[146a] a promising format is nanofibers fabricated by electrospinning or air-spinning, efficient processing methods to manufacture long fiber structures. Air-spinning is an alternative process to classical electrospinning, based on stretching of polymer solutions with a high speed air flow. These fibrous materials possess large surface areas, high porosity, and interconnected network structures. These unique properties have promoted the use of PLA-fibers as useful biomaterials as sutures, implants for bone fixation,[144a] drug delivery vehicles,[184] and tissue engineering scaffolds.[185] Recently, air-spun PLA-fibers have found their applications as biomaterials to coat luminal wall of commercial vascular grafts in vascular surgery.

Vascular grafts are used to replace, bypass, or maintain function of damaged, occluded or diseased blood vessels in small, medium and large diameter. Poly(ethylene terephthalate) (PET) is one of the commercially-available materials for textile vascular prostheses. PET is usually coated with proteins such as gelatin or collagen to prevent blood loss through prosthesis wall.[186] A drawback for the impregnation of proteins involves a dramatic decrease in patency rate with smaller diameters.[187] The use of PLA-based nanofibrous mesh enable to circumvent the problem as well as promote good endothelial cell proliferation in monolayers on the PLA-fiber mesh.[188] Despite these advances, however, several challenges for the use of conventional PLA-fiber mesh to be addressed remain. One challenge is their hydrophobic surface causing non-specific interactions with proteins in the blood. Another challenge involves their limited ability to further conjugation or modification of their surfaces due to their lack of functionalities. Surface modification of PLA nanofibrous materials with chemical functions, desirably hydrophilicity, or biomolecules could strongly enhance their applicability toward the successful vascular tissue engineering applications.

Several approaches to surface modification of nanofibrous materials have been reported. Click-type orthogonal reactions have been used for enhanced specific protein adhesion[189] and anti-fouling properties.[190] Surface-initiated (SI) atom transfer radical polymerization (ATRP)[137a] has also been explored. The SI-ATRP technique allowed for adjusting the surface properties of fibrous materials of polystyrene, PET, PLA, and cellulose. This "grafting from" method was conducted directly from bromine-terminated polystyrene fibers in aqueous solution.[191] However, for most of the fibrous materials, post-immobilization of small molecular weight ATRP initiating species into as-synthesized fibers through either physical absorption[192] or covalent attachment is required prior to SI-ATRP.[193]

Stimuli-responsive degradation (SRD) is a dynamic and powerful platform that involves the cleavage of covalent bonds in response to external stimuli.[123a, 125b] Particularly, disulfides are cleaved to the corresponding thiols in response to reductive reactions,[126a] enabling enhanced release,[172b] changing morphologies,[124a] or tuning lower critical solution temperature.[194] This unique disulfide-thiol chemistry has been explored to develop a variety of reductively-responsive degradable nanomaterials desirable for various biomedical applications. Typical examples include self-assembled micellar nanocarriers,[195] nanocapsules,[196] nanogels,[197] hydrogels,[198] and bioconjugates.[199] Further, PLA fibers modified with sheddable hydrophilic polymers that can undergo reductively-responsive cleavage would be interesting as smart coating materials in constructing PET-based vascular prostheses with tunable surfaces of hydrophobicity and hydrophilicity.

Herein, we report new air-spun PLA nanofibers whose surfaces are modified with reductively-sheddable hydrophilic surfaces as versatile coating biomaterials for vascular surgery. Scheme 6.1 illustrates our approach to synthesis and surface modification of reductive-responsive PLA fibers labeled with disulfide linkages. High molecular weight PLA-ss-Br homopolymers were first synthesized by ring opening polymerization (ROP) in the presence of a double-head initiator labeled with a disulfide (HO-ss-iBuBr) and then processed to PLA-ss-Br fibers by air-spinning. As a proof-of-concept approach, pendant oligo(ethylene glycol)-containing polymethacrylate (POEOMA) was targeted to modify the surfaces of air-spun PLA fibers using a direct SI-ATRP to be hydrophilic. POEOMA is an analog of poly(ethylene oxide) (PEO); PEO is biocompatible material that has been FDA-approved for clinical use, has low toxicity, and prevents nonspecific protein adsorption.[200] The successful grafting of POEOMA

from PLA fibers enabled improved thermal stability and surface properties. Further, the reductive cleavage of disulfide linages resulted in shedding hydrophilic POEOMA from POEOMA-g-PLA fibers, adjusting their surface properties.
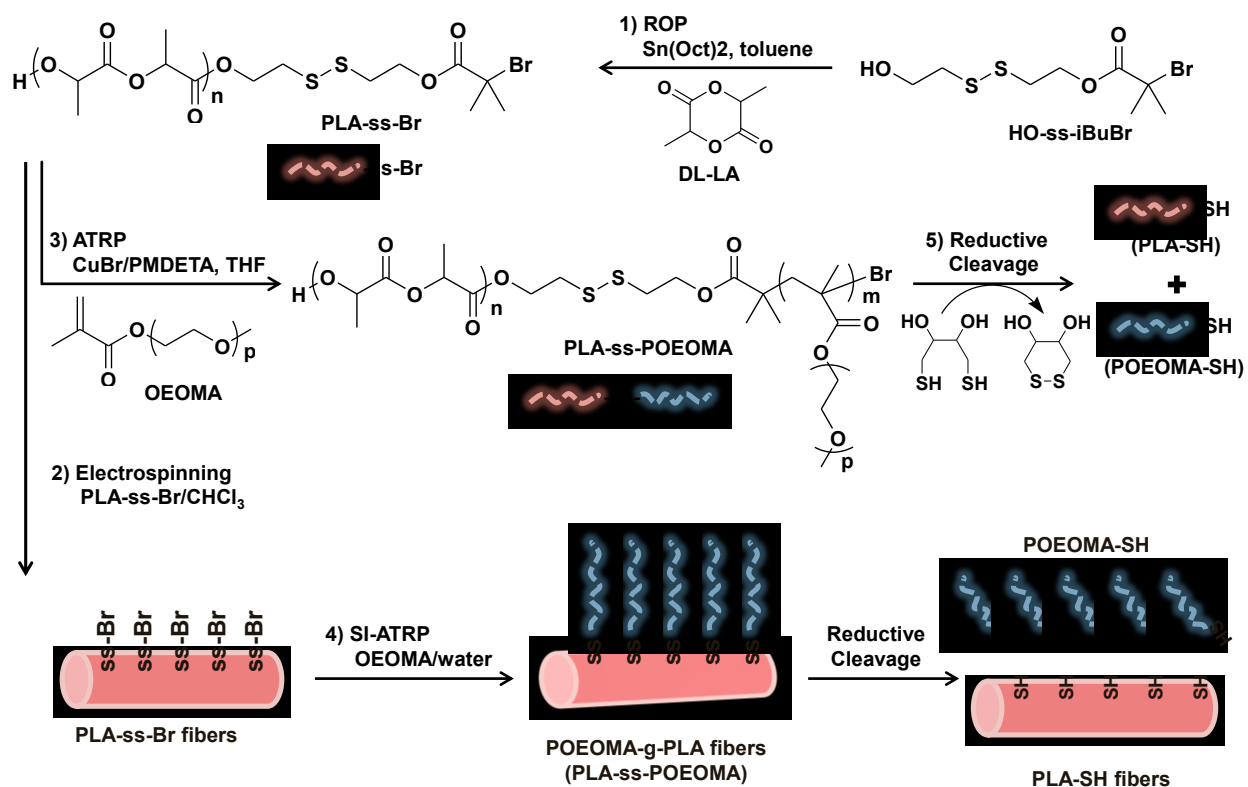
Scheme 6.1. Illustration of our approach to synthesize reductively-sheddable POEOMA-g-PLA fibers based on PLA-ss-POEOMA block copolymers having disulfides at block junctions using surface-initiated atom transfer radical polymerization of OEOMA in the presence of PLA-ss-Br fibrous macroinitiators and their degradation in response to reductive reactions.

6.2 Experimental section

6.2.1 Materials

3,6-Dimethyl-1,4-dioxane-2,5-dione (DL-lactide, LA), tin(II) 2-ethylhexanoate (Sn(Oct)$_2$, 95%), *N,N,N′,N″,N″*-pentamethyldiethylenetriamine (PMDETA, >98%), copper(I) bromide

(CuBr, >99.99%), and poly(ethylene oxide monomethyl ether) (PEOH) with MW = 2,000 g/mol from Aldrich and DL-dithiothreitol (DTT, 99%) from Acros Organics were purchased and used as received. Oligo(ethylene glycol) monomethyl ether methacrylate (OEOMA) with MW = 300 g/mol (#EO units ≈ 5) for OEOMA300 and MW = 950 g/mol (#EO units ≈ 23) for OEOMA950 were purchased from Aldrich and purified by passing them through a column filled with basic alumina to remove the inhibitors. 2-Hydroxyethyl-2′-(bromoisobutyryl)ethyl disulfide (HO-ss-iBuBr) was synthesized as described elsewhere.[29a] Tris(2-pyridylmethyl)amine (TPMA) was synthesized according to literature procedure.[201]

6.2.2 Instrumentation and analysis

^{1}H-NMR spectra were recorded using a 500 MHz Varian spectrometer. The $CDCl_3$ singlet at 7.26 ppm was selected as the reference standard. Molecular weight and molecular weight distribution were determined by gel permeation chromatography (GPC) with an Agilent 1260 Infinity Isocratic Pump and a refractive index (RI) detector. Two Agilent columns (PLgel mixed-D and mixed-C) were used with DMF containing 0.1 mol% LiBr at 50 °C at a flow rate of 1.0 mL/min. Linear polystyrene (PSt) standards were used for calibration. Aliquots of polymer samples were dissolved in DMF/LiBr and the clear solutions were filtered using a 0.25 μm PTFE filter to remove any THF-insoluble species. A drop of anisole was added as a flow rate marker.

6.2.2.1 Scanning Electron Microscopy (SEM)

Nanofiber samples were gold-coated and observed with a scanning electron microscope. Nanofiber images were taken using either an EVO[®] 50 (Carl Zeiss, Göttingen, Germany) equipped with an Everhart-Thornley secondary electron detector at a 10kV accelerating voltage or a Jeol JSM32CF (Soquelec, Montréal, QC, Canada) at a 15kV accelerating voltage. Each image was analyzed with image treatment software (Image J, National Institutes of Health, Bethesda, Maryland, USA). Diameters of fibers were measured on images at 10000x magnification. A total of approximately 150 fibers were randomly selected for each sample.

6.2.2.2 Thermogravimetric analysis (TGA)

TGA measurements were carried out using a TA instruments Q50 analyzer. Typically, aliquots of dried PLA-ss-Br, POEOMA-g-PLA fibers, and PEOH as a control (5-10 mg) were

placed in a platinum pan inside a programmable furnace. The sample was heated from 25 to 500 °C at a heating rate of 10 °C/min under nitrogen flow. Mass loss was then calculated.

6.2.2.3 Water contact angle measurements.

Contact angles on PLA and POEOMA-g-PLA fibrous meshes were measured by sessile drop contact angles of water droplets (1 µL) using a home-made instrument. Drop-shape images were recorded at 10 x magnification using a digital camera (Evolution VF cooled monochrome cooled camera, Media Cybernetics Inc.). ImageJ with Marco Brugnara's contact angle plugin was used to determine the contact angle.

6.2.3 Synthesis of well-controlled PLA-ss-Br homopolymers by ROP

A series of ROP of LA was conducted in the presence of HO-ss-iBuBr and $Sn(Oct)_2$ in toluene at 120 °C under various conditions. A typical procedure to synthesize high molecular weight PLA-9 under the initial mole ratio of $[LA]_0/[\text{HO-ss-iBuBr}]_0/[Sn(Oct)_2]_0 = 2000/1/0.14$ (Table 6.1) is as follows; HO-ss-iBuBr (10.5 mg, 30 µmol), LA (10 g, 69.4 mmol), $Sn(Oct)_2$ (2 mg, 4.9 µmol), and toluene (6 mL) were added to a 25 mL Schlenk flask. The resulting mixture was deoxygenated by three freeze-pump-thaw cycles. The reaction flask was filled with nitrogen, thawed, and then immersed in an oil bath preheated to 120 °C to start the polymerization. After 22 hrs, the polymerization was stopped by cooling down to room temperature. The resulting homopolymer was then precipitated from MeOH for 12 hrs, isolated by vacuum filtration, and washed with MeOH several times. Well controlled PLA-ss-Br was then dried in a vacuum oven at 50 °C overnight, resulting in white solids: molecular weight data, $M_n = 75,600$ g/mol and $M_w/M_n = 1.13$.

Table 6.1. Characteristics and molecular weight data of PLA-ss-Br homopolymers synthesized by ROP of LA in the presence of HO-ss-iBuBr in toluene at 120 C under different conditions.

Entry	$[LA]_0/[OH\text{-}ss\text{-}Br]_0$	$[Sn(Oct)_2]_0/$ $[OH\text{-}ss\text{-}iBuBr]_0$	Time (hrs)	M_n (g/mol)	M_w/M_n	HMS (%)
PLA-1	70	0.07	2	27,600	1.06	16
PLA-2	500	0.07	3	37,800	1.04	5
PLA-3	500	0.07	16	57,900	1.07	31
PLA-4	500	0.07	30	67,100	1.09	27
PLA-5	1,000	0.14	4	25,900	1.03	5
PLA-6	1,000	0.14	5	35,000	1.06	10
PLA-7	1,000	0.14	42	77,700	1.21	41
PLA-8	1,000	0.20	18	72,000	1.18	38
PLA-9	2,000	0.14	22	75,600	1.13	15

6.2.4 Preparation of air-spun PLA-ss-Br nanofibers.

The purified, dried PLA-ss-Br homopolymers were dissolved in chloroform (99.8%, Laboratoire Mat, Québec, QC, Canada). The resulting clear solutions were then injected into an air-spinning device set with the previously optimized parameters of air pressure = 5 MPa, flow rate = 10 mL/hr, needle diameter = 0.25 mm.

6.2.5 Synthesis of PLA-ss-POEOMA BCPs in THF by ATRP.

The dried, purified PLA fibers (0.28 g), OEOMA300 (0.41 g, 1.38 mmol), PMDETA (2.9 μL, 14 μmol), and THF (2.6 mL) were mixed in a 10 mL Schlenk flask. The resulting mixture was deoxygenated by three freeze-pump-thaw cycles. The reaction flask was filled with nitrogen and CuBr (2.0 mg, 14 μmol) was then added to the frozen solution. The flask was sealed, purged with vacuum and backfilled with nitrogen. The mixture was thawed and then the flask was immersed in an oil bath preheated to 47 °C to start the polymerization. The polymerization was stopped at 6 hrs by exposing the reaction contents to air.

For the synthesis of PLA-ss-POEOMA950, a similar procedure with the use of the purified PLA-fibers (0.21 g), OEOMA950 (1.0 g, 1.04 mmol), PMDETA (2.2 μL, 10 μmol), CuBr (1.5 mg, 10 μmol), and THF (2.1 mL) was applied. To purify the resulting polymers, as-synthesized polymer solution was diluted in THF and then passed through a basic aluminum

oxide column filled to remove residual copper species. The polymer solutions were precipitated from hexane and residual solvent was further removed using a vacuum oven at 50 °C overnight.

6.2.6 Synthesis of POEOMA-g-PLA fibers using surface-initiated ATRP.

A mixture consisting of an aliquot of PLA fibrous mesh (0.21 g), OEOMA950 (0.97 g, 1.0 mmol), TPMA (3 mg, 10 µmol), and water (1.6 mL) in a 10 mL Schlenk flask was deoxygenated by three freeze-pump-thaw cycles. The reaction flask was filled with nitrogen and CuBr (1.5 mg, 10 µmol) was then added to the frozen solution. The flask was sealed, purged with vacuum and backfilled with nitrogen. The mixture was thawed and then the flask was immersed in an oil bath preheated to 30 °C to start the polymerization. The polymerization was stopped at 2 hrs by exposing the reaction contents to air. To purify the resulting product fibers by removal of residual copper species and unreacted monomers, the as-synthesized mixtures were placed in a dialysis tubing with MWCO = 12,000 g/mol and dialyzed over water (500 mL) for over 2 days. The resulting fibers were then dried in a vacuum oven at 50 °C overnight.

6.2.7 DTT-responsive cleavage of disulfide linkages of PLA-ss-POEOMA in DMF.

Aliquots of the purified, dried BCP-1 or BCP-3/fibers (10 mg) were dissolved in DMF (10 mL) to form clear solutions at 1 mg/mL. They were then mixed with 10 mM DTT under stirring for 5 days. The resulting mixtures were analyzed using GPC.

6.2.8 DTT-responsive cleavage of disulfide linkages of POEOMA-g-PLA fibers in aqueous solution.

Aliquots of the purified, dried BCP-3/fibers (10 mg) were immersed in 10 mM aqueous DTT solution (10 mL) and water (10 mL) as a control for 5 days without stirring. Note that fibrous mesh were destroyed with even mild stirring. The resulting fibers were washed with water three times, and then dried in a vacuum oven at 50 °C for 2 days. They were then analyzed using ^{1}H-NMR and contact angle measurements.

6.3 Results and Discussion

6.3.1 Synthesis of a series of PLA-ss-Br homopolymers

The synthesis of HO-ss-iBuBr double-head initiator for both ROP and ATRP is described in our previous publication.[29a] In the presence of HO-ss-iBuBr, a series of ROP of D,L-lactide (LA) mediated with tin(II) 2-ethylhexanonate (Sn(Oct)$_2$) in toluene at 120 °C was conducted. The results are summarized in Table 6.1, where the samples are denoted as PLA-x (x: serial number). First, ROP with the targeting degree of polymerization (DP) = 70 defined as the initial mole ratio of $[LA]_0/[HO\text{-}ss\text{-}iBuBr]_0$ = 70/1 yielded PLA-ss-Br homopolymer (PLA-1) with relatively low molecular weight, the number average molecular weight (M_n) = 27.6 kg/mol and narrow molecular weight distribution, M_w/M_n = 1.06. As seen in Figure 6.1, gel permeation chromatography (GPC) trace shows a shoulder in high molecular weight region. Peak analysis using a deconvolution method suggests the content of high molecular weight species (HMS) to be 16%. The formation of HMS could be attributed to undesirable side reactions.[155] In an effort to synthesis of high molecular weight PLA-ss-Br with less HMS content, the important parameters such as targeting DP and $[Sn(Oct)_2]_0/[HO\text{-}ss\text{-}iBuBr]_0$ ratio were varied. When the targeting DP increased to 500 and 1000, relatively high molecular weight PLA-ss-Br homopolymers with M_n = 65 – 75 kg/mol were obtained with longer polymerization time. However, the undesirable HMS content also increased up to 41%. When the amount of Sn(Oct)$_2$ increased, polymerization was fast and the HMS contents also increased (PLA-7 and PLA-8 with targeting DP = 1000) (Figure 6.2). Further increase in targeting DP = 2000 with $[Sn(Oct)_2]_0/[HO\text{-}ss\text{-}iBuBr]_0$ = 0.14/1 yielded high molecular weight PLA-9 with M_n = 75.6 kg/mol and HMS = 15%. These results suggest that the balance of targeting DP, polymerization time, and Sn(Oct)$_2$ content is required for the synthesis of high molecular weight PLA-ss-Br with less HMS content.
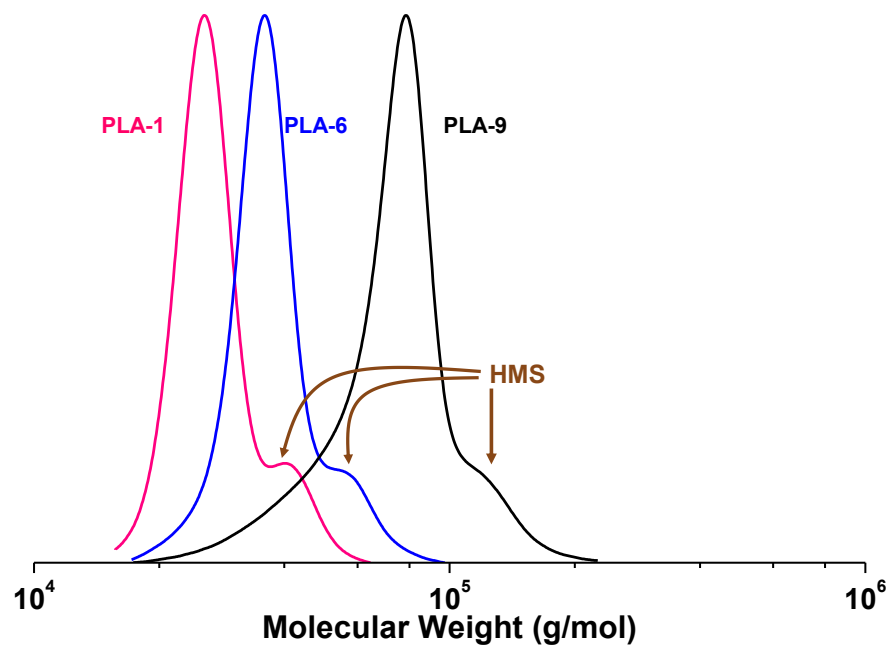
Figure 6.1. GPC traces of PLA-1 (Mn = 27.6 kg/mol), PLA-6 (Mn = 35.0 kg/mol), and PLA-9 (Mn = 75.6 kg/mol).
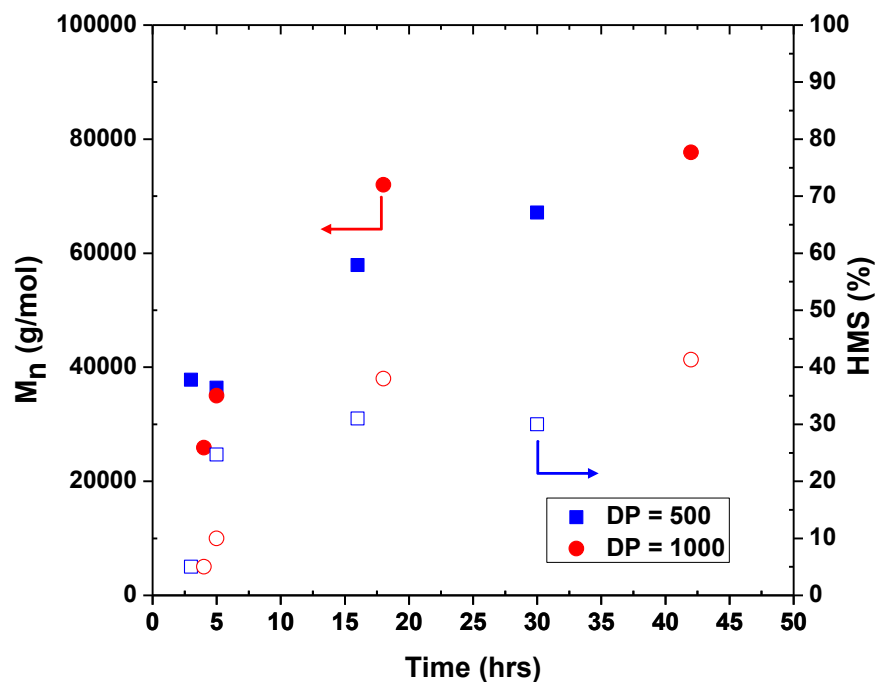
Figure 6.2. Evolution of molecular weights and HMS contents over polymerization time for ROP of LA with targeting DP = 500 and 1000, as summarized in Table 6.1.

6.3.2 Fabrication of air-spun PLA-ss-Br nanofibers.

Next, air-spinning of the PLA-ss-Br homopolymers dissolved in chloroform was examined. Chloroform is a good solvent to use with PLA as it is volatile which is advantageous for spinning purposes. Three homopolymers with different molecular weights, but HMS content < 20%, were selected: PLA-1 (M_n = 27.6 kg/mol), PLA-6 (M_n = 35 kg/mol), and PLA-9 (M_n = 75.6 kg/mol) (see their GPC traces in Figure 6.1). PLA-1 and PLA-6 with relatively low molecular weights (M_n < 40 kg/mol) were not well air-spun, even at as high as 70% concentration. Scanning electron microscopy (SEM) images in Figure 6.3 show the presence of some fibers, but mostly large spheres. Such poor spinninability could be attributed to relatively low molecular weight PLAs, and thus lower solution viscosities even at higher concentrations. Promisingly, PLA-9 with M_n > 70 kg/mol was fabricated through entanglement of PLA chains to fibrous woven at 30% concentration (Figure 6.4a,c). The average diameter was estimated to be 495 ± 240 nm from approximately 150 fibers (Figure 6.9).
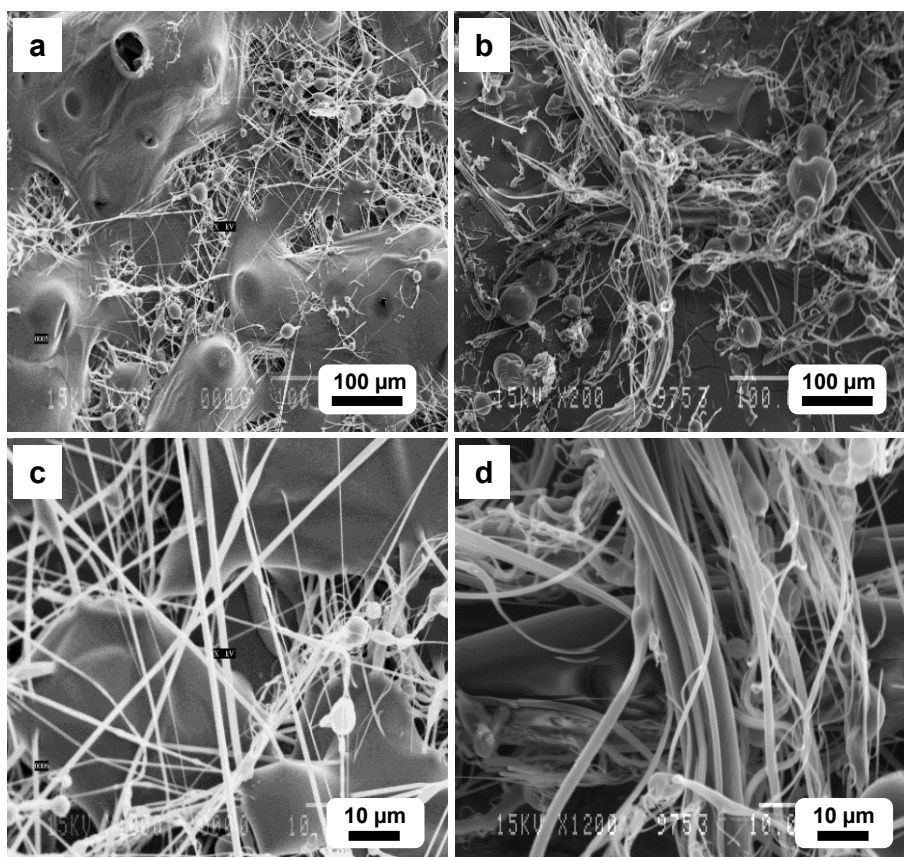
Figure 6.3. SEM images of low molecular weight PLA-1 (M_n = 27.6 kg/mol) (a, c) and PLA-6 (M_n = 35.0 kg/mol) (b, d) at lower (a, b) and higher (c, d) magnititudes.
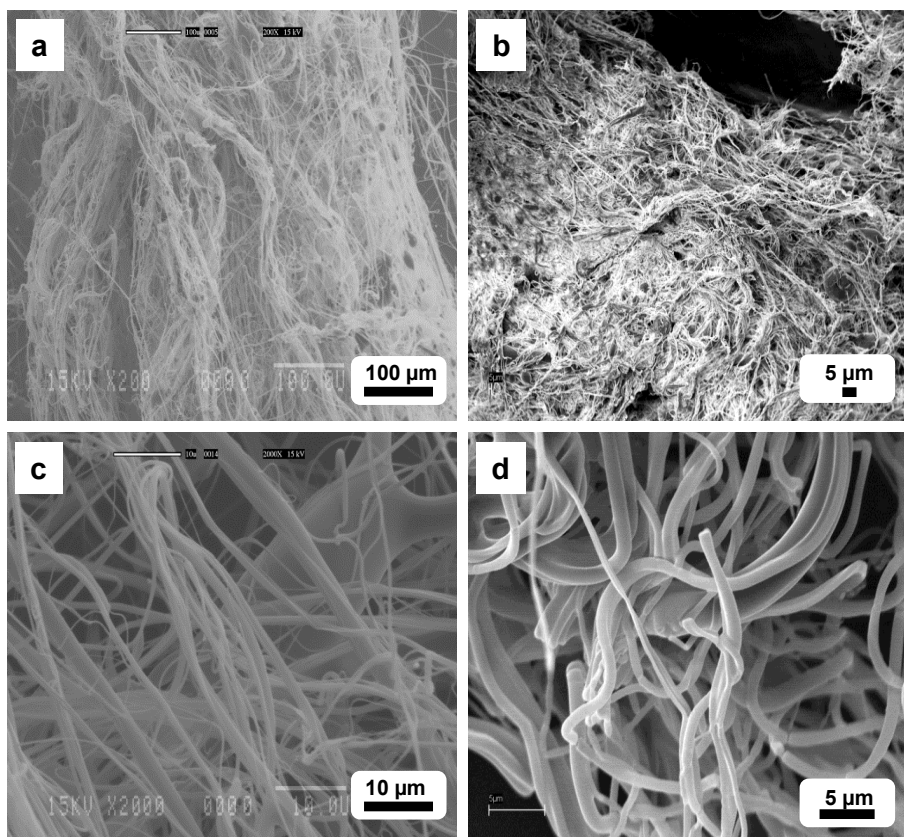
Figure 6.4. SEM images of PLA-9 fibers (M_n = 75.6 kg/mol) (a, c) and POEOMA-g-PLA BCP-3/fibers (b, d) with lower (a, b) and higher (c, d) magnitudes.

6.3.3 SI-ATRP of PLA-ss-Br fibers

The resulting PLA-ss-Br fibers consist of terminal Br groups. In the presence of PLA-ss-Br fibers, SI-ATRP of OEOMA was investigated to synthesize POEOMA grafted from PLA fibers (POEOMA-g-PLA fibers) based on PLA-ss-POEOMA block copolymers (BCPs) consisting of disulfide linkages at the junctions of PLA and POEOMA blocks. Table 6.2 summarizes the results. To see the availability of terminal Br groups in PLA-ss-Br homopolymer fibers, their chain extension was first examined with OEOMA300 with MW = 300 g/mol (BCP-1) and OEOMA950 with MW = 950 g/mol (BCP-2) in homogeneous solution. Aliquots of the dried fibers, OEOMA, and CuBr complex were dissolved in tetrahydrofuran under direct ATRP conditions for 2 hrs. Conversion was determined to be 0.14 for BCP-1 and 0.07 for BCP-2. After purification, their ^{1}H-NMR spectra show typical peaks at 5.0-5.2 ppm (a) corresponding to

methine protons in PLA and 0.9-1.0 ppm (b) to backbone methyl protons in POEOMA (Figure 6.5b for BCP-1 and Figure 6.6 for BCP-2). From the integral ratio of these peaks [(b/3)/(a/2)], the weight ratio of POEOMA/PLA in BCPs was calculated to be 0.22/1 for BCP-1 and 0.42/1 for BCP-2. These values are close to those calculated using the wt ratio of OEOMA/PLA from the recipe and the determined conversion (Table 6.2). GPC traces of the purified BCPs evolved to higher molecular weight region. For example, M_n increased from 71.4 kg/mol to 82.0 kg/mol for BCP-1 (Figure 6.7). These ^{1}H-NMR and GPC results indicate the successful synthesis of PLA-ss-POEOMA BCPs in homogeneous solutions, confirming the presence of terminal Br groups in PLA-ss-Br homopolymer fibers.

Table 6.2. Characteristics and molecular weight data of PLA-ss-POEOMA BCPs synthesized by chain extension of PLA-ss-Br fibers with POEOMA under normal ATRP conditions.

Entry	BCP-1	BCP-2	BCP-3/fibers
PLA fiber (mg)	276	208	198
OEOMA/PLA (wt/wt)	1.5/1	4.8/1	4.8/1
OEOMA [M]	0.53	0.50	0.60
CuBr [mM]	5.3	5.0	6.3
OEOMA monomer	OEOMA300	OEOMA950	OEOMA950
Solvent	THF	THF	water
Time (hrs)	6	2	2
Conv [a]	0.14	0.06	NA
POEOMA/PLA (wt/wt),theo [b]	0.21/1	0.35/1	NA
POEOMA/PLA (wt/wt) [c]	0.22/1	0.42/1	0.13/1
M_n (g/mol) [d]	82,000	77,200	67,200
M_w/M_n [d]	1.11	1.14	1.13

a) Determined by ^{1}H-NMR.

b) Estimated by OEOMA/PLA wt ratio x conversion

c) Determined by ^{1}H-NMR with molecular weight of LA and OEOMA

d) Derermined by GPC with DMF as an eluent.
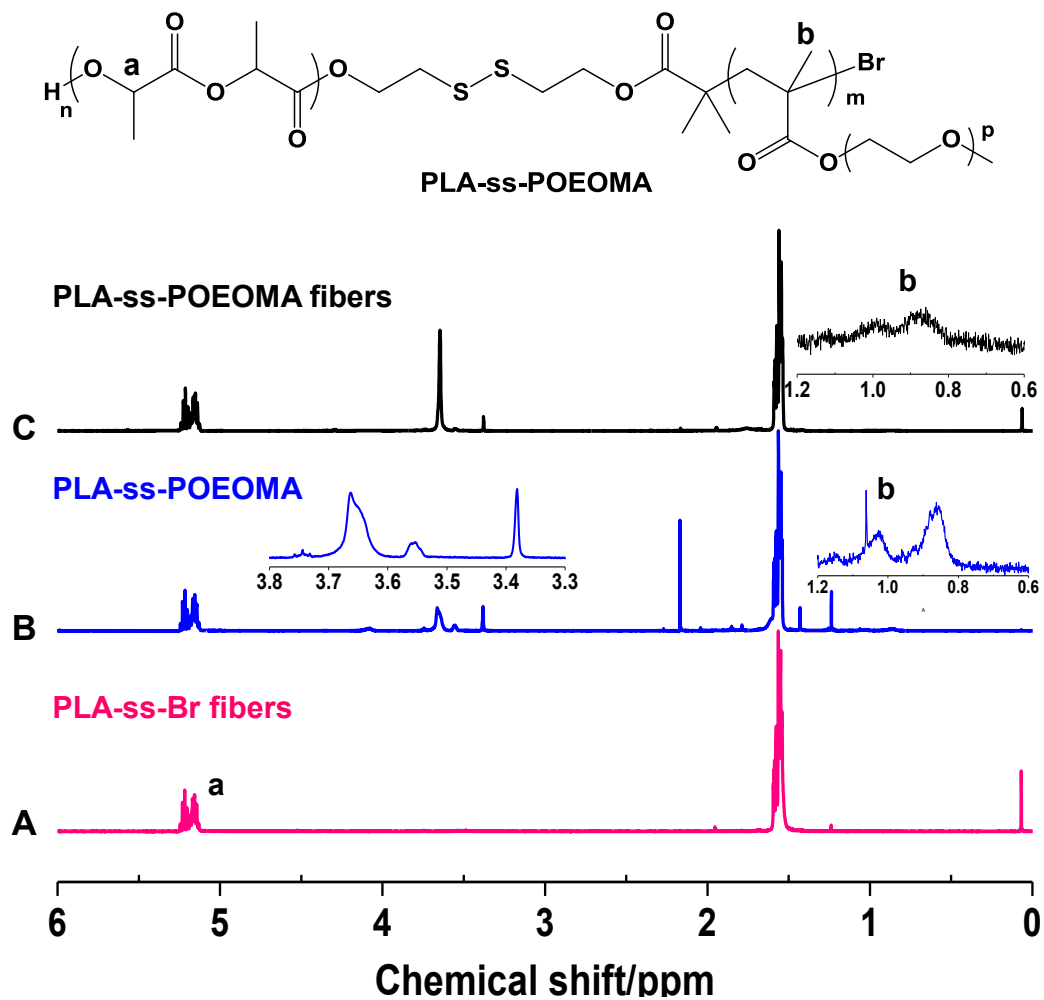
Figure 6.5. ^{1}H-NMR spectra of PLA-9 (A), BCP-1 (B), and BCP-3/fibers (C) in CDCl$_3$.
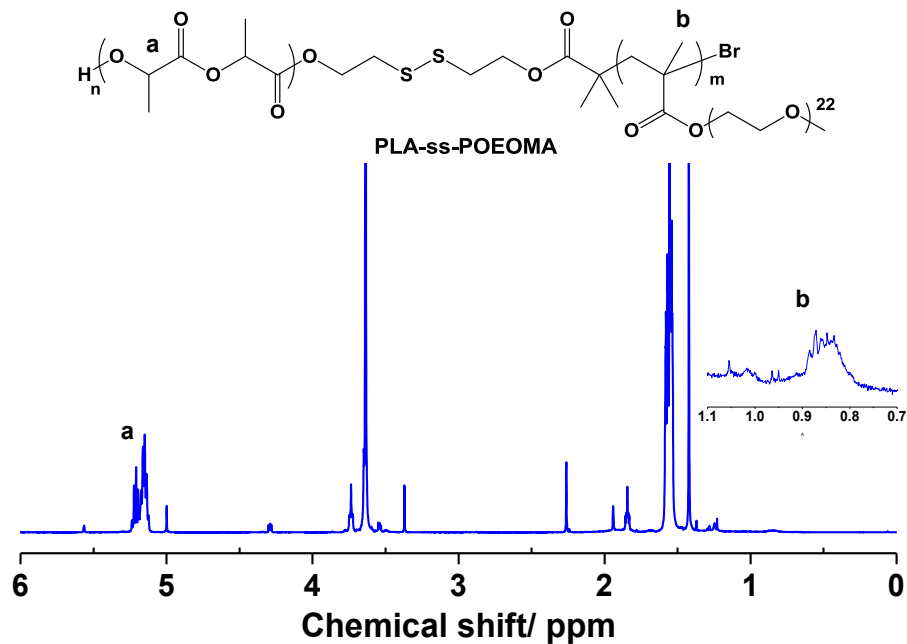
Figure 6.6. ¹H-NMR spectrum of PLA-ss-POEOMA BCP-2 in CDCl₃.
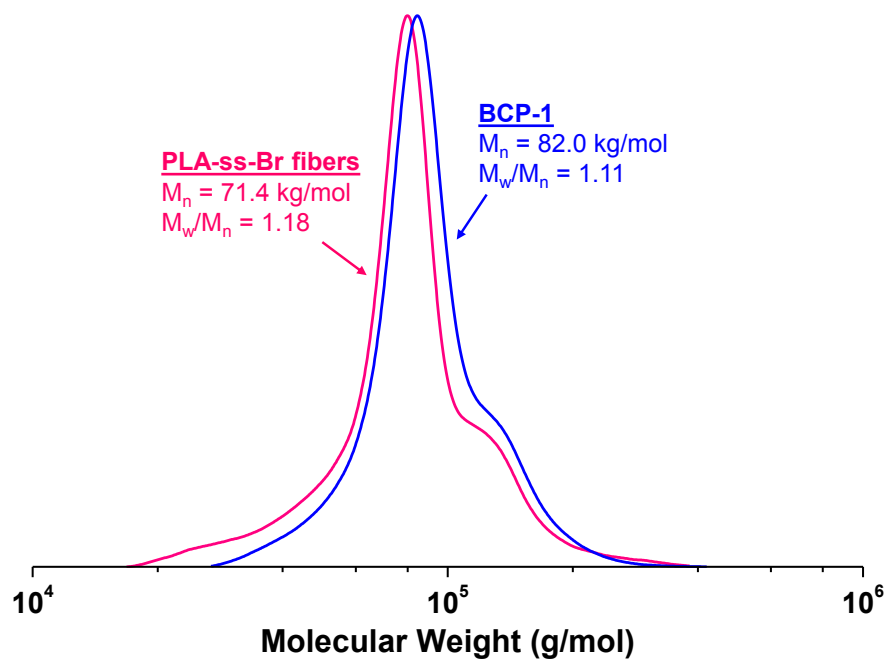
Figure 6.7. GPC traces of PLA-ss-Br fibers and PLA-ss-POEOMA300 (BCP-1) in DMF.

Considering these promising results, grafting POEOMA from PLA-ss-Br fibers through SI-ATRP in aqueous solution was next examined. Solubility test reveals that PLA fibers remained intact in aqueous solution of OEOMA950, while they were dissolved in aqueous solution of OEOMA300 even at room temperature. Consequently, PLA fibrous mesh was soaked in a solution consisting of OEOMA950, Cu complex, and water for 2 hrs. SI-ATRP was then conducted for 2 hrs at 30 °C, below the melting point of amorphous PLA ($\approx$39 °C). The resulting products were purified by extensive dialysis using a dialysis tubing (MWCO = 12 kg/mol) to completely remove unreacted OEOMA950 monomers. ^{1}H-NMR spectrum shows the typical peaks (b) at 0.9-1.0 ppm for POEOMA and 5.0-5.2 ppm (a) for PLA (Figure 6.5c). The wt ratio of POEOMA/PLA was calculated to be 0.13/1 (Table 6.2). Further, the GPC trace of the purified BCP slightly evolved to higher molecular weight region (Figure 6.8). These results suggest the successful grafting POEOMA from PLA fibers, yielding POEOMA-g-PLA fibers (BCP-3/fibers) based on PLA-ss-POEOMA BCPs.
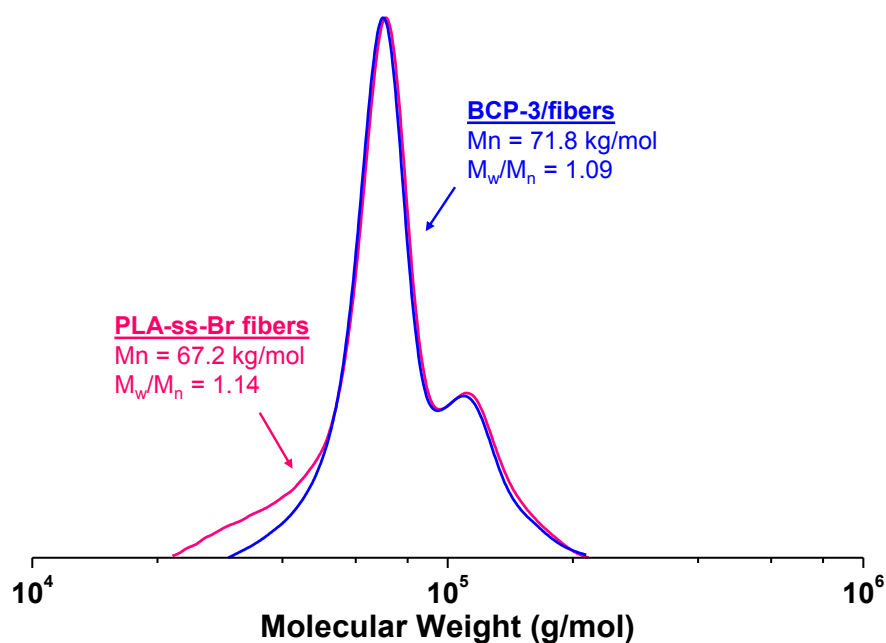
Figure 6.8. GPC traces of PLA-ss-Br fibers and POEOMA-g-PLA fibers based on PLA-ss-POEOMA950 (BCP-3/fibers) in DMF.

Further, the effect of the grafted POEOMA chains was evaluated on fibrous morphologies by SEM, thermal properties using thermogravimetric analysis (TGA), surface properties using contact angle measurements. SEM images show a relatively dense fibrous form (Figure 6.4b,d). The average diameter of the POEOMA-g-PLA fibers was estimated to be 620 ± 220 nm, larger than pristine PLA fibers by approximately 122 nm (Figure 6.9).
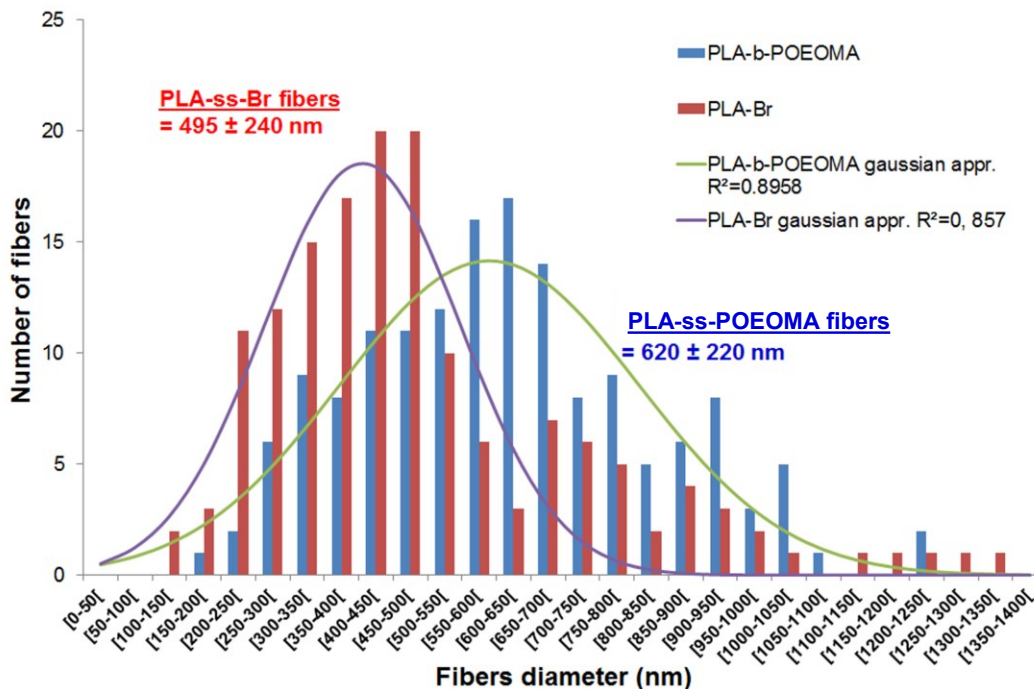
Figure 6.9. Size distribution in diameter of nanofibers of PLA-ss-Br and POEOMA-g-PLA fibers.

Figure 6.10 shows TGA data of the weight loss of BCP-3/fibers, compared with PLA-9 fibers and PEO homopolymers as controls, upon heating. For BCP-3/fibers, the major weight loss started at 236 °C. This temperature is lower than that (315 °C) for PEO homopolymers, but higher than that (215 °C) by 20 °C for PLA fibers. This result suggests that the tethered POEOMA enhances thermal stability of PLA fibers.
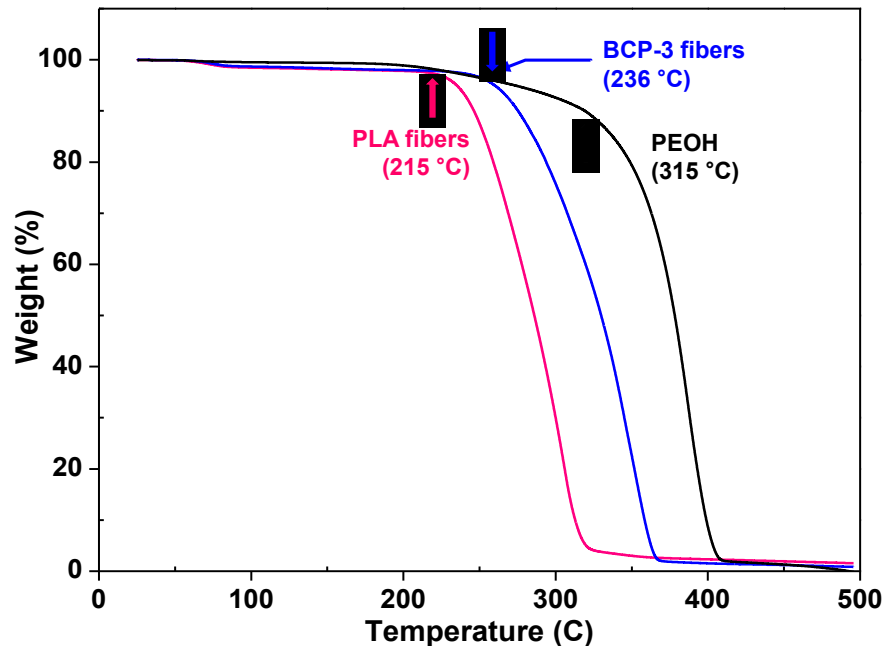
Figure 6.10. TGA diagrams of PLA-ss-Br fibers, BCP-3/fibers, and PEOH with MW = 2,000 g/mol for comparison. Am arrow indicates a temperature where the major weight loss starts.

Figure 6.11 shows the results of contact angle measurements with snapshots of water drops on PLA fibrous mesh before and after surface modification with POEOMA. On POEOMA-g-PLA fibers, water drops were immediately absorbed into fibers within 1.5 sec, resulting in sharp decrease in contact angle (Figure 6.11a). The disappearance of a water drop on BCP fibers was snapshotted in Figure 6.11b. On hydrophobic PLA homopolymer fibers, however, water drops stayed with a contact angle at 120.5 ° over time (Figure 6.11c). This result suggests that the tethered hydrophilic POEOMA increases wettability of hydrophobic PLA fibers, allowing an instantaneous penetration of water, whereas the pristine PLA fibers offered a significant barrier to it. Similar results are reported for other fibrous materials with different chemical structures.[189, 192]

117
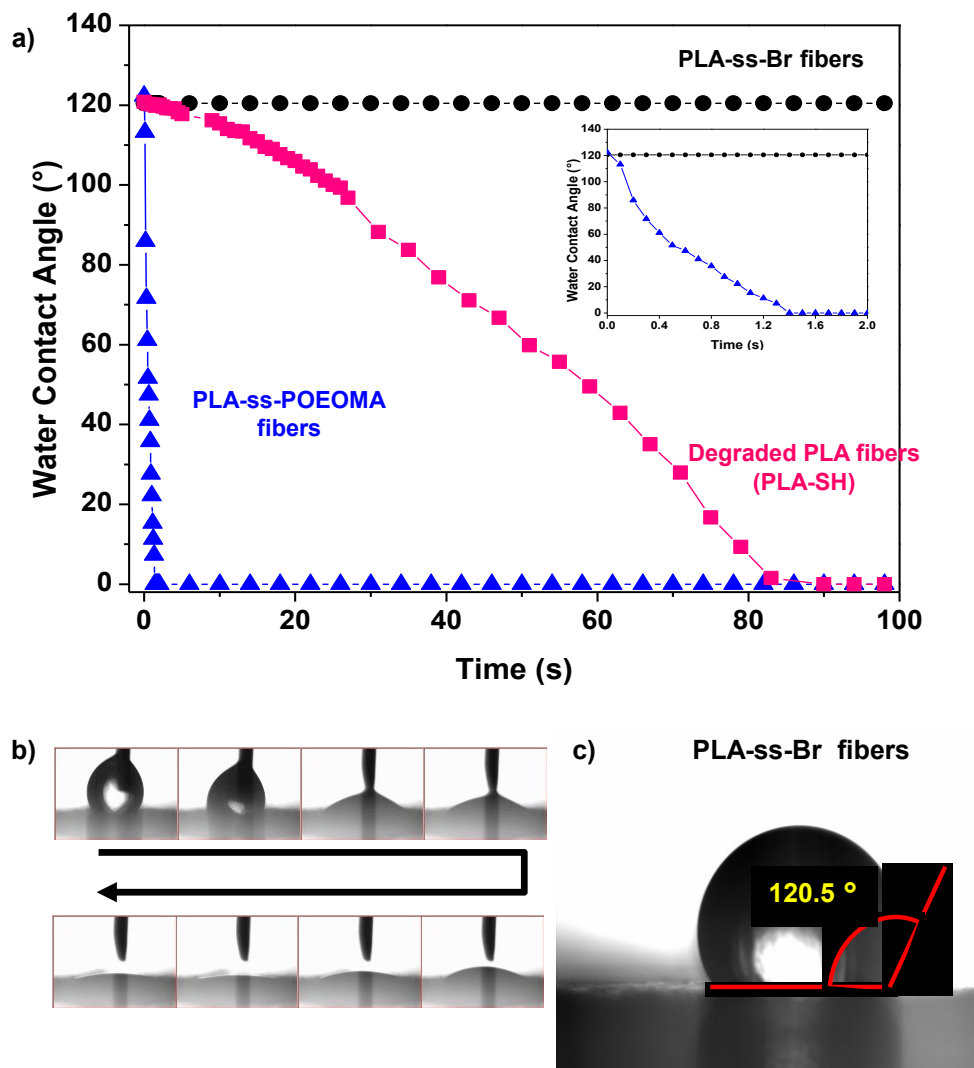
Figure 6.11. Evolution of contact angle on PLA fibers, POEOMA-g-PLA fibers before and after treatment with DTT (a), and snapshots of water droplets on POEOMA-g-PLA fibers after SI-ATRP (b) and PLA-ss-Br fibers in the prisitine state (c). Inset of (a): evolution of contact angle on PLA fibers and POEOMA-g-PLA fibers before DTT treatment.

6.3.4 Reductive degradation of POEOMA-g-PLA fibers

The POEOMA-g-PLA fibers based on PLA-ss-POEOMA BCPs contain disulfides at block junctions. These disulfide linkages could be cleaved in the presence of DTT, a reducing agent, to the corresponding thiols including POEOMA-SH and PLA-SH as linear polymers or fibers (Scheme 6.1). GPC results indicate the decrease in molecular weight of PLA-3/fibers from

$M_n = 71.8$ kg/mol to $M_n = 67.0$ kg/mol in homogeneous DMF solution with excess DTT (Figure 6.12). ^{1}H-NMR was also used to examine the disulfide cleavage in aqueous solution where BCP-3/fibers exist as meshes. In the presence of excess DTT, the typical peaks at 0.9-1.0 ppm corresponding to backbone methyl protons in POEOMA completely disappeared, while being retained in the absence of DTT (Figure 6.13). These GPC and NMR results suggest the significant cleavage of disulfide linkages in reducing environments. Such cleavage could result in shedding POEOMA-SH from POEOMA-g-PLA fibers, thus changing the surface polarity of PLA fibers. As seen in Figure 6.11a, water contact angle on the resulting PLA-SH fibers slowly decreased. After 80 sec, water droplet was completely absorbed in the fibers. Such slow decrease is attributed to the surface of the resulting PLA-SH fibers to be less hydrophilic than POEOMA-g-PLA fibers, but more hydrophilic than pristine PLA fibers.
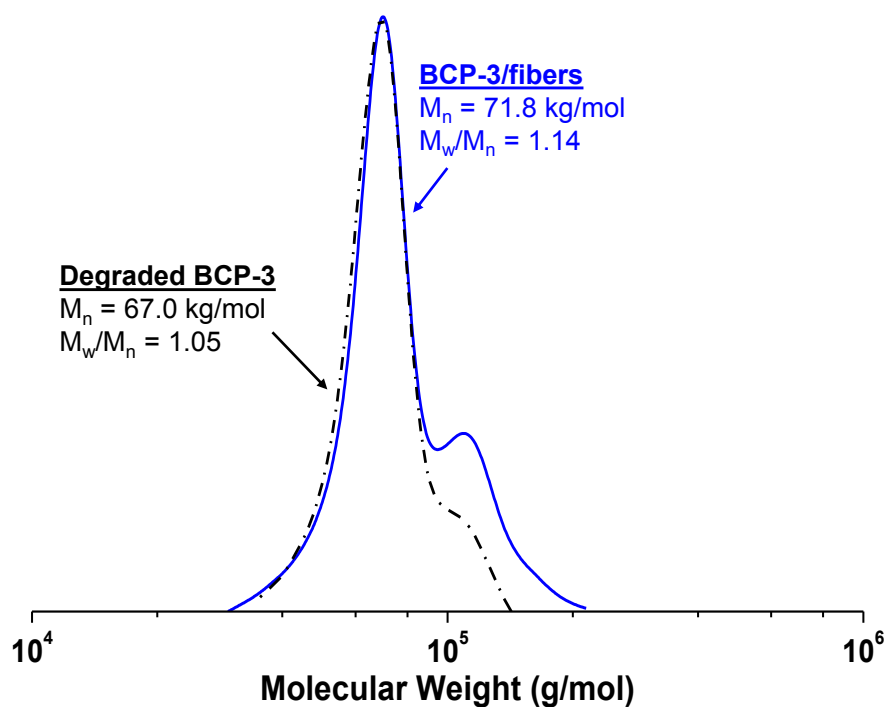
Figure 6.12. Reductive degradation of POEOMA-g-PLA fibers in DMF homogeneous solution monitored by GPC traces.
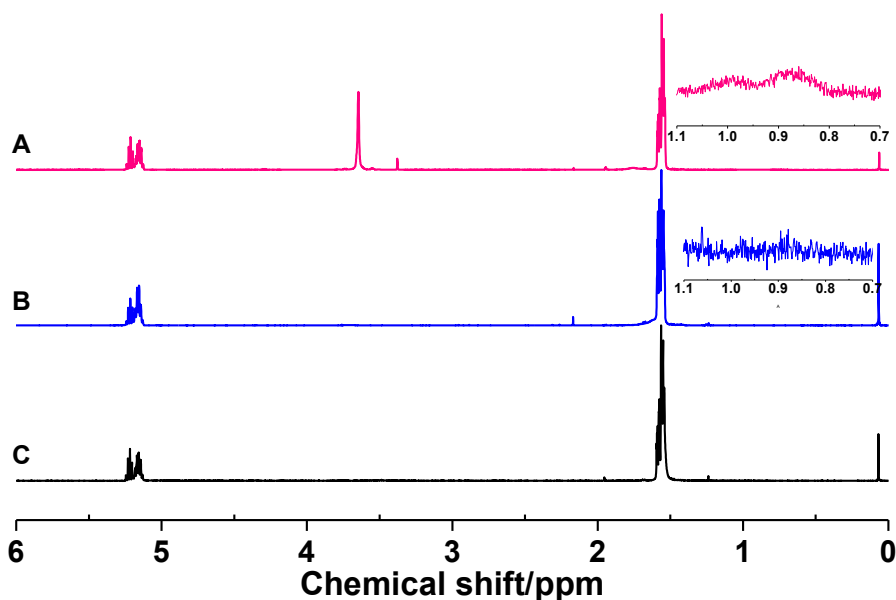
Figure 6.13. ^{1}H-NMR spectra of BCP-3/fibers in the absence (A) and presence (B) of excess DTT in water, compared with the spectrum of pristine PLA-ss-Br fibers (C) in CDCl₃.

6.4 Conclusion

A new class of air-spun PLA nanofibers modified with thiol-responsive sheddable POEOMA was synthesized by a combination of ROP, air-spinning, and SI-ATRP techniques. High molecular weight PLA-ss-Br with less HMS contents (<15%) ensured good spinability, yielding PLA fibers functionalized with terminal Br groups at interfaces. SI-ATRP allowed for the modification of the PLA fibers with tethered hydrophilic POEOMA blocks. The resulting POEOMA-g-PLA fibers with hydrophilic surfaces exhibit improved thermal stability and surface properties such as water content and wetting behavior, confirmed by SEM, TGA, and contact angle measurements. Moreover, shedding hydrophilic POEOMA from POEOMA-g-PLA fibers by the cleavage of disulfide linkages in response to reductive reactions enabled tuning the surface properties. Toward vascular tissue engineering, the controlled and enhanced release of therapeutics upon the cleavage of disulfide linkages in response to reductive reactions[80] of the new POEOMA-g-PLA fibrous mesh as well as by varying hydrophobicity driven by their nanostructures fabricated on PET films[202] is currently under investigation.

Chapter 7 Summary and recommendations for future work

7.1 Summary of thesis

The main focus of my Ph.D. research was to understand SRD, especially reduction-responsive system, and design a variety of new PLA-based nanomaterials in biomedical applications. Disulfide-labeled PLA-based ABPs were synthesized via ROP and ATRP in the presence of HO-ss-iBuBr initiator and they have subsequently been used as building blocks for the fabrication of self-assembled micellar drug carriers; polyplexes for delivery of drugs and genes; and surface-modified air-spun nanofibers. Upon the cleavage of disulfide linkages under a reductive environment, PLA-based nanomaterials degraded, exhibiting the rapid release of anticancer drugs and genes, as well as tuning the surface properties. The obtained results suggest that these novel reduction-responsive PLA-based nanomaterials possess great potentials as effective platforms for multi-functional drug delivery and tissue engineering applications in biomedical fields.

Chapter 3 describes well-established method to synthesize novel disulfide-labeled PLA-based BCPs. A series of PLAs with narrow molecular weight distribution were synthesized by ROP of D,L-LA initiated with double headed HO-ss-iBuBr initiator in a well-controlled manner. The synthetic condition was optimized by adjusting the amount of the $Sn(Oct)_2$ catalyst and the polymerization time to reduce the high molecular weight species (HMS), by-products yielded by side coupling reactions. The results confirmed that the amount of HMS increased in proportion to the amount of catalyst and the polymerization time. Using the resulting PLAs as the macroinitiators, various PLA-based BCPs (PLA-ss-PATRPs) were synthesized via ATRP with various monomers including methacrylates, acrylates, and aromatic monomers. These well-controlled syntheses proceeded in a controlled manner low molecular weight distribution ($M_w/M_n < 1.2$), analyzed by ^{1}H-NMR and GPC. In the presence of the reducing agent DTT, the PLA-ss-PATRPs degraded to the corresponding thiols, including PLA-SH and PATRP-SH, upon the cleavage of disulfide at block junctions. These significant results were used for the development of multifunctional nanomaterials as micelles and as fibers with reduction-responsive degradation.

Chapter 4 of this thesis describes PLA-based polyplexes for dual delivery of drugs and genes. This work expands upon the well-established synthetic method of PLA-based BCPs basic described in Chapter 3 by incorporating positively-charged PDMA as the hydrophilic block constituting the cationic amphiphilic micellar aggregates. Such cationic micelles enabled electrostatic interaction with negatively-charged ssDNA to form C-ssABP micelles and ssDNA polyplexes with a diameter of 90 nm, as well as encapsulation of anticancer drugs in the hydrophobic PLA cores. The optimal ratio of C-ssABP (cationic micelle) and ssDNA (N/P ratio) = 2/1-4/1 was confirmed by agarose gel electrophoresis and zeta potential measurements. From a biological perspective, both cationic micelles and polyplexes exhibit good cell viability up to 200 µg/mL. The GSH-responsive cleavage of disulfide linkages at micelle interfaces resulted in shedding cationic coronas, leading to the controlled release of both anticancer therapeutics and oligonucleotides in cancer cells. The *in vitro* results from CLSM, FC, and gene transfection assay show that the new C-ssABP possesses great potential as an effective nanocarrier for dual chemotherapy and gene therapy.

Chapter 5 focuses the effects of the number and location of disulfide linkages on the PLA-based ABPs. The novel PLA-based triblock copolymer with a single disulfide in the middle of hydrophobic PLA block and two disulfides at PLA/hydrophilic POEOMA block junctions was synthesized. In aqueous solution, these amphiphilic triblock copolymers self-assembled to form multi-cleavable micellar aggregates with disulfides at dual locations, the hydrophobic core and the micellar interface. To evaluate their enhanced degradation rate and rapid drug release, mono-cleavable micelles with disulfides only at the micellar cores were also prepared as a reference. After the cleavage of dual-located disulfide linkages in response to a GSH cellular trigger, multi-cleavable micelles exhibited faster destabilization than a mono-cleavable system, leading to the synergistically enhanced release of encapsulated anticancer drugs. These results suggest that the thiol-responsive, dual-located degradation strategy accelerated the release of encapsulated model drugs from the micelles.

Chapter 6 describes the synthesis of high molecular weight PLAs (M_n >70 kg/mol) with a terminal Br functional group and single disulfide linkages for the fabrication of fibrous nanomaterial. Novel PLA nanofibers with ≈ 495 nm in diameter were fabricated via air-spinning process. These fibrous materials possess large surface area, high porosity, and interconnected network structure. The resulting PLA fibers were then modified via SI-ATRP with hydrophilic

POEOMA blocks. The surface modified POEOMA-g-PLA fibers exhibited improved thermal stability and water wetting behavior. Moreover, the reduction-responsive degradation to sheddable hydrophilic POEOMA from POEOMA-g-PLA fibers enabled the tuning of surface properties. For vascular tissue engineering, this new POEOMA-g-PLA fibrous mesh can be used for the controlled and enhanced release of therapeutics, as well as varying hydrophobicity driven by their nanostructures fabricated on polyethylene terephthalate (PET) films.

7.2 Future work

The current design of dual delivery carriers as described in Chapter 2 shows that the electrostatically interacted nucleic acids are exposed to the aqueous environment, which may reduce the stability of gene delivery carriers, causing a loss of nucleic acids before they reach the target site. To circumvent this weakness, PEG-shielding on the surface of micellar nanocarriers was proposed as a promising approach. PEG is a biocompatible hydrophilic polymer, and coating the surface of nanocarriers with PEG can prevent the opsonisation process, prolonging circulation time in the body (referred to as "stealth" systems). Several PEG-coated gene delivery carriers based on amphiphilic micelles were reported.[203] These core-shell structured micellar gene carriers exhibit improved colloidal stability and cytotoxicity. Therefore, future work on this project should include the modification of the surface of dual-delivery carriers with hydrophilic PEG coronas. In support of the well-established synthetic technique presented in Chapter 3, PEG-labeled PLA-based cationic triblock copolymers can be synthesized. In aqueous solution, these ABPs can form the PEG-shielded micellar nanocarriers consisting of a hydrophobic PLA core that encapsulate drugs and a hydrophilic cationic poly(N,N-dimethylaminoethyl methacrylate) layer.

Chapter 6 describes the air-spun PLA nanofibers and their surface modification with hydrophilic POEOMA via ATRP method. This current approach, however, is very limited to specific hydrophilic monomers demonstrating poor-miscibility with PLA-nanofibers. Typical hydrophilic monomers with low molecular weight such as POEOMA 300 and PEG can conduct a relatively high monomer conversion. However, they can dissolve PLA-nanofibers during polymerization, destroying fibrous structure. Compared with low molecular weight monomers, POEOMA 950 is suitable for surface-initiated grafting of PLA-nanofibers due to its relatively high-molecular weight and poor-miscibility with PLA, but this approach results in very low

monomer conversion (<0.5). To overcome these drawbacks, fabrication of PLA-nanofibers using PLA-based ABPs may be useful. Well-defined PLA-based ABPs consisting of a high molecular weight of the PLA block and hydrophilic block can be synthesized and used for the fabrication of hybrid nanofibers via the air-spinning method. Several research studies have reported the fabrication of nanofibers using a mechanically blended hydrophobic PLA polymer and hydrophilic polymers;[204] however, there are no reports that propose a fabrication strategy of nanofibers using PLA-based ABPs.

Furthermore, the drug can be embedded inside the nanofibers so that these surface-modified nanofibers possessing therapeutics may be adapted to multi-functional biomedical applications. A nanofibrous carrier for drug delivery applications has attracted much interest but very limited studies were reported. As a proof of concept approach, several studies have been demonstrated based on the biodegradable nanofibers including poly(lactide-co-glycolide),[205] poly(ethylene-co-vinyl acetate),[206] poly(ethylene-co-vinyl alcohol),[207] PDLLA,[208] PLLA,[209] and their blends.[210] So it is desirable to embed therapeutics inside the surface-modified nanofibers for both applications of drug delivery and vascular tissue engineering.

References

[1]   Y. Cheng, S. Deng, P. Chen, R. Ruan, *Frontiers of chemistry in China* **2009**, *4*, 259-264.

[2]   D. Campoccia, P. Doherty, M. Radice, P. Brun, G. Abatangelo, D. F. Williams, *Biomaterials* **1998**, *19*, 2101-2127.

[3]   D. Henry, *ASM International, Ohio, USA* **2009**, 151-186.

[4]   O. Dechy-Cabaret, B. Martin-Vaca, D. Bourissou, *Chemical Reviews* **2004**, *104*, 6147-6176.

[5]   D. Attwood, C. Booth, S. G. Yeates, C. Chaibundit, N. M. Ricardo, *International journal of pharmaceutics* **2007**, *345*, 35-41.

[6]   aR. Langer, *Science* **2001**, *293*, 58-59; bR. Duncan, *Nature Reviews Drug Discovery* **2003**, *2*, 347-360.

[7]   aS. V. Vinogradov, T. K. Bronich, A. V. Kabanov, *Advanced drug delivery reviews* **2002**, *54*, 135-147; bH. S. Choi, W. Liu, P. Misra, E. Tanaka, J. P. Zimmer, B. I. Ipe, M. G. Bawendi, J. V. Frangioni, *Nature biotechnology* **2007**, *25*, 1165-1170.

[8]   G. Vilar, J. Tulla-Puche, F. Albericio, *Current Drug Delivery* **2012**, *9*, 367-394.

[9]   aR. Van Furth, Z. Cohn, J. Hirsch, J. Humphrey, W. Spector, H. Langevoort, *Bulletin of the World Health Organization* **1972**, *46*, 845; bM. M. Frank, L. F. Fries, *Immunology today* **1991**, *12*, 322-326.

[10]   aS. S. Davis, L. Illum, *Int. J. pharm* **1998**, *176*, 1-8; bE. V. Batrakova, T. K. Bronich, J. A. Vetro, A. V. Kabanov, *Nanoparticulates as drug carriers* **2006**, 57-93; cC.-M. J. Hu, L. Zhang, *Biochemical pharmacology* **2012**, *83*, 1104-1111.

[11]   R. A. Petros, J. M. DeSimone, *Nature Reviews Drug Discovery* **2010**, *9*, 615-627.

[12]   Y. H. Bae, K. Park, *Journal of Controlled Release* **2011**, *153*, 198-205.

[13]   M. Goldberg, R. Langer, X. Jia, *Journal of Biomaterials Science, Polymer Edition* **2007**, *18*, 241-268.

[14]   aV. V. Ranade, *The Journal of Clinical Pharmacology* **1990**, *30*, 10-23; bS. M. Moghimi, A. C. Hunter, J. C. Murray, *The FASEB Journal* **2005**, *19*, 311-330; cV. Wagner, A. Dullaart, A.-K. Bock, A. Zweck, *Nature biotechnology* **2006**, *24*, 1211-1218; dT. Lammers, W. Hennink, G. Storm, *British journal of cancer* **2008**, *99*, 392-397; eR. Duncan, R. Gaspar, *Molecular pharmaceutics* **2011**, *8*, 2101-2141.

[15]   M. Hans, A. Lowman, *Current Opinion in Solid State and Materials Science* **2002**, *6*, 319-327.

[16]   A. Kader, R. Jalil, *Drug development and industrial pharmacy* **1998**, *24*, 527-534.

[17]   aC. Roney, P. Kulkarni, V. Arora, P. Antich, F. Bonte, A. Wu, N. Mallikarjuana, S. Manohar, H.-F. Liang, A. R. Kulkarni, *Journal of Controlled Release* **2005**, *108*, 193-214; bR. P Pawar, S. U Tekale, S. U Shisodia, J. T Totre, A. J Domb, *Recent Patents on Regenerative Medicine* **2014**, *4*, 40-51.

[18]   aW. R. Gombotz, D. K. Pettit, *Bioconjugate Chemistry* **1995**, *6*, 332-351; bR. Gref, P. Quellec, A. Sanchez, P. Calvo, E. Dellacherie, M. J. Alonso, *European Journal of Pharmaceutics and Biopharmaceutics* **2001**, *51*, 111-118.

[19]   aI.-S. Kim, S.-K. Lee, Y.-M. Park, Y.-B. Lee, S.-C. Shin, K. C. Lee, I.-J. Oh, *International Journal of Pharmaceutics* **2005**, *298*, 255-262; bX. Gao, W. Tao, W. Lu, Q. Zhang, Y. Zhang, X. Jiang, S. Fu, *Biomaterials* **2006**, *27*, 3482-3490; cK. Hu, J. Li, Y. Shen, W. Lu, X. Gao, Q. Zhang, X. Jiang, *Journal of Controlled Release* **2009**, *134*, 55-61.

[20]   R. M. Rasal, A. V. Janorkar, D. E. Hirt, *Progress in polymer science* **2010**, *35*, 338-356.

[21]   L. Xiao, B. Wang, G. Yang, M. Gauthier, *Poly (lactic acid)-based biomaterials: synthesis, modification and applications*, INTECH Open Access Publisher, **2012**.

[22]   Y. Hu, X. Jiang, Y. Ding, L. Zhang, C. Yang, J. Zhang, J. Chen, Y. Yang, *Biomaterials* **2003**, *24*, 2395-2404.

[23]   J. K. Oh, *Soft Matter* **2011**, *7*, 5096-5108.

[24]   N. Kumar, M. N. Ravikumar, A. Domb, *Advanced drug delivery reviews* **2001**, *53*, 23-44.

[25]   A. Hoshino, Y. Isono, *Biodegradation* **2002**, *13*, 141-147.
[26]   M. S. Reeve, S. P. McCarthy, M. J. Downey, R. A. Gross, *Macromolecules* **1994**, *27*, 825-831.
[27]   aJ. Bergsma, W. De Bruijn, F. Rozema, R. Bos, G. Boering, *Biomaterials* **1995**, *16*, 25-31; bR. Suuronen, T. Pohjonen, J. Hietanen, C. Lindqvist, *Journal of Oral and Maxillofacial Surgery* **1998**, *56*, 604-614.
[28]   aS. W. Zielhuis, J. F. W. Nijsen, J.-H. Seppenwoolde, C. J. G. Bakker, G. C. Krijger, H. F. J. Dullens, B. A. Zonnenberg, P. P. van Rijk, W. E. Hennink, A. D. van het Schip, *Biomaterials* **2007**, *28*, 4591-4599; bJ. Lu, J. Jackson, M. Gleave, H. Burt, *Cancer Chemother Pharmacol* **2008**, *61*, 997-1005; cA.-Z. Chen, Y. Li, F.-T. Chau, T.-Y. Lau, J.-Y. Hu, Z. Zhao, D. K.-w. Mok, *Acta Biomaterialia* **2009**, *5*, 2913-2919; dD. Lensen, K. van Breukelen, D. M. Vriezema, J. C. M. van Hest, *Macromolecular Bioscience* **2010**, *10*, 475-480.
[29]   aB. Khorsand Sourkohi, A. Cunningham, Q. Zhang, J. K. Oh, *Biomacromolecules* **2011**, *12*, 3819-3825; bA. Cunningham, J. K. Oh, *Macromolecular rapid communications* **2013**, *34*, 163-168; cA. Cunningham, N. R. Ko, J. K. Oh, *Colloids and Surfaces B: Biointerfaces* **2014**, *122*, 693-700; dN. Chan, S. Y. An, J. K. Oh, *Polymer Chemistry* **2014**, *5*, 1637-1649.
[30]   aC. de las Heras Alarcón, S. Pennadam, C. Alexander, *Chemical Society Reviews* **2005**, *34*, 276-285; bQ. Zhang, N. R. Ko, J. K. Oh, *Chemical Communications* **2012**, *48*, 7542-7552; cB. Wang, K. Chen, R. Yang, F. Yang, J. Liu, *Carbohydrate polymers* **2014**, *103*, 510-519.
[31]   A. Ghosh, M. Haverick, K. Stump, X. Yang, M. F. Tweedle, J. E. Goldberger, *Journal of the American Chemical Society* **2012**, *134*, 3647-3650.
[32]   S. Ganta, H. Devalapally, A. Shahiwala, M. Amiji, *Journal of Controlled Release* **2008**, *126*, 187-204.
[33]   aM.-H. Li, P. Keller, *Soft Matter* **2009**, *5*, 927-937; bS. Mura, J. Nicolas, P. Couvreur, *Nature materials* **2013**, *12*, 991-1003.
[34]   aJ. Lu, E. Choi, F. Tamanoi, J. I. Zink, *Small* **2008**, *4*, 421-426; bH.-M. Lin, W.-K. Wang, P.-A. Hsiung, S.-G. Shyu, *Acta biomaterialia* **2010**, *6*, 3256-3263; cG. Liu, C.-M. Dong, *Biomacromolecules* **2012**, *13*, 1573-1583.
[35]   J. M. Schumers, C. A. Fustin, J. F. Gohy, *Macromolecular rapid communications* **2010**, *31*, 1588-1607.
[36]   F. Calliada, R. Campani, O. Bottinelli, A. Bozzini, M. G. Sommaruga, *European Journal of Radiology* **1998**, *27, Supplement 2*, S157-S160.
[37]   H. Li, J. Wang, P. Wang, J. Zheng, F. Song, T. Yin, G. Zhou, R. Zheng, C. Zhang, *Chemical Communications* **2014**, *50*, 15163-15166.
[38]   E. Fleige, M. A. Quadir, R. Haag, *Advanced Drug Delivery Reviews* **2012**, *64*, 866-884.
[39]   aW. G. Pitt, G. A. Husseini, B. J. Staples, *Expert opinion on drug delivery* **2004**, *1*, 37-56; bP. Wust, B. Hildebrandt, G. Sreenivasa, B. Rau, J. Gellermann, H. Riess, R. Felix, P. Schlag, *The lancet oncology* **2002**, *3*, 487-497.
[40]   aA. Prokop, Y. Iwasaki, A. Harada; bT. Kodama, Y. Tomita, K.-i. Koshiyama, M. J. Blomley, *Ultrasound in medicine & biology* **2006**, *32*, 905-914.
[41]   R. Li, W. Wu, Q. Liu, P. Wu, L. Xie, Z. Zhu, M. Yang, X. Qian, Y. Ding, L. Yu, X. Jiang, W. Guan, B. Liu, *PLoS ONE* **2013**, *8*, e69643.
[42]   T. L. Andresen, S. S. Jensen, K. Jørgensen, *Progress in lipid research* **2005**, *44*, 68-97.
[43]   C. Minelli, S. B. Lowe, M. M. Stevens, *Small* **2010**, *6*, 2336-2357.
[44]   S. Hansson, P. Antoni, H. Bergenudd, E. Malmström, *Polymer Chemistry* **2011**, *2*, 556-558.
[45]   P. Vaupel, F. Kallinowski, P. Okunieff, *Cancer research* **1989**, *49*, 6449-6465.
[46]   C. Rijcken, O. Soga, W. Hennink, C. Van Nostrum, *Journal of Controlled Release* **2007**, *120*, 131-148.
[47]   T. Ziglari, A. Allameh, *The Significance of Glutathione Conjugation in Aflatoxin Metabolism*, **2013**.
[48]   aE. Pebay-Peyroula, G. Rummel, J. P. Rosenbusch, E. M. Landau, *Science* **1997**, *277*, 1676-1681; bG. Saito, J. A. Swanson, K.-D. Lee, *Advanced drug delivery reviews* **2003**, *55*, 199-215.

[49]   aS. Aluri, S. M. Janib, J. A. Mackay, *Advanced drug delivery reviews* **2009**, *61*, 940-952; bD. S. Manickam, J. Li, D. A. Putt, Q.-H. Zhou, C. Wu, L. H. Lash, D. Oupický, *Journal of Controlled Release* **2010**, *141*, 77-84.

[50]   aN. V. Tsarevsky, K. Matyjaszewski, *Macromolecules* **2005**, *38*, 3087-3092; bC. Li, J. Madsen, S. P. Armes, A. L. Lewis, *Angewandte Chemie International Edition* **2006**, *45*, 3510-3513.

[51]   M. Talelli, C. J. Rijcken, S. Oliveira, R. van der Meel, P. M. van Bergen en Henegouwen, T. Lammers, C. F. van Nostrum, G. Storm, W. E. Hennink, *Journal of Controlled Release* **2011**, *151*, 183-192.

[52]   aG. J. Charrois, T. M. Allen, *Biochimica et Biophysica Acta (BBA)-Biomembranes* **2004**, *1663*, 167-177; bM. R. Shaik, M. Korsapati, D. Panati, *International Journal Of Pharma Sciences* **2012**, *2*, 112-116; cM. E. Davis, D. M. Shin, *Nature reviews Drug discovery* **2008**, *7*, 771-782.

[53]   H. Ringsdorf, in *Journal of Polymer Science: Polymer Symposia, Vol. 51*, Wiley Online Library, **1975**, pp. 135-153.

[54]   Y. Su, Y. Hu, Y. Du, X. Huang, J. He, J. You, H. Yuan, F. Hu, *Molecular Pharmaceutics* **2015**, *12*, 1193-1202.

[55]   G. M. Soliman, A. Sharma, D. Maysinger, A. Kakkar, *Chemical Communications* **2011**, *47*, 9572-9587.

[56]   R. K. Kainthan, S. R. Hester, E. Levin, D. V. Devine, D. E. Brooks, *Biomaterials* **2007**, *28*, 4581-4590.

[57]   J. Lim, A. Chouai, S.-T. Lo, W. Liu, X. Sun, E. E. Simanek, *Bioconjugate Chemistry* **2009**, *20*, 2154-2161.

[58]   A. V. Kabanov, S. V. Vinogradov, *Angewandte Chemie International Edition* **2009**, *48*, 5418-5429.

[59]   X. Zhang, S. Malhotra, M. Molina, R. Haag, *Chemical Society Reviews* **2015**, *44*, 1948-1973.

[60]   aD. Missirlis, R. Kawamura, N. Tirelli, J. A. Hubbell, *European journal of pharmaceutical sciences* **2006**, *29*, 120-129; bA. V. Kabanov, V. Y. Alakhov, *Critical Reviews™ in Therapeutic Drug Carrier Systems* **2002**, *19*.

[61]   F. Sultana, M. Manirujjaman, M. A. Imran-Ul-Haque, S. Sharmin, *Journal of Applied Pharmaceutical Science Vol* **2013**, *3*, S95-S105.

[62]   D. Dorwal, *Int J Pharm Pharm Sci* **2012**, *4*, 67-74.

[63]   H. P. Yap, A. P. R. Johnston, G. K. Such, Y. Yan, F. Caruso, *Advanced Materials* **2009**, *21*, 4348-4352.

[64]   A. Nelson-Mendez, S. Aleksanian, M. Oh, H.-S. Lim, J. K. Oh, *Soft Matter* **2011**, *7*, 7441-7452.

[65]   G. S. Kwon, *Critical Reviews™ in Therapeutic Drug Carrier Systems* **1998**, *15*.

[66]   F. Alexis, E. Pridgen, L. K. Molnar, O. C. Farokhzad, *Molecular pharmaceutics* **2008**, *5*, 505-515.

[67]   M. Ferrari, *Nature Reviews Cancer* **2005**, *5*, 161-171.

[68]   aJ. You, F.-Q. Hu, Y.-Z. Du, H. Yuan, *Nanotechnology* **2008**, *19*, 255103; bA. Mazzaglia, A. Valerio, V. Villari, A. Rencurosi, L. Lay, S. Spadaro, L. M. Scolaro, N. Micali, *New journal of chemistry* **2006**, *30*, 1662-1668; cD.-Q. Wu, Z.-Y. Li, C. Li, J.-J. Fan, B. Lu, C. Chang, S.-X. Cheng, X.-Z. Zhang, R.-X. Zhuo, *Pharmaceutical research* **2010**, *27*, 187-199; dT. Noh, Y. H. Kook, C. Park, H. Youn, H. Kim, E. T. Oh, E. K. Choi, H. J. Park, C. Kim, *Journal of Polymer Science Part A: Polymer Chemistry* **2008**, *46*, 7321-7331.

[69]   aN. Chan, B. Khorsand, S. Aleksanian, J. K. Oh, *Chemical Communications* **2013**, *49*, 7534-7536; bN. R. Ko, J. K. Oh, *Biomacromolecules* **2014**, *15*, 3180-3189.

[70]   B. Khorsand Sourkohi, R. Schmidt, J. K. Oh, *Macromolecular Rapid Communications* **2011**, *32*, 1652-1657.

[71]   A. Cunningham, J. K. Oh, *Macromolecular Rapid Communications* **2013**, *34*, 163-168.

[72]   B. Khorsand, G. Lapointe, C. Brett, J. K. Oh, *Biomacromolecules* **2013**, *14*, 2103-2111.

[73]   Q. Zhang, S. Aleksanian, S. M. Noh, J. K. Oh, *Polymer Chemistry* **2013**, *4*, 351-359.

[74]   L. Sun, J. Liu, H. Zhao, *Polymer Chemistry* **2014**, *5*, 6584-6592.

[75]   J.-H. Ryu, S. Jiwpanich, R. Chacko, S. Bickerton, S. Thayumanavan, *Journal of the American Chemical Society* **2010**, *132*, 8246-8247.

[76]   W. Chen, Y. Zou, J. Jia, F. Meng, R. Cheng, C. Deng, J. Feijen, Z. Zhong, *Macromolecules* **2013**, *46*, 699-707.

[77]   P. Pinnel, A. Mendez-Nelson, S. M. Noh, J. H. Nam, J. K. Oh, *Macromolecular Chemistry and Physics* **2012**, *213*, 678-685.

[78]   aH. Sun, B. Guo, R. Cheng, F. Meng, H. Liu, Z. Zhong, *Biomaterials* **2009**, *30*, 6358-6366; bT. Thambi, G. Saravanakumar, J.-U. Chu, R. Heo, H. Ko, V. Deepagan, J.-H. Kim, J. Park, *Macromolecular Research* **2013**, *21*, 100-107; cZ. Huang, H. Cang, R. Huang, Z. Cai, H. Zhang, *Polymer Science Series B* **2014**, *56*, 883-894.

[79]   A. Cunningham, N. R. Ko, J. K. Oh, *Colloids and Surfaces B: Biointerfaces* **2014**, *122*, 693-700.

[80]   H. Sun, B. Guo, R. Cheng, F. Meng, H. Liu, Z. Zhong, *Biomaterials* **2009**, *30*, 6358-6366.

[81]   Y.-C. Wang, F. Wang, T.-M. Sun, J. Wang, *Bioconjugate Chemistry* **2011**, *22*, 1939-1945.

[82]   H.-Y. Wen, H.-Q. Dong, W.-j. Xie, Y.-Y. Li, K. Wang, G. M. Pauletti, D.-L. Shi, *Chemical Communications* **2011**, *47*, 3550-3552.

[83]   J. Li, M. Huo, J. Wang, J. Zhou, J. M. Mohammad, Y. Zhang, Q. Zhu, A. Y. Waddad, Q. Zhang, *Biomaterials* **2012**, *33*, 2310-2320.

[84]   Y. Sun, X. Yan, T. Yuan, J. Liang, Y. Fan, Z. Gu, X. Zhang, *Biomaterials* **2010**, *31*, 7124-7131.

[85]   aN. Fomina, C. McFearin, M. Sermsakdi, O. Edigin, A. Almutairi, *Journal of the American Chemical Society* **2010**, *132*, 9540-9542; bG. Pasparakis, M. Vamvakaki, *Polymer Chemistry* **2011**, *2*, 1234-1248; cD. Han, X. Tong, Y. Zhao, *Langmuir* **2012**, *28*, 2327-2331; dX. Jiang, G. Lu, C. Feng, Y. Li, X. Huang, *Polymer Chemistry* **2013**, *4*, 3876-3884; eW.-C. Wu, Y.-S. Kuo, C.-H. Cheng, *Journal of Polymer Research* **2015**, *22*, 1-10.

[86]   R. E. Drumright, P. R. Gruber, D. E. Henton, *Advanced materials* **2000**, *12*, 1841-1846.

[87]   S.-H. Hyon, K. Jamshidi, Y. Ikada, *Biomaterials* **1997**, *18*, 1503-1508.

[88]   R. A. Auras, L.-T. Lim, S. E. Selke, H. Tsuji, *Poly (lactic acid): synthesis, structures, properties, processing, and applications, Vol. 10*, John Wiley & Sons, **2011**.

[89]   aW. H. Carothers, F. J. V. Natta, *Journal of the American Chemical Society* **1930**, *52*, 314-326; bJ. W. Hill, *Journal of the American Chemical Society* **1930**, *52*, 4110-4114; cW. H. Carothers, G. L. Dorough, F. J. v. Natta, *Journal of the American Chemical Society* **1932**, *54*, 761-772; dF. J. v. Natta, J. W. Hill, W. H. Carothers, *Journal of the American Chemical Society* **1934**, *56*, 455-457.

[90]   D. W. Grijpma, A. J. Pennings, *Macromolecular Chemistry and Physics* **1994**, *195*, 1633-1647.

[91]   aJ. Dahlmann, G. Rafler, K. Fechner, B. Mehlis, *British Polymer Journal* **1990**, *23*, 235-240; bD. W. Grijpma, G. J. Zondervan, A. J. Pennings, *Polymer Bulletin* **1991**, *25*, 327-333; cH. R. Kricheldorf, J. Meier-Haack, *Die Makromolekulare Chemie* **1993**, *194*, 715-725; dA. C. Albertsson, M. Gruvegård, *Polymer* **1995**, *36*, 1009-1016.

[92]   A. Stjerndahl, A. Finne-Wistrand, A. C. Albertsson, C. M. Bäckesjö, U. Lindgren, *Journal of Biomedical Materials Research Part A* **2008**, *87A*, 1086-1091.

[93]   R. Mehta, V. Kumar, H. Bhunia, S. Upadhyay, *Journal of Macromolecular Science, Part C: Polymer Reviews* **2005**, *45*, 325-349.

[94]   I. Engelberg, J. Kohn, *Biomaterials* **1991**, *12*, 292-304.

[95]   L. Fambri, A. Pegoretti, R. Fenner, S. Incardona, C. Migliaresi, *Polymer* **1997**, *38*, 79-85.

[96]   C. Fraschini, R. Plesu, J. R. Sarasua, R. E. Prud'Homme, *Journal of Polymer Science Part B: Polymer Physics* **2005**, *43*, 3308-3315.

[97]   J. Brandrup, E. H. Immergut, E. A. Grulke, A. Abe, D. R. Bloch, *Polymer handbook, Vol. 89*, Wiley New York, **1999**.

[98]   G. Moad, J. Chiefari, R. T. Mayadunne, C. L. Moad, A. Postma, E. Rizzardo, S. H. Thang, in *Macromolecular Symposia, Vol. 182*, Wiley-Blackwell, 111 River Street Hoboken NJ 07030-5774 USA, **2002**, pp. 65-80.

[99]   G. Zhang, I. Y. Song, K. H. Ahn, T. Park, W. Choi, *Macromolecules* **2011**, *44*, 7594-7599.

[100]   K. Matyjaszewski, T. P. Davis, *Handbook of radical polymerization*, Wiley Online Library, **2002**.

[101]   K. Matyjaszewski, J. Xia, *Chemical reviews* **2001**, *101*, 2921-2990.
[102]   aY. Chong, T. P. Le, G. Moad, E. Rizzardo, S. H. Thang, *Macromolecules* **1999**, *32*, 2071-2074; bV. Mishra, R. Kumar, *Journal of Applied Polymer Science* **2012**, *124*, 4475-4485.
[103]   R. D. Puts, D. Y. Sogah, *Macromolecules* **1996**, *29*, 3323-3325.
[104]   K. Matyjaszewski, *Macromolecules* **2012**, *45*, 4015-4039.
[105]   N. X. Thanh, M. Hsieh, R. Philp, *Organic Geochemistry* **1999**, *30*, 119-132.
[106]   R. H. Colby, L. J. Fetters, W. W. Graessley, *Macromolecules* **1987**, *20*, 2226-2237.
[107]   D. M. Meunier, J. W. Lyons, J. J. Kiefer, Q. J. Niu, L. M. DeLong, Y. Li, P. S. Russo, R. Cueto, N. J. Edwin, K. J. Bouck, H. C. Silvis, C. J. Tucker, T. H. Kalantar, *Macromolecules* **2014**, *47*, 6715-6729.
[108]   aW. Roorda, J. Bouwstra, M. de Vries, H. Junginger, *Pharmaceutical Research* **1988**, *5*, 722-725; bE. Fukuoka, M. Makita, S. Yamamura, *Chemical and Pharmaceutical Bulletin* **1989**, *37*, 1047-1050; cS. Neau, G. Flynn, *Pharmaceutical Research* **1990**, *7*, 1157-1162; dJ. J. Gerber, J. G. vanderWatt, A. P. Lötter, *International Journal of Pharmaceutics* **1991**, *73*, 137-145.
[109]   B. He, V. Martin, F. Setterwall, *Energy* **2004**, *29*, 1785-1804.
[110]   A. Cooper, M. A. Nutley, A. Wadood, Oxford University Press, Oxford, NY, **2000**, pp. 287-318.
[111]   R. V. Siriwardane, J. A. Poston Jr, E. P. Fisher, M.-S. Shen, A. L. Miltz, *Applied Surface Science* **1999**, *152*, 219-236.
[112]   K. Desai, K. Kit, *Polymer* **2008**, *49*, 4046-4050.
[113]   I. A. Nyrkova, A. N. Semenov, *The European Physical Journal E* **2005**, *17*, 327-337.
[114]   M. Eagleson, *Concise encyclopedia chemistry*, Walter de Gruyter, **1994**.
[115]   S. D. Fowler, W. J. Brown, J. Warfel, P. Greenspan, *Journal of lipid research* **1987**, *28*, 1225-1232.
[116]   P. Greenspan, E. P. Mayer, S. D. Fowler, *The Journal of cell biology* **1985**, *100*, 965-973.
[117]   G.-H. Huang, G. Chen, F. Chen, *Biomass and Bioenergy* **2009**, *33*, 1386-1392.
[118]   A. S. H. Makhlouf, I. Tiginyanu, *Nanocoatings and ultra-thin films: Technologies and applications*, Elsevier, **2011**.
[119]   L. Giannuzzi, F. Stevie, *Micron* **1999**, *30*, 197-204.
[120]   F. Bouyer, N. Sanson, M. Destarac, C. Gerardin, *New Journal of Chemistry* **2006**, *30*, 399-408.
[121]   T. Mosmann, *Journal of Immunological Methods* **1983**, *65*, 55-63.
[122]   aC. Alexander, K. M. Shakesheff, *Advanced Materials* **2006**, *18*, 3321-3328; bN. Rapoport, *Progress in Polymer Science* **2007**, *32*, 962-990; cM. Motornov, Y. Roiter, I. Tokarev, S. Minko, *Progress in Polymer Science* **2010**, *35*, 174-211; dD. Roy, J. N. Cambre, B. S. Sumerlin, *Progress in Polymer Science* **2010**, *35*, 278-301; eH.-i. Lee, J. Pietrasik, S. S. Sheiko, K. Matyjaszewski, *Progress in Polymer Science* **2010**, *35*, 24-44.
[123]   aK. Loomis, K. McNeeley, R. V. Bellamkonda, *Soft Matter* **2011**, *7*, 839-856; bQ. Zhang, N. R. Ko, J. K. Oh, *Chemical Communications* **2012**, *48*, 7542-7552.
[124]   aW.-F. Dong, A. Kishimura, Y. Anraku, S. Chuanoi, K. Kataoka, *Journal of the American Chemical Society* **2009**, *131*, 3804-3805; bT.-H. Ku, M.-P. Chien, M. P. Thompson, R. S. Sinkovits, N. H. Olson, T. S. Baker, N. C. Gianneschi, *Journal of the American Chemical Society* **2011**, *133*, 8392-8395; cA. Ghosh, M. Haverick, K. Stump, X. Yang, M. F. Tweedle, J. E. Goldberger, *Journal of the American Chemical Society* **2012**, *134*, 3647-3650.
[125]   aC. J. F. Rijcken, T. F. J. Veldhuis, A. Ramzi, J. D. Meeldijk, N. C. F. van, W. E. Hennink, *Biomacromolecules* **2005**, *6*, 2343-2351; bY. Wang, H. Xu, X. Zhang, *Advanced Materials* **2009**, *21*, 2849-2864; cO. J. Cayre, N. Chagneux, S. Biggs, *Soft Matter* **2011**, *7*, 2211-2234.
[126]   aN. V. Tsarevsky, K. Matyjaszewski, *Macromolecules* **2002**, *35*, 9009-9014; bC. Li, J. Madsen, S. P. Armes, A. L. Lewis, *Angewandte Chemie, International Edition* **2006**, *45*, 3510-3513; cY.-Z. You, Q.-H. Zhou, D. S. Manickam, L. Wan, G.-Z. Mao, D. Oupicky, *Macromolecules* **2007**, *40*, 8617-8624.
[127]   J.-H. Ryu, R. Roy, J. Ventura, S. Thayumanavan, *Langmuir* **2010**, *26*, 7086-7092.

[128] aJ. Liu, Y. Pang, W. Huang, Z. Zhu, X. Zhu, Y. Zhou, D. Yan, *Biomacromolecules* **2011**, *12*, 2407-2415; bL. Sun, W. Liu, C.-M. Dong, *Chemical Communications* **2011**, *47*, 11282-11284; cJ. Chen, X. Qiu, J. Ouyang, J. Kong, W. Zhong, M. M. Q. Xing, *Biomacromolecules* **2011**, *12*, 3601-3611; dB. Khorsand, R. Schmidt, J. K. Oh, *Macromol Rapid Commun* **2011**, *32*, 1652-1657; eS. Li, C. Ye, G. Zhao, M. Zhang, Y. Zhao, *Journal of Polymer Science, Part A: Polymer Chemistry* **2012**, *50*, 3135-3148.

[129] aY. Li, B. S. Lokitz, S. P. Armes, C. L. McCormick, *Macromolecules* **2006**, *39*, 2726-2728; bZ. Jia, L. Wong, T. P. Davis, V. Bulmus, *Biomacromolecules* **2008**, *9*, 3106-3113; cE. Kim, D. Kim, H. Jung, J. Lee, S. Paul, N. Selvapalam, Y. Yang, N. Lim, C. G. Park, K. Kim, *Angewandte Chemie, International Edition* **2010**, *49*, 4405-4408; dJ.-H. Ryu, R. T. Chacko, S. Jiwpanich, S. Bickerton, R. P. Babu, S. Thayumanavan, *Journal of the American Chemical Society* **2010**, *132*, 17227-17235; eA. W. Jackson, D. A. Fulton, *Macromolecules* **2012**, *45*, 2699-2708; fK. Wang, G.-F. Luo, Y. Liu, C. Li, S.-X. Cheng, R.-X. Zhuo, X.-Z. Zhang, *Polymer Chemistry* **2012**, *3*, 1084-1090.

[130] aX.-J. Cai, H.-Q. Dong, W.-J. Xia, H.-Y. Wen, X.-Q. Li, J.-H. Yu, Y.-Y. Li, D.-L. Shi, *Journal of Materials Chemistry* **2011**, *21*, 14639-14645; bT.-B. Ren, Y. Feng, Z.-H. Zhang, L. Li, Y.-Y. Li, *Soft Matter* **2011**, *7*, 2329-2331; cW. Wang, H. Sun, F. Meng, S. Ma, H. Liu, Z. Zhong, *Soft Matter* **2012**, *8*, 3949-3956.

[131] aM. Kang, B. Moon, *Macromolecules* **2009**, *42*, 455-458; bH. Zhao, W. Gu, E. Sterner, T. P. Russell, E. B. Coughlin, P. Theato, *Macromolecules* **2011**, *44*, 6433-6440; cH. Zhao, E. S. Sterner, E. B. Coughlin, P. Theato, *Macromolecules* **2012**, *45*, 1723-1736.

[132] M. Zhang, L. Yang, S. Yurt, M. J. Misner, J.-T. Chen, E. B. Coughlin, D. Venkataraman, T. P. Russell, *Advanced Materials* **2007**, *19*, 1571-1576.

[133] aA. Klaikherd, S. Ghosh, S. Thayumanavan, *Macromolecules* **2007**, *40*, 8518-8520; bA. Klaikherd, C. Nagamani, S. Thayumanavan, *Journal of the American Chemical Society* **2009**, *131*, 4830-4838; cJ. Liu, Y. Pang, W. Huang, X. Huang, L. Meng, X. Zhu, Y. Zhou, D. Yan, *Biomacromolecules* **2011**, *12*, 1567-1577.

[134] aH.-Y. Wen, H.-Q. Dong, W.-j. Xie, Y.-Y. Li, K. Wang, G. M. Pauletti, D.-L. Shi, *Chemical Communications* **2011**, *47*, 3550-3552; bQ. Zhang, N. R. Ko, J. K. Oh, *RSC Advances* **2012**, *DOI:10.1039/C2RA21209A*.

[135] B. Khorsand, A. Cunningham, Q. Zhang, J. K. Oh, *Biomacromolecules* **2011**, *12*, 3819-3825.

[136] S. Penczek, M. Cypryk, A. Duda, P. Kubisa, S. Slomkowski, *Progress in Polymer Science* **2007**, *32*, 247-282.

[137] aK. Matyjaszewski, J. Xia, *Chemical Reviews* **2001**, *101*, 2921-2990; bM. Kamigaito, T. Ando, M. Sawamoto, *Chemical Reviews* **2001**, *101*, 3689-3745.

[138] aY. Zheng, K. Yao, J. Lee, D. Chandler, J. Wang, C. Wang, F. Chu, C. Tang, *Macromolecules* **2010**, *43*, 5922-5924; bP. A. Wilbon, Y. Zheng, K. Yao, C. Tang, *Macromolecules* **2010**, *43*, 8747-8754.

[139] A. Kowalski, A. Duda, S. Penczek, *Macromolecular Rapid Communications* **1998**, *19*, 567-572.

[140] J. L. Eguiburu, J. J. Iruin, M. J. Fernandez-Berridi, J. San Roman, *Polymer* **1998**, *39*, 6891-6897.

[141] aP. Sarazin, D. Favis Basil, *Biomacromolecules* **2003**, *4*, 1669-1679; bE. Zuza, A. Lejardi, J. M. Ugartemendia, N. Monasterio, E. Meaurio, J.-R. Sarasua, *Macromolecular Chemistry and Physics* **2008**, *209*, 2423-2433.

[142] P. Pinnel, A. Mendez-Nelson, S. M. Noh, J. H. Nam, J. K. Oh, *Macromolecular Chemistry and Physics* **2012**, *213*, 678-685.

[143] aC. Allen, D. Maysinger, A. Eisenberg, *Colloids and Surfaces, B: Biointerfaces* **1999**, *16*, 3-27; bN. Nishiyama, K. Kataoka, *Advances in Polymer Science* **2006**, *193*, 67-101; cA. Harada, K. Kataoka, *Progress in Polymer Science* **2006**, *31*, 949-982; dA. S. Mikhail, C. Allen, *Journal of Controlled Release* **2009**, *138*, 214-223; eX.-B. Xiong, A. Falamarzian, S. M. Garg, A. Lavasanifar, *Journal of Controlled Release* **2011**, *155*, 248-261.

[144] aR. E. Drumright, P. R. Gruber, D. E. Henton, *Advanced Materials* **2000**, *12*, 1841-1846; bA. Kumari, S. K. Yadav, S. C. Yadav, *Colloids and Surfaces, B: Biointerfaces* **2010**, *75*, 1-18.

[145] A. Cunningham, J. K. Oh, *Macromolecular Rapid Communications* **2013**, *34*, 163-168.

[146] aJ.-K. Oh, *Soft Matter* **2011**, *7*, 5096-5108; bY. Liu, A. H. Ghassemi, W. E. Hennink, S. P. Schwendeman, *Biomaterials* **2012**, *33*, 7584-7593.

[147] aS. C. Kim, D. W. Kim, Y. H. Shim, J. S. Bang, H. S. Oh, S. W. Kim, M. H. Seo, *Journal of Controlled Release* **2001**, *72*, 191-202; bO. C. Farokhzad, J. Cheng, B. A. Teply, I. Sherifi, S. Jon, P. W. Kantoff, J. P. Richie, R. Langer, *Proc. Nat. Acad. Sci. U. S. A.* **2006**, *103*, 6315-6320; cY. Dong, S.-S. Feng, *J. Biomed. Mater. Res. Part A* **2006**, *78A*, 12-19; dJ. Yang, C.-H. Lee, H.-J. Ko, J.-S. Suh, H.-G. Yoon, K. Lee, Y.-M. Huh, S. Haam, *Angewandte Chemie, International Edition* **2007**, *46*, 8836-8839; eQ. Shi, Y. Huang, X. Chen, M. Wu, J. Sun, X. Jing, *Biomaterials* **2009**, *30*, 5077-5085.

[148] aL. Zhang, R. Guo, M. Yang, X. Jiang, B. Liu, *Advanced Materials* **2007**, *19*, 2988-2992; bF. F. Wolf, N. Friedemann, H. Frey, *Macromolecules* **2009**, *42*, 5622-5628; cE. Jubeli, L. Moine, G. Barratt, *Journal of Polymer Science, Part A: Polymer Chemistry* **2010**, *48*, 3178-3187; dZ. Cao, Q. Yu, H. Xue, G. Cheng, S. Jiang, *Angewandte Chemie, International Edition* **2010**, *49*, 3771-3776; eM. Barz, F. K. Wolf, F. Canal, K. Koynov, M. J. Vicent, H. Frey, R. Zentel, *Macromolecular Rapid Communications* **2010**, *31*, 1492-1500.

[149] aH. Wang, J. Zhuang, S. Thayumanavan, *ACS Macro Letters* **2013**, *2*, 948-951; bJ. Zhuang, R. Chacko, D. F. Amado Torres, H. Wang, S. Thayumanavan, *ACS Macro Letters* **2014**, *3*, 1-5; cP. Huang, C. Yang, J. Liu, W. Wang, S. Guo, J. Li, Y. Sun, H. Dong, L. Deng, J. Zhang, J. Liu, A. Dong, *Journal of Materials Chemistry B: Materials for Biology and Medicine* **2014**, *2*, 4021-4033.

[150] aM. A. Mintzer, E. E. Simanek, *Chemical Reviews* **2009**, *109*, 259-302; bS. W. Kim, *Journal of Controlled Release* **2011**, *155*, 116-118.

[151] aT. Froehlich, E. Wagner, *Soft Matter* **2010**, *6*, 226-234; bW. Liang, J. K. W. Lam, *Molecular Regulation of Endocytosis* **2012**, 429-456; cX. Guo, L. Huang, *Accounts of Chemical Research* **2012**, *45*, 971-979.

[152] aD. S. W. Benoit, S. Srinivasan, A. D. Shubin, P. S. Stayton, *Biomacromolecules* **2011**, *12*, 2708-2714; bA. M. Alhoranta, J. K. Lehtinen, A. O. Urtti, S. J. Butcher, V. O. Aseyev, H. J. Tenhu, *Biomacromolecules* **2011**, *12*, 3213-3222; cD. J. Gary, H. Lee, R. Sharma, J.-S. Lee, Y. Kim, Z. Y. Cui, D. Jia, V. D. Bowman, P. R. Chipman, L. Wan, Y. Zou, G. Mao, K. Park, B.-S. Herbert, S. F. Konieczny, Y.-Y. Won, *ACS Nano* **2011**, *5*, 3493-3505; dS. Agarwal, Y. Zhang, S. Maji, A. Greiner, *Materials Today* **2012**, *15*, 388-393.

[153] aJ. H. Jeong, L. V. Christensen, J. W. Yockman, Z. Zhong, J. F. J. Engbersen, W. J. Kim, J. Feijen, S. W. Kim, *Biomaterials* **2007**, *28*, 1912-1917; bC. Lin, Z. Zhong, M. C. Lok, X. Jiang, W. E. Hennink, J. Feijen, J. F. J. Engbersen, *Bioconjugate Chemistry* **2007**, *18*, 138-145; cJ. Chen, C. Wu, D. Oupicky, *Biomacromolecules* **2009**, *10*, 2921-2927; dS. Son, R. Namgung, J. Kim, K. Singha, W. J. Kim, *Accounts of Chemical Research* **2012**, *45*, 1100-1112.

[154] aS. Takae, K. Miyata, M. Oba, T. Ishii, N. Nishiyama, K. Itaka, Y. Yamasaki, H. Koyama, K. Kataoka, *Journal of the American Chemical Society* **2008**, *130*, 6001-6009; bH. Sun, B. Guo, X. Li, R. Cheng, F. Meng, H. Liu, Z. Zhong, *Biomacromolecules* **2010**, *11*, 848-854; cK. Miyata, N. Nishiyama, K. Kataoka, *Chemical Society Reviews* **2012**, *41*, 2562-2574.

[155] N. R. Ko, K. Yao, C. Tang, J. K. Oh, *Journal of Polymer Science, Part A: Polymer Chemistry* **2013**, *51*, 3071-3080.

[156] aM. Spasova, L. Mespouille, O. Coulembier, D. Paneva, N. Manolova, I. Rashkov, P. Dubois, *Biomacromolecules* **2009**, *10*, 1217-1223; bN. Karanikolopoulos, M. Zamurovic, M. Pitsikalis, N. Hadjichristidis, *Biomacromolecules* **2010**, *11*, 430-438; cM. A. Kryuchkov, C. Detrembleur, R. Jerome, R. E. Prud'homme, C. G. Bazuin, *Macromolecules* **2011**, *44*, 5209-5217.

[157] V.-T. Huynh, P. de Souza, M. H. Stenzel, *Macromolecules* **2011**, *44*, 7888-7900.

[158]   aY. Ping, D. Wu, J. N. Kumar, W. Cheng, C. L. Lay, Y. Liu, *Biomacromolecules* **2013**, *14*, 2083-2094; bS. Sevimli, S. Sagnella, M. Kavallaris, V. Bulmus, T. P. Davis, *Biomacromolecules* **2013**, *14*, 4135-4149; cF. Zhao, H. Yin, Z. Zhang, J. Li, *Biomacromolecules* **2013**, *14*, 476-484.

[159]   R. Wei, L. Cheng, M. Zheng, R. Cheng, F. Meng, C. Deng, Z. Zhong, *Biomacromolecules* **2012**, *13*, 2429-2438.

[160]   aX.-Q. Zhang, X.-L. Wang, P.-C. Zhang, Z.-L. Liu, R.-X. Zhuo, H.-Q. Mao, K. W. Leong, *Journal of Controlled Release* **2005**, *102*, 749-763; bN. Wiradharma, Y. W. Tong, Y.-Y. Yang, *Biomaterials* **2009**, *30*, 3100-3109; cA. K. Varkouhi, G. Mountrichas, R. M. Schiffelers, T. Lammers, G. Storm, S. Pispas, W. E. Hennink, *European Journal of Pharmaceutical Sciences* **2012**, *45*, 459-466.

[161]   aA. Prokop, J. M. Davidson, *Journal of Pharmaceutical Sciences* **2008**, *97*, 3518-3590; bO. C. Farokhzad, R. Langer, *ACS Nano* **2009**, *3*, 16-20.

[162]   aS. Taurin, H. Nehoff, K. Greish, *Journal of Controlled Release* **2012**, *164*, 265-275; bJ. W. Nichols, Y. H. Bae, *Nano Today* **2012**, *7*, 606-618; cL. Zhang, Y. Li, J. C. Yu, *Journal of Materials Chemistry B: Materials for Biology and Medicine* **2014**, *2*, 452-470.

[163]   aS. D. Conner, S. L. Schmid, *Nature* **2003**, *422*, 37-44; bL. M. Bareford, P. W. Swaan, *Advanced Drug Delivery Reviews* **2007**, *59*, 748-758.

[164]   D. Klinger, K. Landfester, *Polymer* **2012**, *53*, 5209-5231.

[165]   aC. J. F. Rijcken, O. Soga, W. E. Hennink, C. F. van Nostrum, *Journal of Controlled Release* **2007**, *120*, 131-148; bY. Zhao, *Macromolecules* **2012**, *45*, 3647-3657; cA. W. Jackson, D. A. Fulton, *Polymer Chemistry* **2013**, *4*, 31-45; dC. Alvarez-Lorenzo, A. Concheiro, *Chemical Communications* **2014**, *50*, 7743-7765.

[166]   aS. Binauld, M. H. Stenzel, *Chemical Communications* **2013**, *49*, 2082-2102; bE. R. Gillies, T. B. Jonsson, J. M. J. Frechet, *Journal of the American Chemical Society* **2004**, *126*, 11936-11943.

[167]   aL. Sun, B. Zhu, Y. Su, C.-M. Dong, *Polymer Chemistry* **2014**, *5*, 1605-1613; bO. Bertrand, E. Poggi, J.-F. Gohy, C.-A. Fustin, *Macromolecules* **2014**, *47*, 183-190.

[168]   M.-H. Xiong, Y. Bao, X.-J. Du, Z.-B. Tan, Q. Jiang, H.-X. Wang, Y.-H. Zhu, J. Wang, *ACS Nano* **2013**, *7*, 10636-10645.

[169]   N. V. Tsarevsky, K. Matyjaszewski, *Macromolecules* **2005**, *38*, 3087-3092.

[170]   S. S. Hassan, G. Rechnitz, *Analytical Chemistry* **1982**, *54*, 1972-1976.

[171]   aA. Russo, W. DeGraff, N. Friedman, J. B. Mitchell, *Cancer Research* **1986**, *46*, 2845-2848; bG. Saito, J. A. Swanson, K.-D. Lee, *Advanced Drug Delivery Reviews* **2003**, *55*, 199-215.

[172]   aR. Cheng, F. Feng, F. Meng, C. Deng, J. Feijen, Z. Zhong, *Journal of Controlled Release* **2011**, *152*, 2-12; bH. Wei, R.-X. Zhuo, X.-Z. Zhang, *Progress in Polymer Science* **2013**, *38*, 503-535; cM. Huo, J. Yuan, L. Tao, Y. Wei, *Polymer Chemistry* **2014**, *5*, 1519-1528.

[173]   aM. Ding, J. Li, X. He, N. Song, H. Tan, Y. Zhang, L. Zhou, Q. Gu, H. Deng, Q. Fu, *Advanced Materials* **2012**, *24*, 3639-3645; bX. Jiang, M. Zhang, S. Li, W. Shao, Y. Zhao, *Chemical Communications* **2012**, *48*, 9906-9908; cD.-L. Liu, X. Chang, C.-M. Dong, *Chemical Communications* **2013**, *49*, 1229-1231.

[174]   aS. Aleksanian, B. Khorsand, R. Schmidt, J. K. Oh, *Polymer Chemistry* **2012**, *3*, 2138-2147; bH. Fan, J. Huang, Y. Li, J. Yu, J. Chen, *Polymer* **2010**, *51*, 5107-5114; cS. Yu, C. He, J. Ding, Y. Cheng, W. Song, X. Zhuang, X. Chen, *Soft Matter* **2013**, *9*, 2637-2645.

[175]   aL. Yuan, J. Liu, J. Wen, H. Zhao, *Langmuir* **2012**, *28*, 11232-11240; bQ. Zhang, S. Aleksanian, S. M. Noh, J. K. Oh, *Polymer Chemistry* **2013**, *4*, 351-359.

[176]   aA. P. Bapat, J. G. Ray, D. A. Savin, B. S. Sumerlin, *Macromolecules* **2013**, *46*, 2188-2198; bZ. Zhang, L. Yin, C. Tu, Z. Song, Y. Zhang, Y. Xu, R. Tong, Q. Zhou, J. Ren, J. Cheng, *ACS Macro Letters* **2013**, *2*, 40-44; cW. Chen, M. Zheng, F. Meng, R. Cheng, C. Deng, J. Feijen, Z. Zhong, *Biomacromolecules* **2013**, *14*, 1214-1222; dL.-Y. Tang, Y.-C. Wang, Y. Li, J.-Z. Du, J. Wang, *Bioconjugate Chemistyr* **2009**, *20*, 1095-1099; eN. Chan, S. Y. An, N. Yee, J. K. Oh, *Macromolecular Rapid Communications* **2014**, *35*, 752-757.

[177] aQ. Zhang, N. R. Ko, J. K. Oh, *RSC Advanced* **2012**, *2*, 8079-8086; bW. Yuan, H. Zou, W. Guo, T. Shen, J. Ren, *Polymer Chemistry* **2013**, *4*, 2658-2661; cW. Chen, Y. Zou, F. Meng, R. Cheng, C. Deng, J. Feijen, Z. Zhong, *Biomacromolecules* **2014**, *15*, 900-907; dJ. Xuan, D. Han, H. Xia, Y. Zhao, *Langmuir* **2014**, *30*, 410-417; eR. Tong, X. Lu, H. Xia, *Chemical Communications* **2014**, *50*, 3575-3578; fL. Jia, D. Cui, J. Bignon, A. Di Cicco, J. Wdzieczak-Bakala, J. Liu, M.-H. Li, *Biomacromolecules* **2014**, *15*, 2206-2217; gW. Yuan, T. Shen, J. Wang, H. Zou, *Polymer Chemistry* **2014**, *5*, 3968-3971.

[178] C. Nicky, K. Na Re, A. So Young, K. Behnoush, O. Jung Kwon, in *Controlled Radical Polymerization: Materials, Vol. 1188*, American Chemical Society, **2015**, pp. 273-291.

[179] N. Chan, S. Y. An, J. K. Oh, *Polymer Chemistry* **2014**, *5*, 1637-1649.

[180] aK. E. Uhrich, S. M. Cannizzaro, R. S. Langer, K. M. Shakesheff, *Chemical Reviews* **1999**, *99*, 3181-3198; bO. Dechy-Cabaret, B. Martin-Vaca, D. Bourissou, *Chemical Reviews* **2004**, *104*, 6147-6176.

[181] aA. P. Goodwin, J. L. Mynar, Y. Ma, G. R. Fleming, J. M. J. Frechet, *Journal of the American Chemical Society* **2005**, *127*, 9952-9953; bJ. Jiang, X. Tong, D. Morris, Y. Zhao, *Macromolecules* **2006**, *39*, 4633-4640.

[182] R. Hong, G. Han, J. M. Fernandez, B.-j. Kim, N. S. Forbes, V. M. Rotello, *Journal of the American Chemical Society* **2006**, *128*, 1078-1079.

[183] Y. Jin, L. Song, Y. Su, L. Zhu, Y. Pang, F. Qiu, G. Tong, D. Yan, B. Zhu, X. Zhu, *Biomacromolecules* **2011**, *12*, 3460-3468.

[184] aC. Wang, K.-W. Yan, Y.-D. Lin, P. C. H. Hsieh, *Macromolecules* **2010**, *43*, 6389-6397; bS. Torres-Giner, A. Martinez-Abad, J. V. Gimeno-Alcaniz, M. J. Ocio, J. M. Lagaron, *Advanced Biomaterials* **2012**, B112-B122; cF. Zheng, S. Wang, M. Shen, M. Zhu, X. Shi, *Polymer Chemistry* **2013**, *4*, 933-941.

[185] aS. He, T. Xia, H. Wang, L. Wei, X. Luo, X. Li, *Acta Biomaterialia* **2012**, *8*, 2659-2669; bC. Zhou, Q. Shi, W. Guo, L. Terrell, A. T. Qureshi, D. J. Hayes, Q. Wu, *ACS Applied Materials & Interfaces* **2013**, *5*, 3847-3854; cH. Lee, S. Ahn, H. Choi, D. Cho, G. Kim, *Journal of Materials Chemistry B: Materials for Biology and Medicine* **2013**, *1*, 3670-3677.

[186] R. Y. Kannan, H. J. Salacinski, P. E. Butler, G. Hamilton, A. M. Seifalian, *Journal of Biomedical Materials Research, Part B: Applied Biomaterials* **2005**, *74B*, 570-581.

[187] S. E. Greenwald, C. L. Berry, *The Journal of pathology* **2000**, *190*, 292-299.

[188] aS. Francois, N. Chakfe, B. Durand, G. Laroche, *Acta Biomaterialia* **2009**, *5*, 2418-2428; bS. Francois, C. Sarra-Bournet, A. Jaffre, N. Chakfe, B. Durand, G. Laroche, *Journal of Biomedical Materials Research, Part B: Applied Biomaterials* **2010**, *93B*, 531-543.

[189] A. Lancuski, F. Bossard, S. Fort, *Biomacromolecules* **2013**, *14*, 1877-1884.

[190] H. S. Kim, H. O. Ham, Y. J. Son, P. B. Messersmith, H. S. Yoo, *Journal of Materials Chemistry B: Materials for Biology and Medicine* **2013**, *1*, 3940-3949.

[191] G. D. Fu, J. Y. Lei, C. Yao, X. S. Li, F. Yao, S. Z. Nie, E. T. Kang, K. G. Neoh, *Macromolecules* **2008**, *41*, 6854-6858.

[192] C. Gualandi, C. D. Vo, M. L. Focarete, M. Scandola, A. Pollicino, G. Di Silvestro, N. Tirelli, *Macromolecular Rapid Communications* **2013**, *34*, 51-56.

[193] aA. E. Ozcam, K. E. Roskov, J. Genzer, R. J. Spontak, *ACS Applied Materials & Interfaces* **2012**, *4*, 59-64; bT. J. Menkhaus, H. Varadaraju, L. Zhang, S. Schneiderman, S. Bjustrom, L. Liu, H. Fong, *Chemical Communications* **2010**, *46*, 3720-3722.

[194] aD. J. Phillips, M. I. Gibson, *Chemical Communications* **2012**, *48*, 1054-1056; bK. Rahimian-Bajgiran, N. Chan, Q. Zhang, S. M. Noh, H.-i. Lee, J. K. Oh, *Chemical Communications* **2013**, *49*, 807-809.

[195] aF. Meng, W. E. Hennink, Z. Zhong, *Biomaterials* **2009**, *30*, 2180-2198; bR. Cheng, F. Feng, F. Meng, C. Deng, J. Feijen, Z. Zhong, *Journal of Controlled Release* **2011**, *152*, 2-12.

[196] W. Li, J. A. Yoon, K. Matyjaszewski, *Journal of the American Chemical Society* **2010**, *132*, 7823-7825.

[197]   aK. Miyata, Y. Kakizawa, N. Nishiyama, A. Harada, Y. Yamasaki, H. Koyama, K. Kataoka, *Journal of the American Chemical Society* **2004**, *126*, 2355-2361; bR. A. Petros, P. A. Ropp, J. M. DeSimone, *Journal of the American Chemical Society* **2008**, *130*, 5008-5009; cW. Lv, S. Liu, W. Feng, J. Qi, G. Zhang, F. Zhang, X. Fan, *Macromolecular Rapid Communications* **2011**, *32*, 1101-1107.

[198]   aH. A. Aliyar, P. D. Hamilton, N. Ravi, *Biomacromolecules* **2005**, *6*, 204-211; bJ. A. Yoon, S. A. Bencherif, B. Aksak, E. K. Kim, T. Kowalewski, J. K. Oh, K. Matyjaszewski, *Chemistry-An Asian Journal* **2011**, *6*, 128-136.

[199]   aD. Bontempo, L. Heredia Karina, A. Fish Benjamin, D. Maynard Heather, *Journal of the American Chemical Society* **2004**, *126*, 15372-15373; bC. Boyer, V. Bulmus, J. Liu, T. P. Davis, M. H. Stenzel, C. Barner-Kowollik, *Journal of the American Chemical Society* **2007**, *129*, 7145-7154; cC. Boyer, J. Liu, L. Wong, M. Tippett, V. Bulmus, T. P. Davis, *Journal of Polymer Science, Part A: Polymer Chemistry* **2008**, *46*, 7207-7224.

[200]   aL. Brannon-Peppas, *Journal of Controlled Release* **2000**, *66*, 321; bK. Knop, R. Hoogenboom, D. Fischer, U. S. Schubert, *Angewandte Chemie, International Edition* **2010**, *49*, 6288-6308.

[201]   G. J. P. Britovsek, J. England, A. J. P. White, *Inorganic Chemistry* **2005**, *44*, 8125-8134.

[202]   H. Xu, H. Li, J. Chang, *Journal of Materials Chemistry B: Materials for Biology and Medicine* **2013**, *1*, 4182-4188.

[203]   aS. R. Bhattarai, S. Y. Kim, K. Y. Jang, H. K. Yi, Y. H. Lee, N. Bhattarai, S. Y. Nam, D. Y. Lee, H. Y. Kim, P. H. Hwang, *Gene Therapy* **2006**, *14*, 476-483; bH. J. Kim, K. Miyata, T. Nomoto, M. Zheng, A. Kim, X. Liu, H. Cabral, R. J. Christie, N. Nishiyama, K. Kataoka, *Biomaterials* **2014**, *35*, 4548-4556; cD. G. Abebe, R. Kandil, T. Kraus, M. Elsayed, O. M. Merkel, T. Fujiwara, *Macromolecular Bioscience* **2015**, n/a-n/a.

[204]   aC. Nyambo, A. K. Mohanty, M. Misra, *Biomacromolecules* **2010**, *11*, 1654-1660; bP. Ni, S. Fu, M. Fan, G. Guo, S. Shi, J. Peng, F. Luo, Z. Qian, *International journal of nanomedicine* **2011**, *6*, 3065; cN. Shimada, N. Ogata, K. Nakane, T. Ogihara, *Journal of Applied Polymer Science* **2012**, *125*, E384-E389; dY. Wang, G. Guo, H. Chen, X. Gao, R. Fan, D. Zhang, L. Zhou, *International journal of nanomedicine* **2014**, *9*, 1991.

[205]   N. Nihant, C. Grandfils, R. Jérôme, P. Teyssié, *Journal of Controlled Release* **1995**, *35*, 117-125.

[206]   R. Langer, J. Folkman, *Nature* **1976**, *263*, 797-800.

[207]   T. J. Sill, H. A. von Recum, *Biomaterials* **2008**, *29*, 1989-2006.

[208]   X. Zong, K. Kim, D. Fang, S. Ran, B. S. Hsiao, B. Chu, *Polymer* **2002**, *43*, 4403-4412.

[209]   J. Zeng, X. Xu, X. Chen, Q. Liang, X. Bian, L. Yang, X. Jing, *Journal of Controlled Release* **2003**, *92*, 227-231.

[210]   E.-R. Kenawy, G. L. Bowlin, K. Mansfield, J. Layman, D. G. Simpson, E. H. Sanders, G. E. Wnek, *Journal of Controlled Release* **2002**, *81*, 57-64.